PB82-220161

REPORT NO.
UCB/EERC-82/02
JANUARY 1982

EARTHQUAKE ENGINEERING RESEARCH CENTER

SHAKING TABLE TESTS OF A TUBULAR STEEL FRAME MODEL

by

YUSOF GHANAAT
RAY W. CLOUGH

Report to
American Petroleum Institute
National Science Foundation

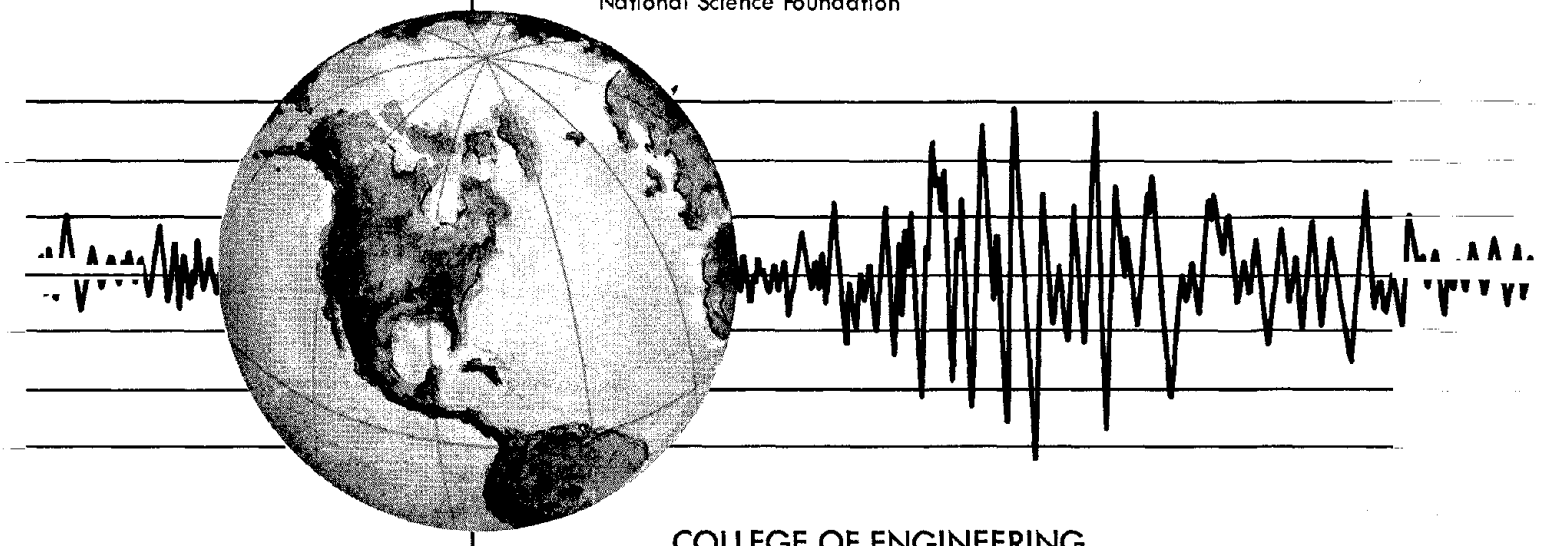

COLLEGE OF ENGINEERING

UNIVERSITY OF CALIFORNIA · Berkeley, California

For sale by the National Technical Information Service, U.S. Department of Commerce, Springfield, Virginia 22161.

See back of report for up to date listing of EERC reports.

DISCLAIMER

SHAKING TABLE TESTS OF A TUBULAR STEEL FRAME MODEL

by

Yusof Ghanaat

and

Ray W. Clough

Report to

American Petroleum Institute

and

National Science Foundation

Report No. UCB/EERC-82/02
Earthquake Engineering Research Center
University of California
Berkeley, California

January 1982

ABSTRACT

This report presents the experimental results of a 2-D (two dimensional) x-braced tubular steel offshore platform model subjected to shaking table motions simulating earthquake excitations. The test frame was a 5/48 scale model of a representative Southern California platform designed according to American Petroleum Institute wave and earthquake criteria. The main purpose of this research was to measure the dynamic response and failure mechanism to be expected of a typical offshore frame subjected to damaging earthquake motions.

This experiment was the first dynamic test of a large single plane frame model performed on the 20-ft square shaking table of the University of California at Berkeley. The model test frame was 17 ft 9 in. (5.4 m) high and consisted of three braced panels with the thinnest members having a wall thickness of 0.049 in. (1.24 mm) and a D/t ratio of 51. A special testing system was designed to provide lateral support to the test model while introducing no constraints in the longitudinal and vertical directions. This arrangement permitted applying a lateral force sufficient to produce major failure in the single test frame, whereas a complete structure including two parallel frames like this could not have been subjected to a failure load.

The 2-D offshore platform model was loaded by 40,000 lb (18,342 kg) of concrete blocks to simulate the prototype dead load, and was subjected to a series of earthquake motions derived from the 1940 El Centro and the 1952 Taft earthquake records. Experimental data are presented indicating when the primary buckling of braces occurred, which braces were affected, and the extent of damage in such members. Time history plots of the table motions and global responses of the test frame, such as lateral forces and displacements, are included. Global lateral force versus displacement hysteresis

loops are presented for the test frame and deterioration of the frame strength and stiffness are discussed. These experimental data provide information on the global inelastic behavior of tubular braced frames, which can be used to verify and extend the ability of existing analytical techniques for predicting the behavior of offshore structures under extreme earthquake conditions. Also presented are data on the local dynamic response of selected bracing members, including force-displacement hysteresis loops for these members.

ACKNOWLEDGMENTS

The experiment reported herein was originally conceived as part of the long term program of research on the use of the EERC shaking table in earthquake engineering, sponsored by the National Science Foundation. In order to improve the efficiency of this test procedure, it was decided to develop a test fixture to permit testing of two-dimensional structures. With funding for the test fixture and for actual performance of the experiment provided by NSF, American Petroleum Institute Committee No. PRAC 32 became interested in the project. They were responsible for planning the test, designing the test model, and providing funding for its construction.

Consequently the authors of this report gratefully acknowledge the two sources of support that made the study possible: National Science Foundation Research Grant No. PFR-79-08257, and API Committee No. PRAC 32, with special thanks to the enthusiastic contributions of its chairman, Mr. Peter Marshall.

TABLE OF CONTENTS

LIST OF TABLES

LIST OF FIGURES

1. INTRODUCTION

Offshore platforms frequently are constructed in parts of the world where significant seismic activity has been recorded or where the region is considered to be seismically active. Structures in such seismic regions may be subjected to intense ground shaking, causing the platform to experience deformations well into the inelastic range. Because the severity of measured earthquake motions has been escalating in recent years, concern for structural safety and the environmental impact of possible structural collapse under an intense ground motion has increased.

The new API platform design recommendations[1] require both strength and ductility in platforms designed to be installed in seismic zones. "Strength Level" or operating level criteria of the API require a structure to be sufficiently strong so that its members remain within the yield or buckling stress levels during a moderate earthquake, one which has a high probability of occurrence in the lifetime of the structure. "Ductility" requirements of the API demand that sufficient energy absorption capacity be provided to insure structural integrity and to prevent collapse in the very rare event of an extremely strong earthquake motion.

The primary ductile deformations in offshore structures which provide the desired energy absorption capability, are developed in the braces. Consequently, the applicability of the ductile design concept depends on the energy dissipation capacity offered by the brace members. Obviously, the inelastic dynamic response of offshore structures has to be thoroughly investigated before the ductile design concept can be applied with confidence.

1.1 Background

In the last several years numerous experimental and analytical investigations have been directed toward evaluating the inelastic behavior of offshore structures subjected to severe seismic loadings. Early experimental studies were related to bending, buckling and post-buckling behavior of the tubular sections[2,3], cyclic inelastic behavior of individual tubular members[4,5], and cyclic inelastic behavior of tubular braced subassemblages[6]. The experimental data on the behavior of individual members provided information which led to development of failure algorithms such as the Marshall strut[7,8]. Also, analytical studies which rely heavily on such algorithms have led to inelastic dynamic analysis computer programs such as DYNAS[9] and INTRA[10].

Furthermore, inelastic cyclic tests performed on two frame models[11] of the Southern California Example Structure[12] have provided data regarding the overall behavior of braced offshore structures subjected to lateral loads. This study showed that the overall structural behavior of offshore platforms depended greatly on the buckling mode of the braces; buckling of the braces was concentrated in one brace of a full diagonal. The S-shape mode of buckling occurred only in diagonal braces of the frame having a low D/t ratio.

The experimental data provided by such inelastic cyclic tests with imposed quasi-static deformation histories contributed much valuable information; however, they can verify only certain aspects of the analytical models. More realistic and general inelastic dynamic behavior of a test structure can be observed if it is subjected to actual earthquake ground motions scaled to produce the desired response intensity. The sequence of lateral forces due to an earthquake acceleration time history generally

differs from those provided in the quasi-static tests. On the other hand, the driving force capacity of the available earthquake simulator (nominally 150 kips) limits such shaking table tests to rather small scale models. One of the objectives of the present study was to develop a technique for shaking table testing of a planar (2D) frame rather than a 3D model; by this approach it was possible to increase significantly the scale of the structure to be tested because only a single frame was subjected to lateral force.

1.2 Objectives and Scope

The primary objective of this study was to obtain experimental data on the seismic behavior of a two dimensional tubular x-braced offshore frame by means of a shaking table. The test model represented a 5/8 scale model of Popov's Frame I[11]; thus, it was a 5/48 scale model of the Southern California Example Structure used in previous analytical studies[9,10,12]. Because of this similarity, this test can provide many useful comparisons with earlier studies; furthermore, it can provide actual dynamic response data for direct computer analysis correlation.

In addition, this investigation had two other specific objectives, as follows:

1. Evaluation of the overall dynamic response of the test frame subjected to scaled earthquakes of differing intensities, simulating the API "Strength Level", "Ductility Level", and "Maximum Credible" earthquake motions.
2. To provide observations of the actual dynamic inelastic behavior of brace members and the failure mechanism of the test frame.

The special test fixture designed to make possible dynamic experimentation with two-dimensional frame structures, as well as details of the test model and its material properties are discussed in Chapter 2. Descriptions of the

structural response instrumentation and of the experimental procedures employed are presented in Chapter 3 and Chapter 4, respectively.

The observed dynamic response of the test model is presented in the form of graphical displays in Chapter 5. Time history plots of the table motions and global responses of the test frame (such as lateral forces and displacements) are discussed, and the global lateral force versus lateral displacement hysteresis loops are examined. Also, the deterioration of global frame strength and stiffness are discussed. In addition to these data on the global response, most of which were included in the preliminary report submitted to the API project sponsors, the present report also gives detailed information on some aspects of the local dynamic response, such as brace deformations and buckling behavior.

2. TEST MODEL AND PROPERTIES

Dynamic testing by shaking table excitation of a single offshore platform tubular frame model required development of a special testing system to provide lateral support to the test structure. This unique test fixture along with design criteria, geometry, and material properties of the test model are described in this chapter.

2.1 Test Fixture

One unique feature of this investigation was that for the first time a dynamic study of a large planar frame model was attempted on the 20-ft square shaking table at the Earthquake Engineering Research Center. The choice of a 2D test model was made for two prime reasons: one was to provide dynamic test results which are directly comparable with the static test results obtained from the model studied previously by E. P. Popov[11], the other was to maximize the size of the test structure while keeping its total strength within the force capabilities of the shaking table. An additional factor of considerable importance is that a 2-D model costs much less than a 3-D model. However, to permit dynamic testing of a 2-D frame required design of a special lateral support fixture which is described briefly in this section.

The complete testing system employed in this investigation consisted of the lateral support fixture, the test model, a steel platform for carrying the test mass, and a set of lateral support linkages, as shown in Figs. 2.1A and 2.1B. The lateral support frame consisted of two steel frames placed parallel to the plane of table motion with a bracing system between them. These frames provided support for the lateral linkage mechanisms connected to the test model, as well as for the linkages controlling the added mass.

The dimensions of the test fixture were 9 x 14 ft in plan and 18 ft in height. Its lateral stability was provided by angle x-braces in the longitudinal direction and rod-turnbuckle braces in the lateral direction.

The 5/48 scale test model may be seen housed within the test fixture in the photographs, Figs. 2.1A and 2.1B. Design criteria and a detailed description of this model are given later in this chapter.

A rigid 6 x 20 ft platform to carry the concrete block, added mass was fabricated from 20 ft long W16 x 58 chord members, connected by eight 6 ft long W8 x 17 cross beams with supplementary angle diagonal braces, as shown in Figs. 2.1C and 2.1D. This was bolted to the top of the test model through the deck module. A one inch space was provided between the lower surface of this platform and the top beams of the test fixture to permit its free movement, but still prevent its dropping on the shaking table if the frame model should collapse.

The lateral support linkages were specially designed to allow the test model to move freely in the longitudinal and vertical directions (plane of table motion) but prevent any lateral (out-of-plane) movements. An analysis of the lateral support linkages is given in Appendix A. These mechanisms consisted of two 45-in. long bracing arms attached to the test fixture at one end and to a 16 in. coupler beam at the other end (as may be seen in Figs. 2.1B, 2.1C and 2.1D). The bracing arms were horizontal in the pre-test position, with the coupler perpendicular to them and connected to the test frame (or deck platform) at its center by a pin. All linkage attachments were provided by spherical bearing joints (HEIM ARE-20M) so that both longitudinal and vertical motions were possible. A total of six linkages were used, four of which were mounted on the test frame legs with vertical couple beams at the locations of horizontal braces. The other two were attached with horizontal couplers to provide guidance for the mass-platform,

as may be seen in Fig. 2.1C.

2.2 Design Criteria for Test Model

The 2D frame tested on the shaking table (see Fig. 2.2) was a scale model of part of a small four-pile offshore production platform designed according to the API wave and earthquake criteria applicable to Southern California[1]. Design of the model for dynamic testing on the shaking table was carried out by API Committee No. PRAC #14, and was governed by the following considerations:

1. Dimension constraints imposed by the shaking table size, and a height limitation associated with the table overturning capacity.
2. Restrictions depending on the availability of the tube sizes, especially those involved in the expected failure mechanism.
3. Limitations imposed by the table payload capacity with regard to survivability of the test model under so called "Maximum Credible" earthquake excitation.

As was noted earlier, the test frame represents a 5/8 model of the frame tested by Popov[11], which in itself was a 1/6 scale model of one frame of the prototype Southern California example structure. In the API design of the shaking table model, the measured strength and stiffness of the Popov Model I (D/t of 48) was scaled up to prototype dimensions. Also the deck mass was increased 30% so that the scaled-up structure would just reach yield stresses for API Seismic Zone 4 and soil type C strength level criteria. This prototype was then scaled down to the shaking table size model, requiring a superimposed weight of 38 kips. The pin-connected base detail used by Popov was retained so that the correspondence of test results would be preserved in this regard.

This geometrically scaled frame with mass distribution similar to the

prototype, represented a model which was dynamically similar to the prototype offshore platform, using an appropriate time scaling factor. Therefore, the experimental results of the test model can be extrapolated to define prototype response, using the standard similitude ratios shown in Table 2.1.

2.3 Geometry and Member Sizes

The 5/48 scale test model was 75 in. (190.5 cm) wide, 17 ft 9-1/2 in. (5.4 m) high and consisted of two diagonal x-braced panels and one k-braced half-panel forming a complete bent (see Fig. 2.2). All brace members and jacket legs were selected from available steel tubing, approximately proportioned for the 5/48 scale size. The horizontals and upper panel diagonal brace members were 2-1/2 in. outer diameter tubes with a wall thickness of 0.049 in. (D/t = 51). They were cold rolled electric-welded tubing (CREW1010) fabricated from A513 mild steel. The failure mechanism for the test structure developed in these tubes, and it is noteworthy that their wall thickness was within 6% of the true scaled dimension.

Diagonal braces used in the lower panel, and k-brace members of the top half-panel were tubes with the wall thickness of 0.083 in. and with outer diameters of 3 in. and 3.5 in., respectively. They were Drawn-Over-Mandrill mechanical tubings, also fabricated from A513 mild steel. The jacket legs of the test frame, with outer diameter of 8 in. and D/t ratio of 43, were chosen from WD-AWWA water pipe sections fabricated from A200 mild steel. Nominal tube sizes and their section properties are summarized in Table 2.2.

The deck module of the test frame was built from two W14 x 22 wide flange sections of A36 steel, welded side by side (see Fig. 2.2) with enough stiffener plates to insure rigid action. It was then attached to the tubular frame by full penetration welds.

Details of the upper and center brace-to-jacket joints are shown in Fig. 2.3A. An intentional offset of 1/2 in. was introduced at the intersection of diagonal and jacket center lines, providing clear distances of from 0.74 to 1.4 in. between the tube walls to facilitate the welding process. This offset and separation between non-overlapping braces are both within the limits allowed by the API[1] for simple joints.

The diagonal cross-joints between braces were fabricated according to the details shown in Fig. 2.3B. Stubs with thick walls were inserted in the through diagonals to prevent any premature failure of cross-joints prior to inelastic action of the diagonal braces[11]. The same procedure was employed in constructing load cells which were inserted at inflection points of the diagonals. The thick wall stubs used in the load cells assured that they would remain elastic when the diagonals yielded or buckled; therefore, axial strains measured in these devices are directly proportional to the member axial forces.

The test frame fabrication process was carefully planned to prevent any undesirable eccentricity and mis-alignment. Full penetration TIG (Tungsten-Insert Gas) welds were used in all tube connections. Tube ends were beveled, and special efforts were taken to have reasonably close fits between the tube members. Also, all welds were checked by radiograph tests for possible flaws.

2.4 Material Properties

As was mentioned, all bracing tubes used in the test frame were fabricated from A513 mild steel. According to the manufacturer's report, the yield strength of such tubing was 58 ksi, which is considerably higher than the yield strength of the A36 mild steel tubing commonly used in full-scale offshore construction. To obtain strength properties in the test frame braces

similar to their corresponding full-scale members, the brace tubings were annealed by heating them at 1600°F for one hour and then oven-cooling to 600°F. The strain-stress curves of coupon tensile tests shown in Fig. 2.4 demonstrate that the annealing process reduced the yield strength of the tubing and produced a substantial plastic plateau which is essential to ductile behavior of the braces.

Three coupon tensile tests were performed for each tube section size of the bracing members. A summary of these test results along with the measured wall thicknesses is given in Table 2.3. Tubes with wall thickness of t = 0.083 in. used in the lower x-braces and in the top half-panel k-braces had an average yield strength of 32 ksi and an average ultimate strength of 53 ksi. According to the API criteria for the yield strength of F_y = 32 ksi, a section is considered fully compact for $D/t \leq 41$ and partially compact if $41 \leq D/t \leq 59$. Based on this criterion the tube section of the lower x-braces with D/t = 36 is fully compact, whereas the tube section of the k-braces with D/t = 42 is considered partially compact.

The yield and ultimate strength of tube sections with measured wall thickness of t = 0.046 in., used in the upper x-braces and the horizontal brace members were 19.6 ksi and 41 ksi, respectively. This unexpectedly low yield strength showed that the thinner sections should have been annealed separately and under milder temperature condition. Under the API compactness requirement (F_y = 19.6 ksi, $D/t \leq 66$), this thin section with D/t = 54 (t = 0.046 in.) is regarded as a fully compact section.

The jacket-legs were not annealed because it was believed that these members would behave elastically in the dynamic tests. Also, because of their larger sizes it was considered appropriate to treat these members as they would be in full-scale construction. Two coupon tensile tests were performed for these members, showing the average yield strength to be 48 ksi.

TABLE 2.1

SCALE FACTORS FOR DYNAMIC RESPONSE OF OFFSHORE PLATFORM

PARAMETER	ONE TRUSS PROTOTYPE/ONE TRUSS MODEL
Length	f*
Area	f^2
Time	$\sqrt{f}$
Period	$\sqrt{f}$
Displacement	f
Velocity	$\sqrt{f}$
Acceleration	1
Mass	f^2
Force	f^2
Moment	f^3
Moment of Inertia	f^4
Stress	1
Strain	1

* f = 48/5 geometric scale factor of prototype/model.

TABLE 2.2

NOMINAL TUBE SIZE AND YIELD STRENGTHS

Member	Tube Size O.D. x Wall Thickness	Section Area ($in.^2$)	Yield Strength (kips)	D/t
1,2,3,4,11,12,13*	2-1/2" ϕ x .049"	0.377	21.87	51
5,6,7,8	3" ϕ x .083	0.761	44.14	36
9,10	3-1/2" ϕ x .083	0.890	51.62	42
Jacket Legs	8 ϕ x .188	4.610	~	43
2-1/2" ϕ Insert	2-1/2" ϕ x .156	1.149	66.64	16
3" ϕ Insert	3" ϕ x .250	2.160	125.28	12

σ_y = 58 ksi according to manufacturer's report.

~ σ_y not available.

* For member numbers see Fig. 3.4.

TABLE 2.3

SUMMARY OF COUPON TEST RESULTS

	Nominal Section O.D. x t	Measured Thickness (in.)	σ_y (ksi)	$\sigma_{ult.}$ (ksi)
1	2-1/2" x .049"	.046	21.90	42.9
2	2-1/2" x .049"	.046	19.45	41.2
3	2-1/2" x .049	.046	17.29	38.9
4	3" x .083"	.083	34.9	53.9
5	3" x .083"	.083	28.6	53.0
6	3" x .083"	.083	30.9	51.9
7	3-1/2" x .083"	.083	30.8	53.1
8	3-1/2" x .083"	.083	33.1	52.8
9	3-1/2" x .083"	.083	32.3	51.2
10	8" x .188"	.194	49.0	62.6
11	8" x .188"	.194	47.6	61.9

Brace Members	Brace Member	Jacket Legs
t = 0.046"	t = 0.083"	t = 0.194"
$\bar{\sigma}_y$ = 19.6 ksi	$\bar{\sigma}_y$ = 32 ksi	$\bar{\sigma}_y$ = 48 ksi
$\bar{\sigma}_{ult}$ = 41 ksi	$\bar{\sigma}_{ult}$ = 53 ksi	$\bar{\sigma}_{ult}$ = 62 ksi

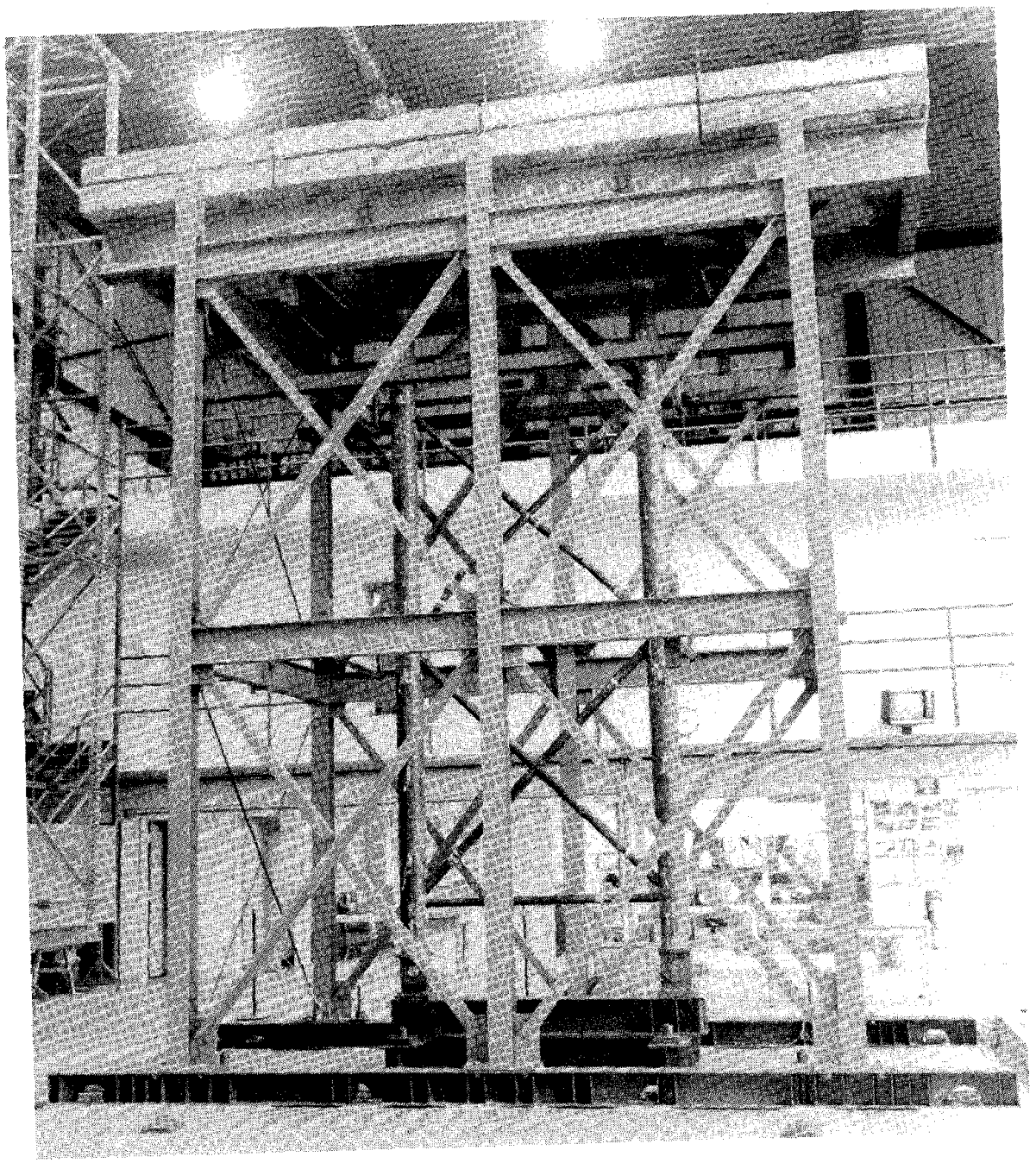

Fig. 2.1A Front View of the Test Model and the Lateral Support Fixture.

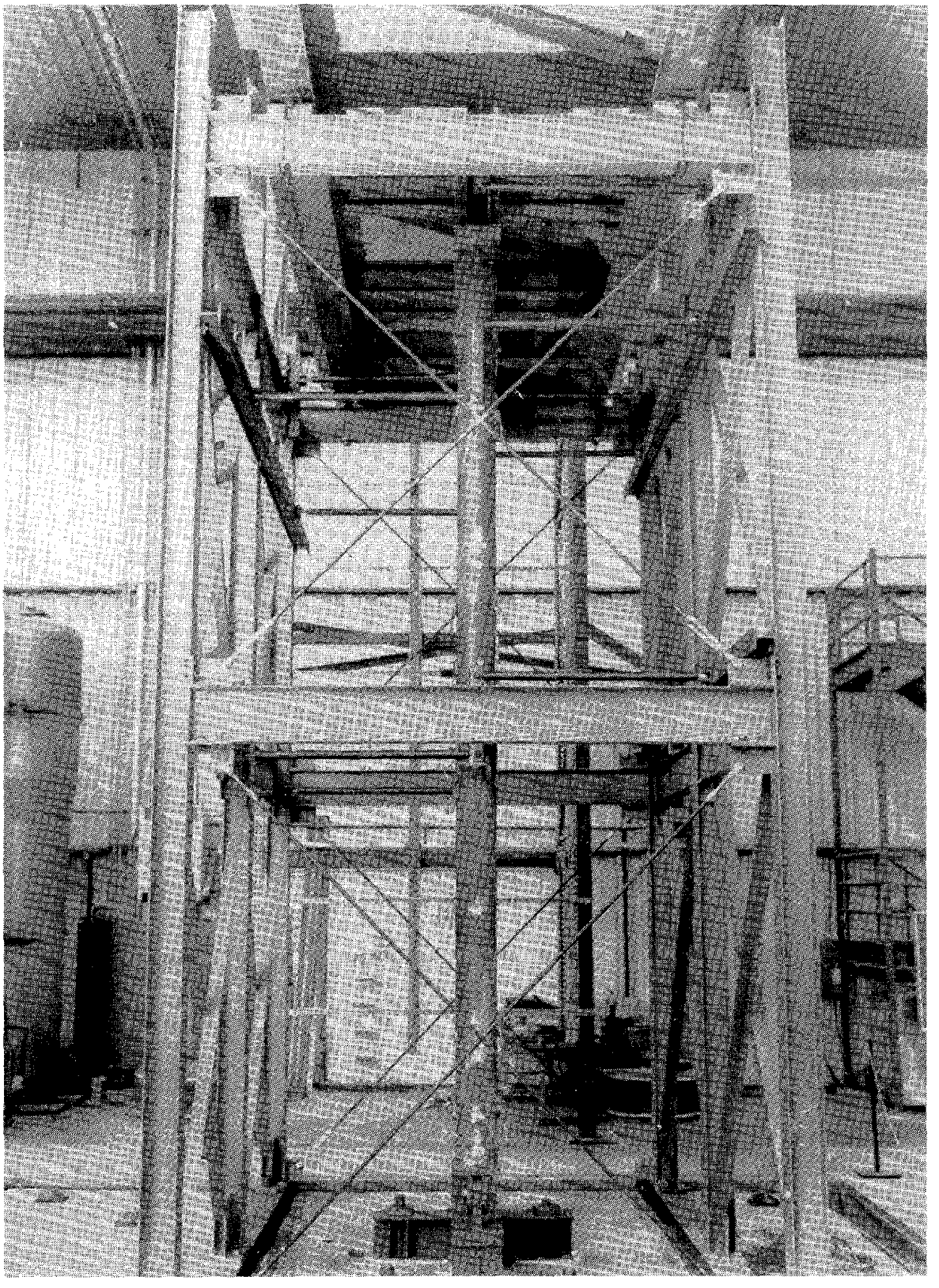

Fig. 2.1B Longitudinal View of Test Setup Showing Lateral Bracing of Test Model to Support Fixture.

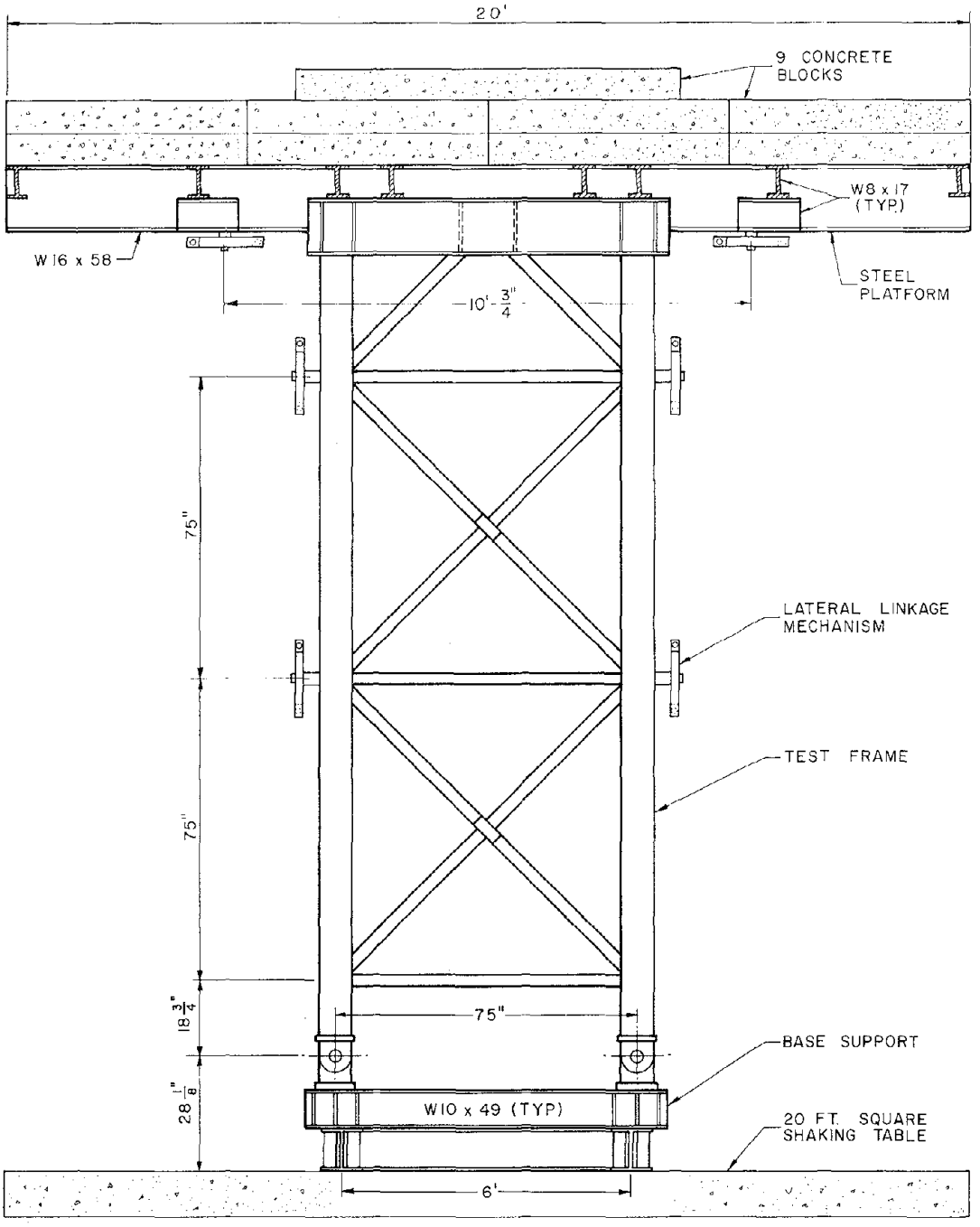

Fig. 2.1C Front View of the Test Setup.

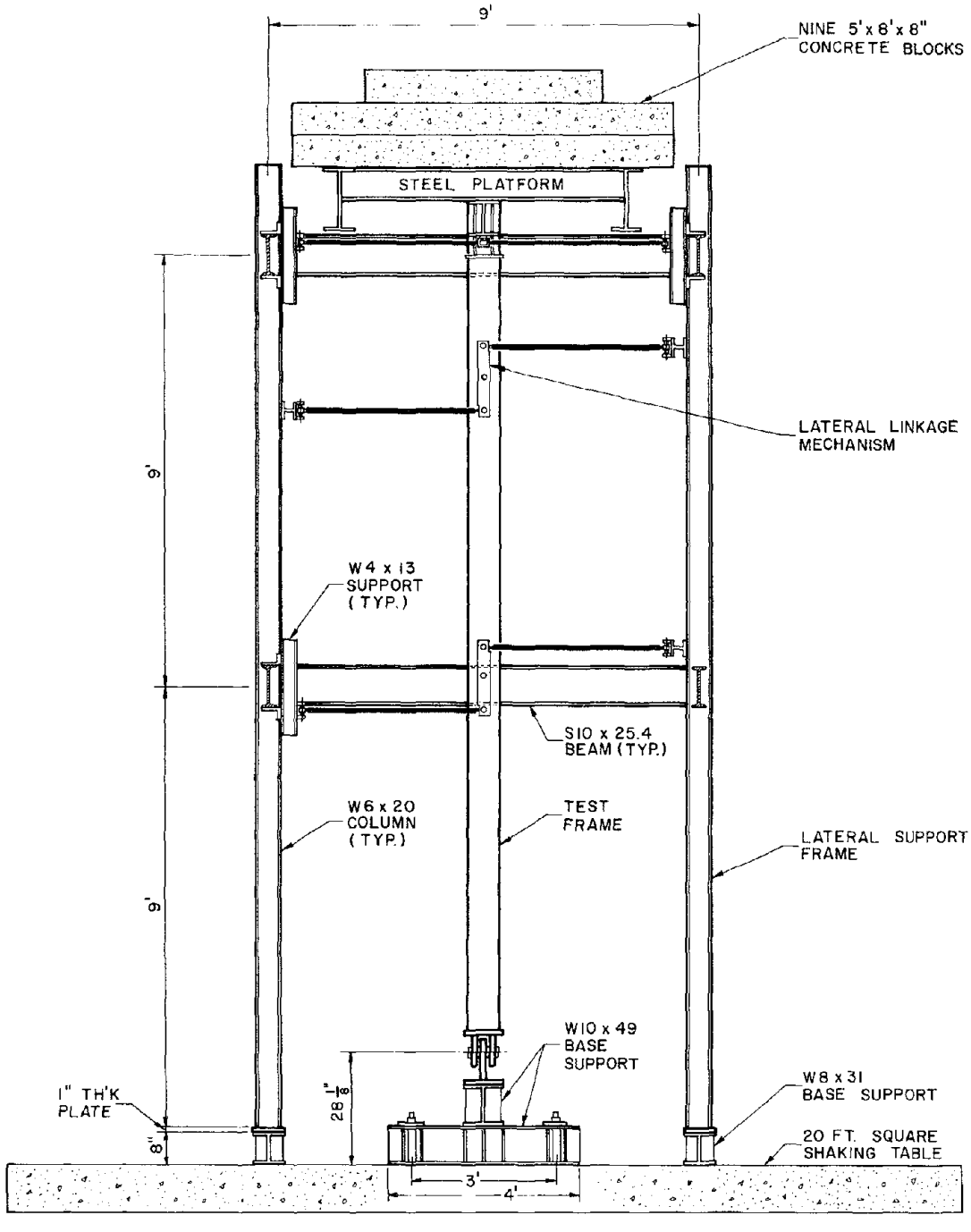

Fig. 2.1D Side View of the Test Setup.

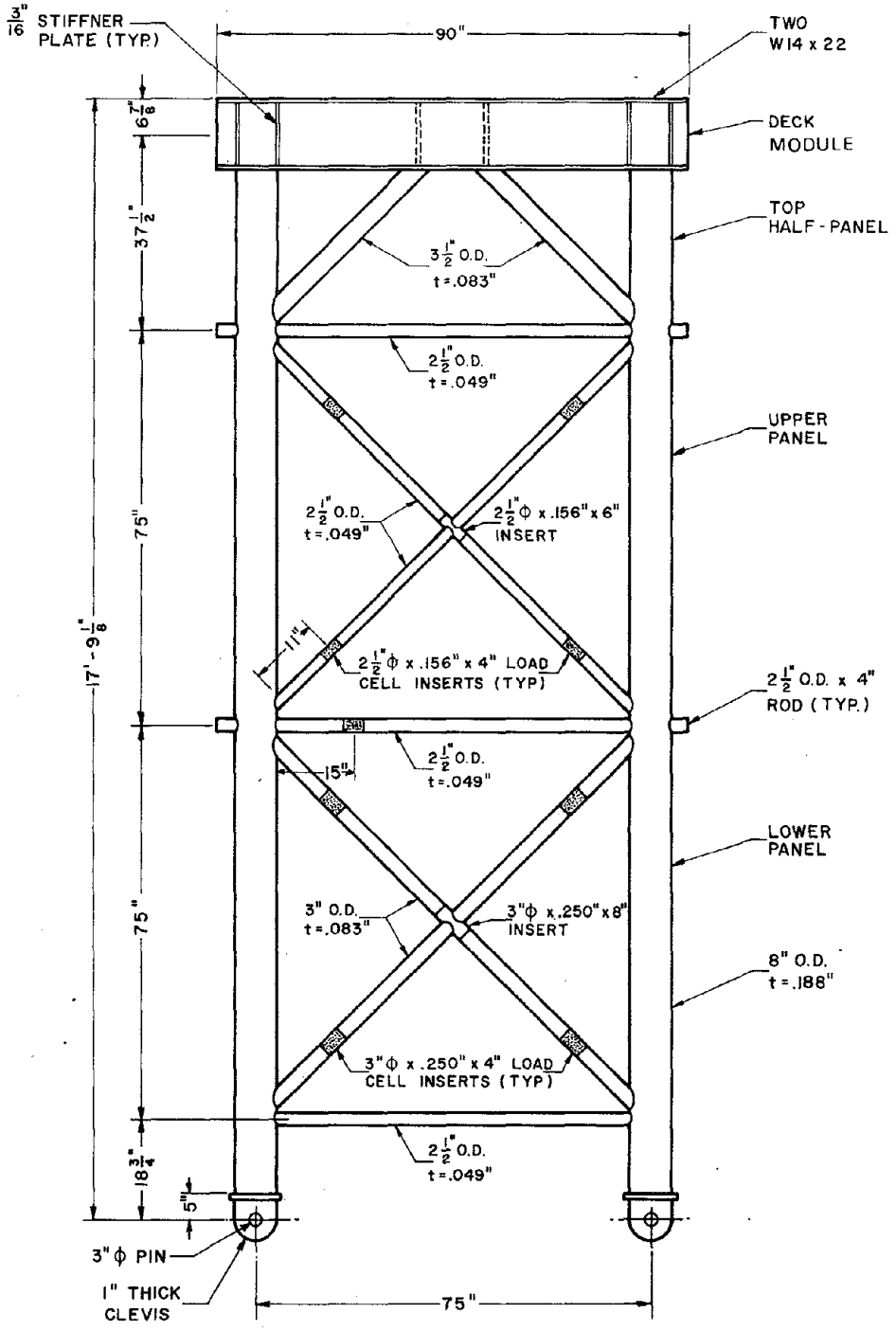

Fig. 2.2 Nominal Dimensions of the Offshore Test Frame.

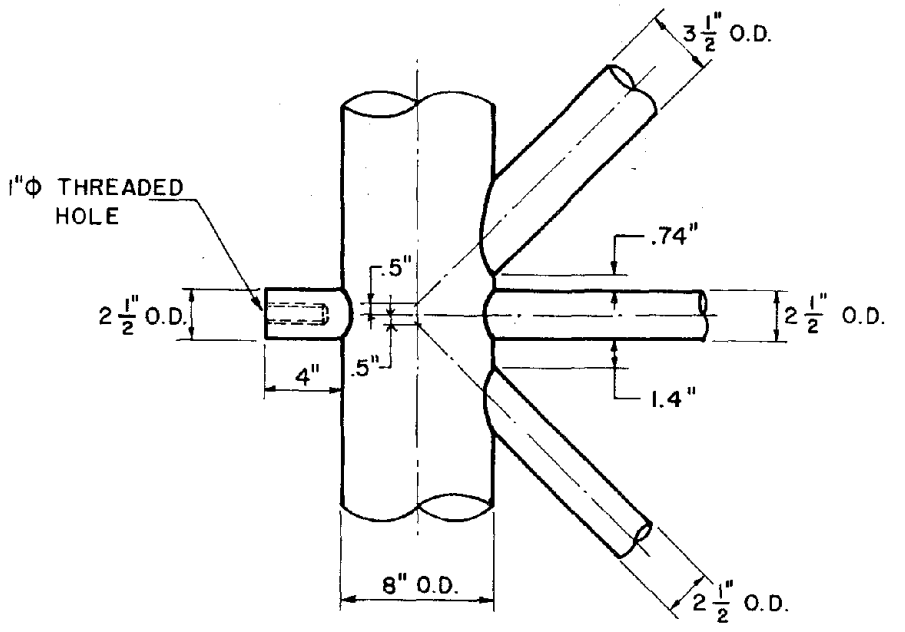

(a) UPPER JOINT

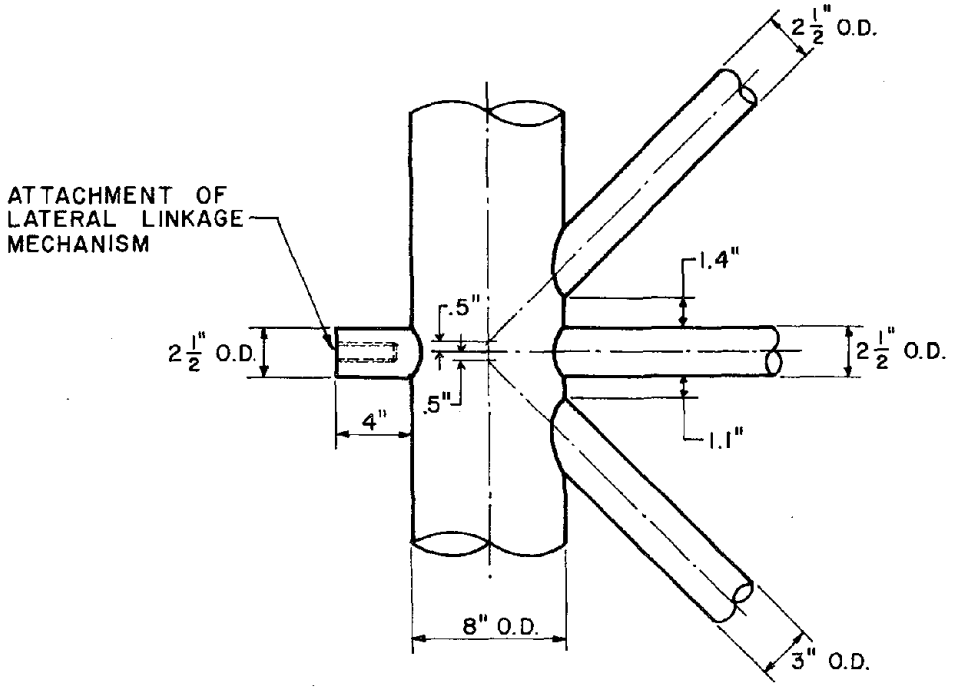

(b) CENTER JOINT

Fig. 2.3A Details of Upper and Center Brace-To-Jacket Joints.

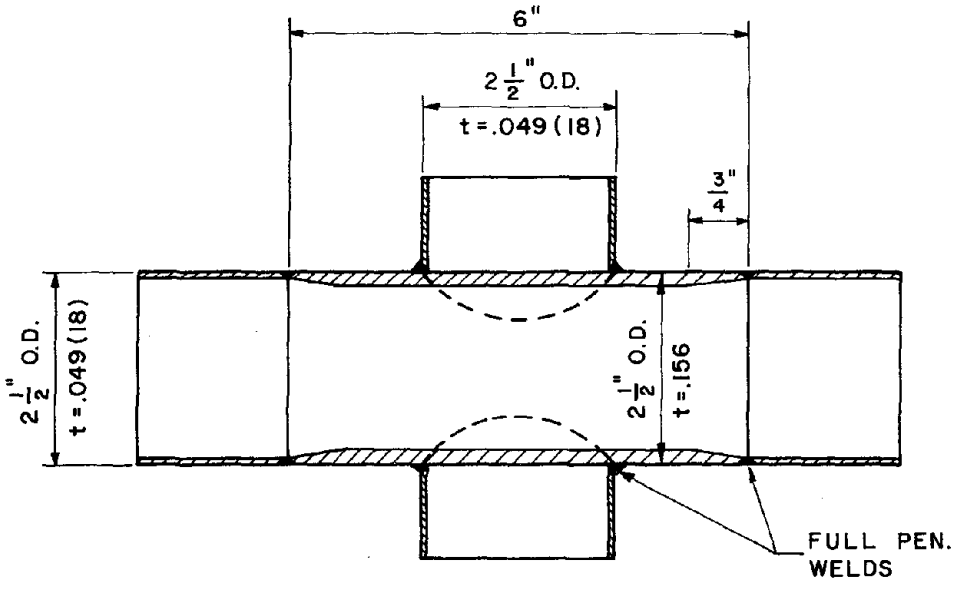

UPPER BRACE CROSS JOINT

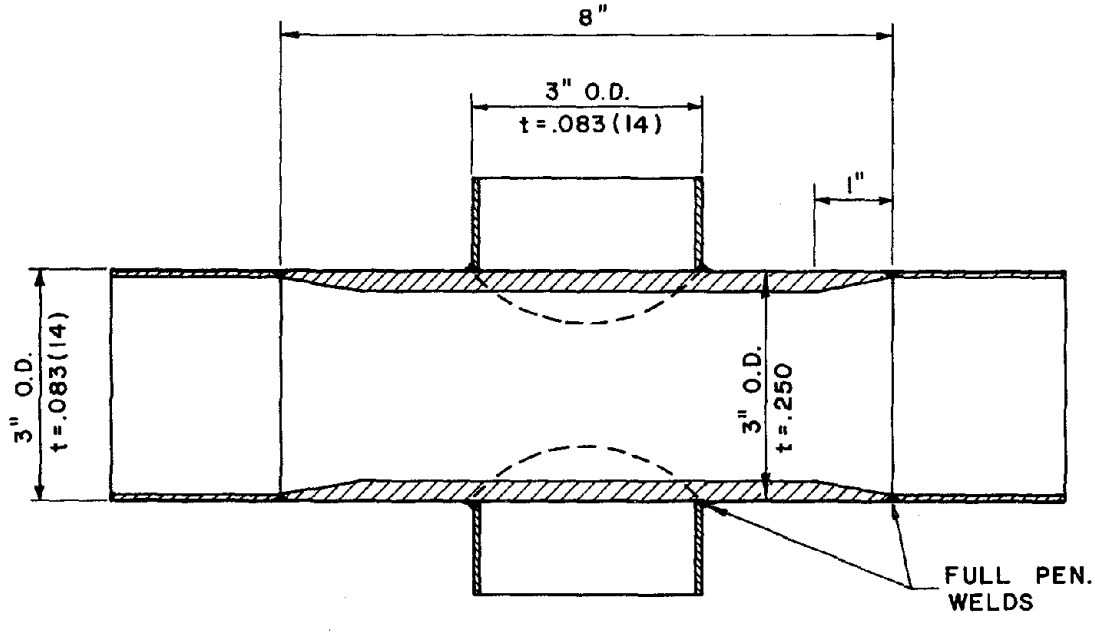

LOWER BRACE CROSS JOINT

Fig. 2.3B Details of Upper and Lower Diagonal Cross-Joints.

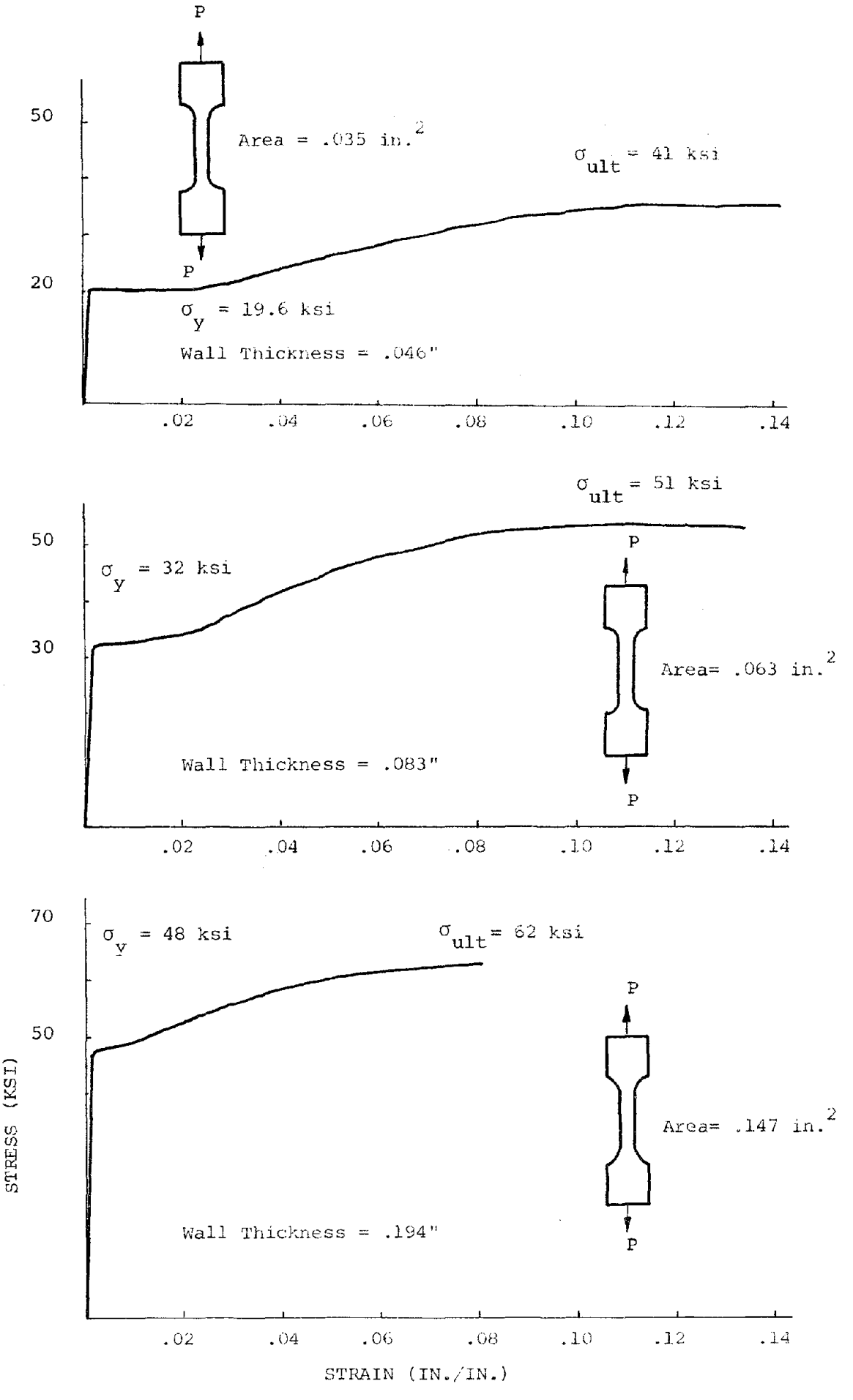

Fig. 2.4 Stress-Strain Curves of Coupon Tensile Tests.

3. TEST SYSTEM AND INSTRUMENTATION

Over one hundred channels of instrumentation were used to measure the shaking table motions and earthquake response of the test model. The measured response quantities consisted of the various accelerations and displacements required to represent the overall response of the test model, as well as forces and strains suitable to describe the behavior of the individual members. A complete list of the data channels is given in Appendix B.

3.1 Table Motion

Dynamic testing of the test model was carried out on the 20 ft. square shaking table of the University of California at Berkeley. This table, which is essentially a one foot thick reinforced and post-tensioned concrete slab driven by an electro-hydraulic actuator system, is able to produce any desired motions independently in the vertical and one horizontal direction.

The limiting values of shaking table motions (displacements, velocities, and accelerations) are shown in Fig. 3.1. These limitations are imposed by the capacity of the actuators and pumping system as described fully by Rea and Penzien[13]. The desired table motions were based on actual earthquake records and were input to the control system in analog displacement form on magnetic tape. The actual table motions were monitored by accelerometers and Direct-Current-Differential-Transformers (DCDT's) mounted at the location of each actuator. In addition to the vertical and translation components, the horizontal pitch, roll and twist accelerations of the table also were measured.

3.2 Structural Response

The response of the test model was monitored by various accelerometers and displacement measuring potentiometers located as shown in Fig. 3.2. A detailed description and discussion of the accuracy of these instruments is given in Reference (14). Longitudinal and possible transverse and rotational accelerations of the platform supporting the concrete blocks were measured by three Kistler accelerometers located at the positions shown in Fig. 3.2a. Thus, the gross base shear could be computed from inertia forces at this deck level calculated from the corresponding measured longitudinal accelerations. In addition, longitudinal and possible transverse and rotational displacements of the deck were monitored by three linear potentiometers shown in Fig. 3.2a.

In addition, seven potentiometers located either on the test fixture or on a non-moving reference frame off the table, were used to measure the longitudinal displacements of the frame at the joint levels and the out-of-plane movements of the brace cross joints. These displacements combined with the table displacement information provided relative displacements at each joint which were used in evaluating the force-displacement hysteresis loops of the complete frame as well as those of each panel.

3.3 Local Behavior

Local behavior of individual structural members was determined from axial and bending strains measured by strain gages placed on appropriate sections.

Axial displacements of the braces were measured using DCDT's connected between the center of brace-jacket joints and the center of the brace cross-joints (photographs "c" and "d" of Fig. 3.3). The members for which axial displacements were measured included x-braces 1 to 8 and horizontal brace 12

as indicated in Fig. 3.4. Out-of-plane movements of the brace cross-joints were measured by linear potentiometers as mentioned previously.

Axial loads in the braces were obtained from the load cells consisting of heavy tubing inserts, as mentioned before, with externally mounted strain gages (see photographs "a" and "b" in Fig. 3.3 and also Fig. 3.5). All four strain gages of each load cell were model CEA-06-250UM-120 manufactured by Micro-Measurement. Braces 9 to 11, and 13 were expected to behave elastically; therefore, strain gages were placed directly on these brace members and no load cell inserts were used.

In-plane and out-of-plane bending strains were measured at the two ends of brace 4. (Coincidentally, brace 4 experienced more severe damage due to buckling than the other braces). For this purpose, four post-yield strain gages (EP-08-250BG-120) manufactured by Micro-Measurement were applied at each end section as shown in Fig. 3.5.

Axial forces in the jacket legs were measured by mounting a pair of strain gages on opposite faces of the jacket tubes. These strain gages were placed at the mid-height of the bottom, lower, and upper panels of the frame (see Fig. 3.6). Bending strains in the jackets were also monitored at critical locations next to the joints, using the same type of post-yield gages mentioned above.

3.4 Data Acquisition

The analog signals from all transducers were scanned and digitized at the rate of 100 samples per second per channel, by a NEFF 620 data acquisition system. The data were temporarily stored on a mini-computer magnetic-disk for immediate extreme values print out, and then were copied on magnetic tapes for permanent storage and subsequent processing.

3.5 Load Cell Calibration

Load cells were used to measure the axial loads in the brace members. Each load cell consisted of a heavy tubing stub with four strain gages mounted externally at 90 degree angles. Thick wall tubing was used to maintain elastic behavior of the load cell, and the four measured strains were averaged so that the axial force in the brace would be interpreted directly from the strain reading.

To verify the accuracy of the load cells, 12 in. lengths were cut from the bracing members including the 4 in. long load cell inserts in their mid sections. These then were subjected to increasing compressive axial loads until they failed. The results of these tests on two sets of four load cells each are summarized in Table 3.1, where the measured EA factors for computation of axial forces from axial strains, and the ultimate load capacity of each specimen are given. In these tests, the applied axial forces were plotted versus the axial strains measured by each pair of strain gages mounted on opposite sides of the load cells. Differences in the slopes of those plots indicated that reliable results could be obtained only from the average readings of all four strain gages on each load cell.

TABLE 3.1

TEST RESULTS OF THE LOAD CELL CALIBRATION

Load Cell	Area ($in.^2$)	Measured EA (kips)	Ultimate Load (kips)	Average EA (kips)
2-1/2" x .165	1.21	31,265.4	8.64	35,139
2-1/2" x .165	1.21	36,796.7	10.00	
2-1/2" x .165	1.21	36,460.5	8.80	
2-1/2" x .165	1.21	36,033.0	9.96	
3" x .261	2.246	70,781	30.75	66,482
3" x .261	2.246	64,735	29.30	
3" x .261	2.246	63,930	29.30	
3" x .261	2.246	~	28.00	

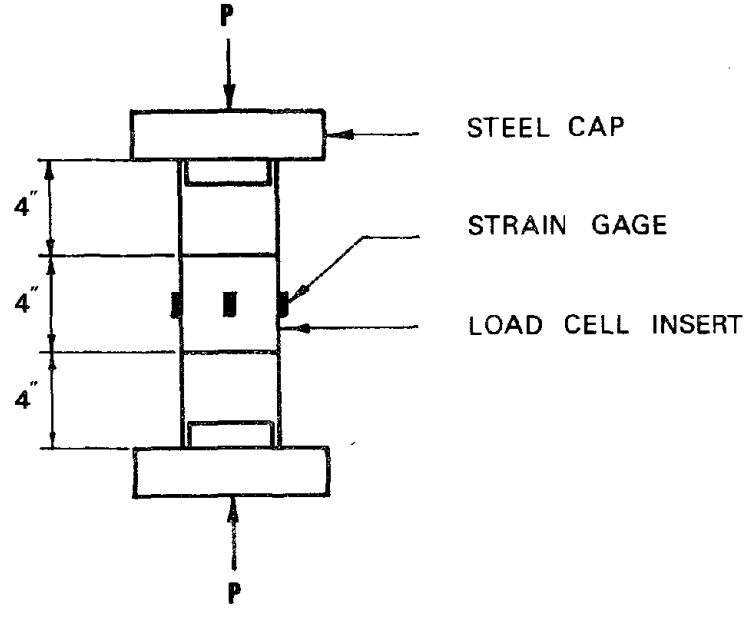

TEST SPECIMEN

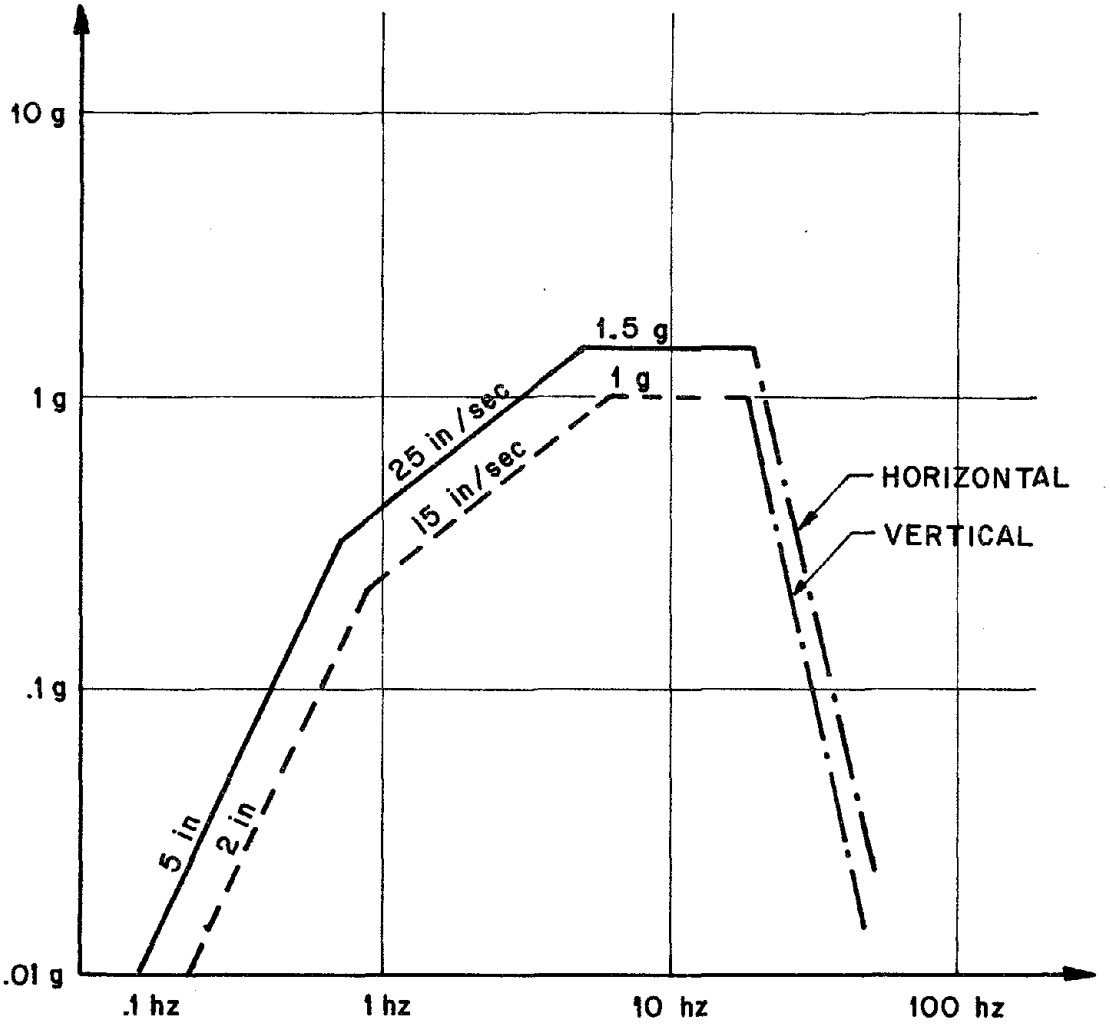

Fig. 3.1 Shaking Table Motion Capabilities.

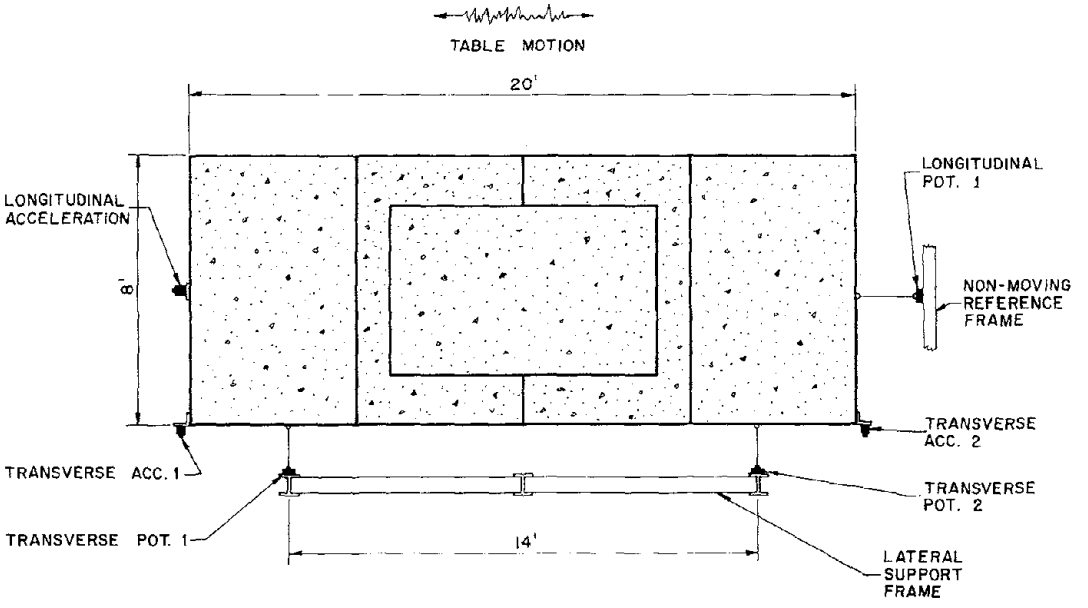

(a) Plan View of Deck Instrumentation.

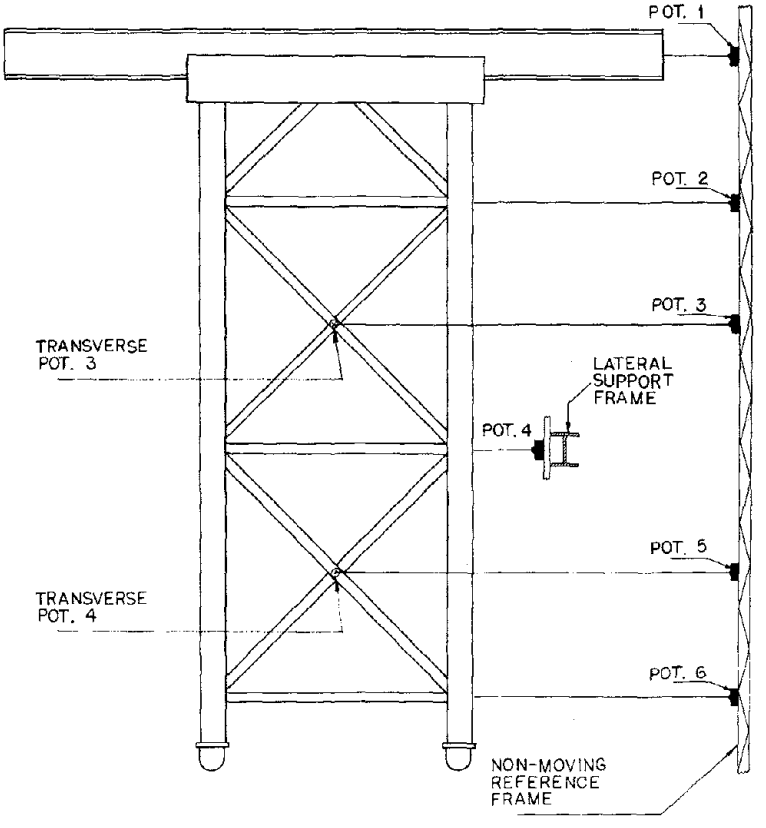

(b) Longitudinal Displacement Measurement.

Fig. 3.2 Acceleration and Displacement Measurements.

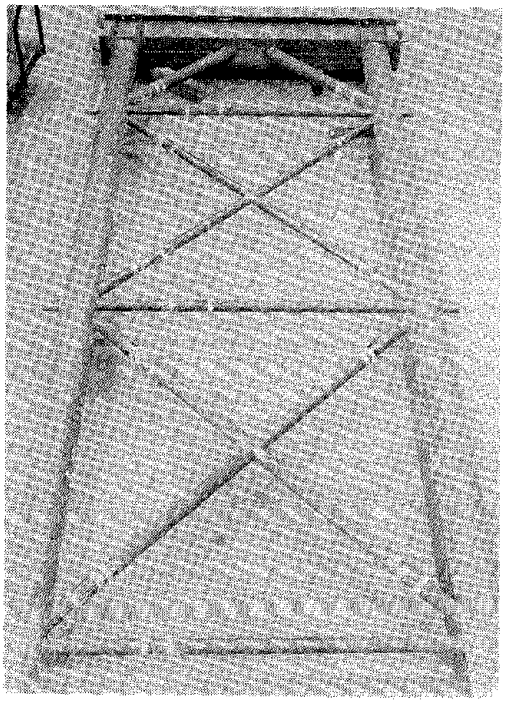

(a) Offshore Frame Model.

(b) Brace Load Cell.

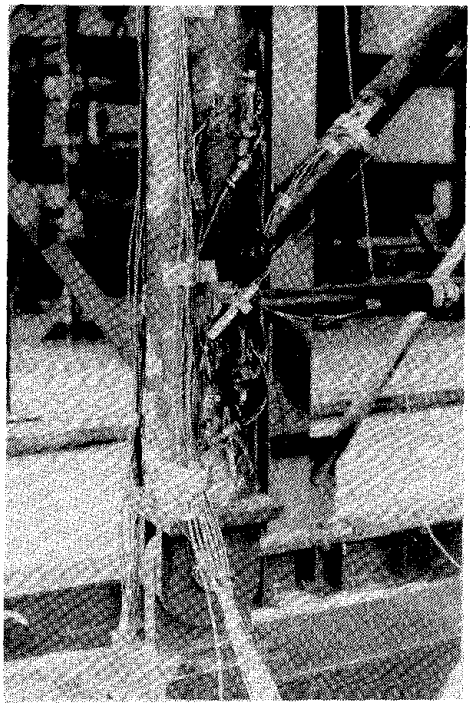

(c) Instrumentation of the Lower Joint.

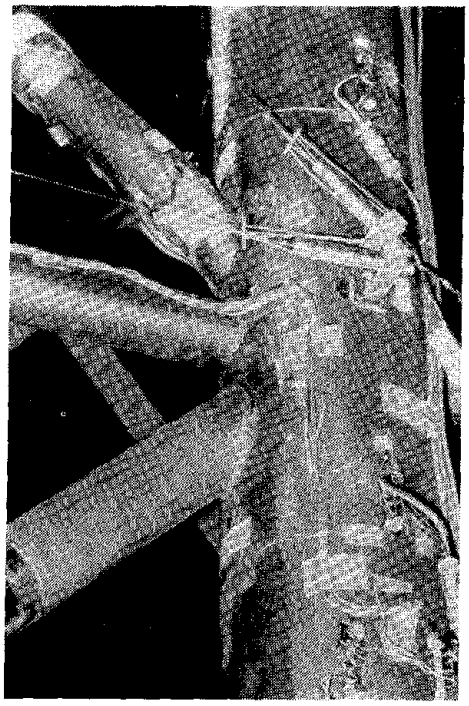

(d) Instrumentation of the Center Joint

Fig. 3.3 Instrumentation of the Test Model.

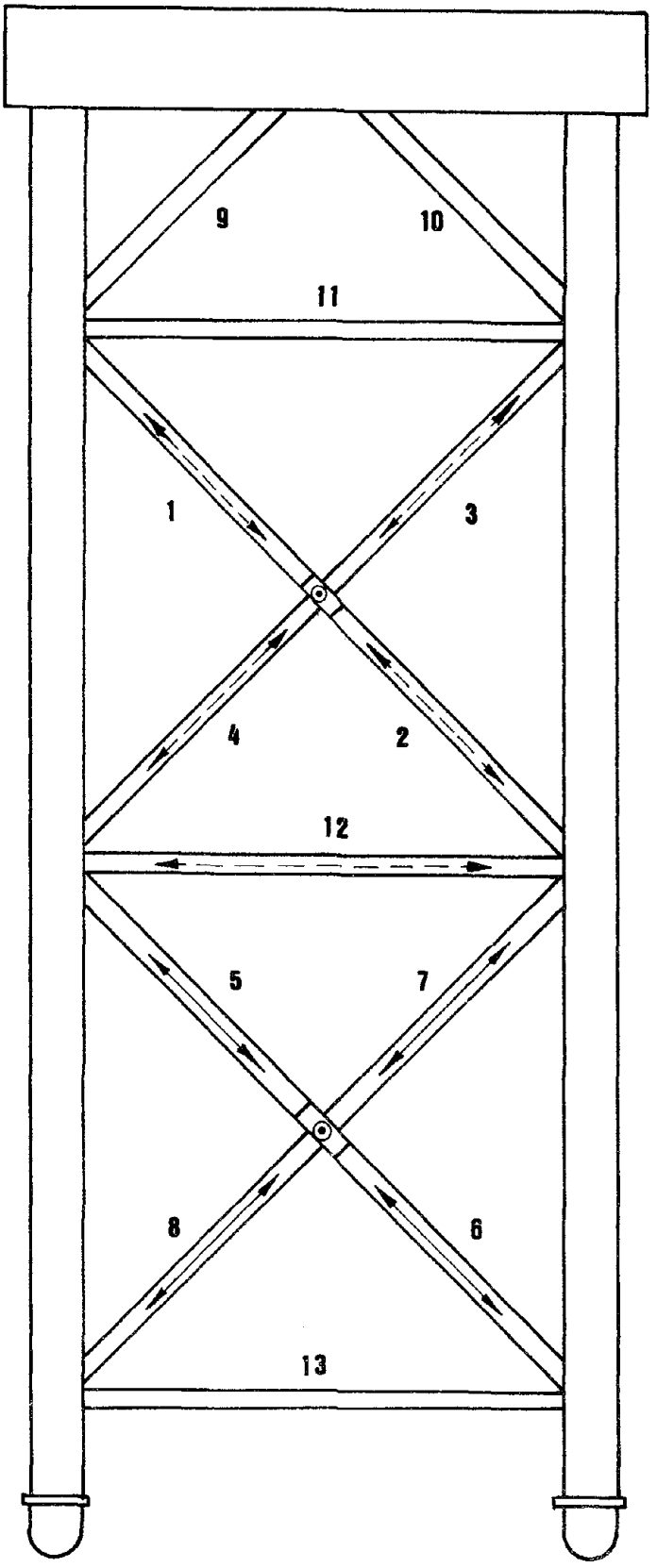

Fig. 3.4 Location of DCDT's Measuring Axial Displacement of the Braces.

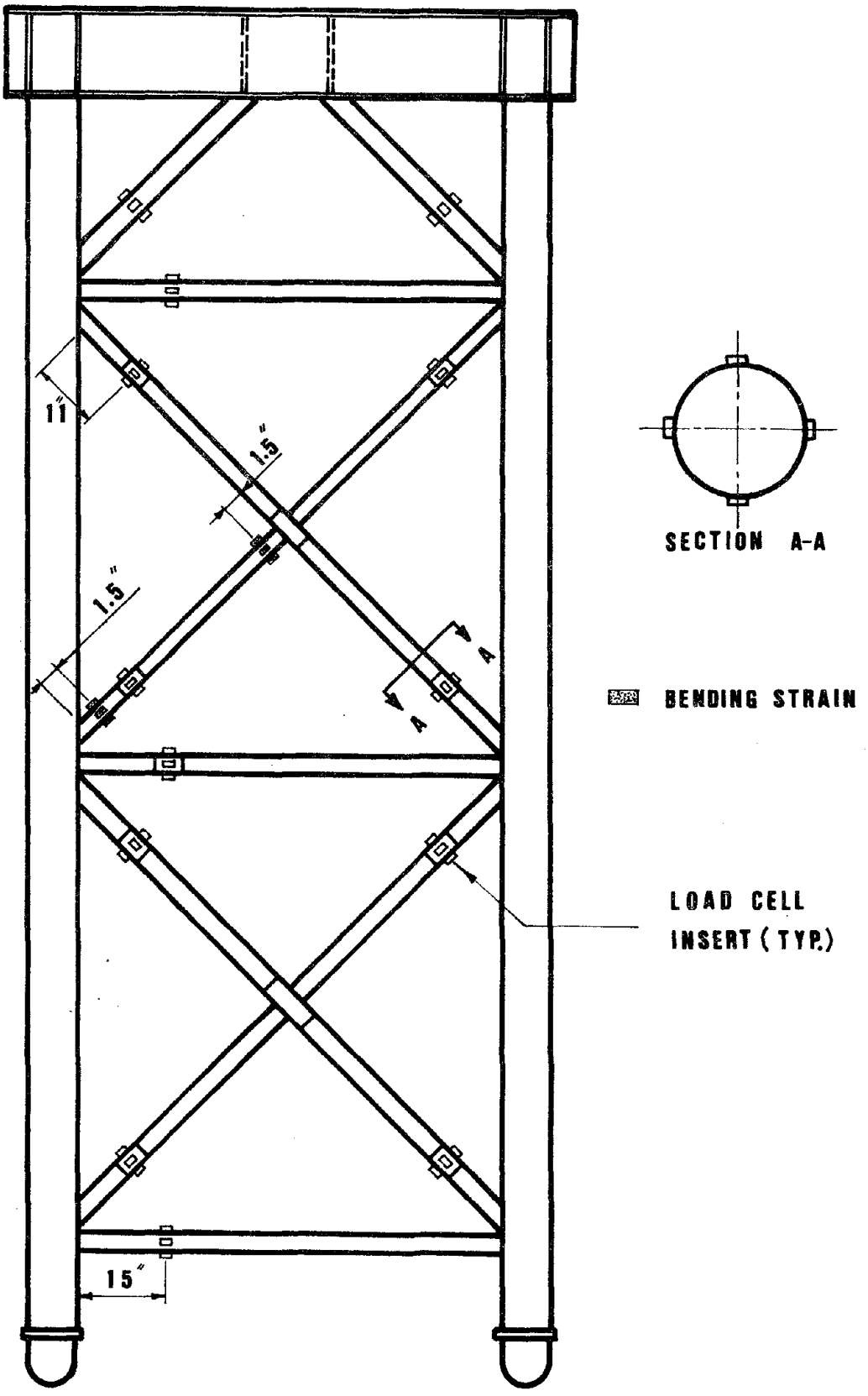

Fig. 3.5 Location of Brace Load Cells and Strain Gages.

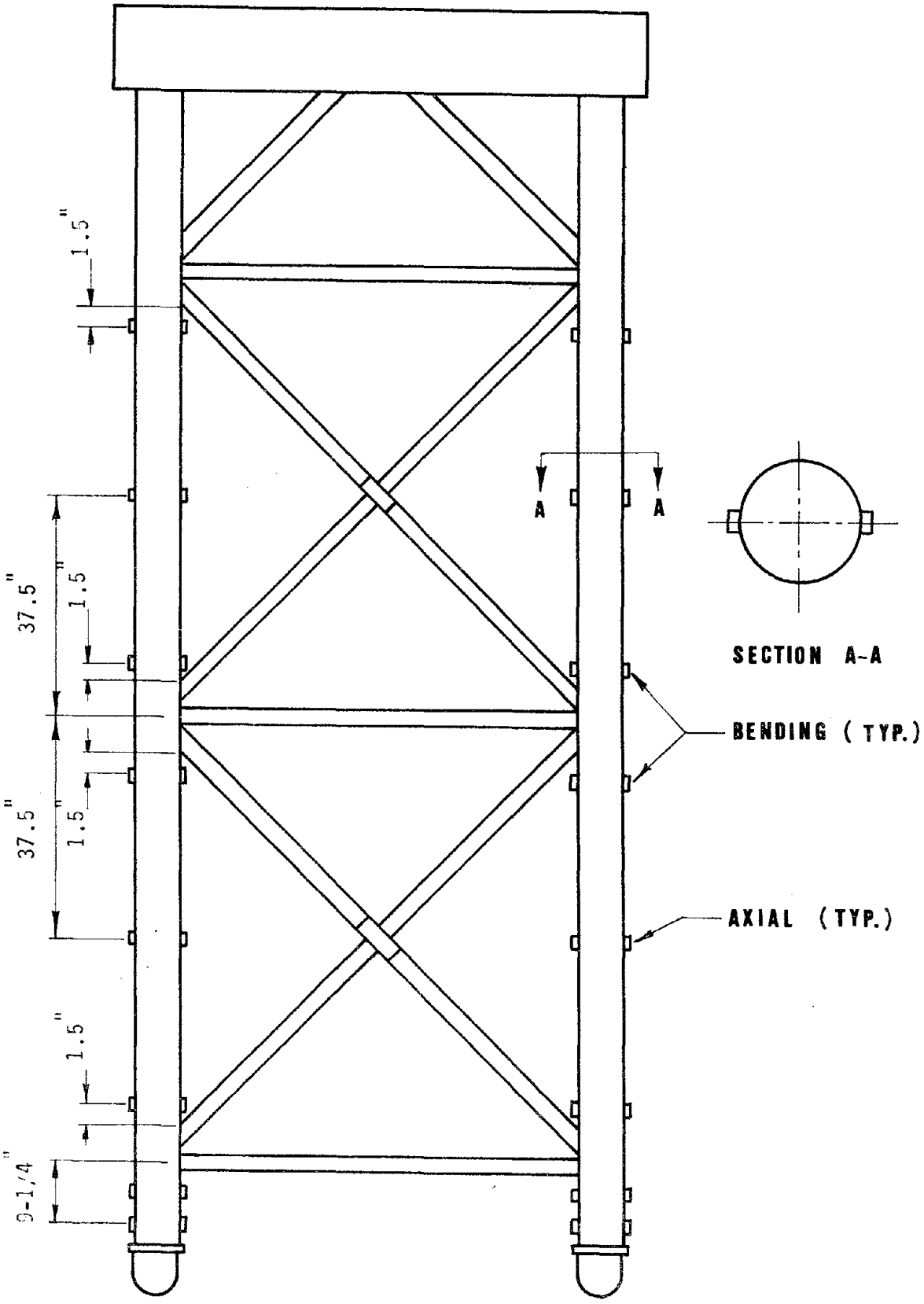

Fig. 3.6 Location of the Jacket Strain Gages.

4. TEST PROGRAM

The test program involved shaking table excitation of the frame model at three earthquake intensity levels: the so-called API "Strength", "Ductility", and "Maximum Credible" earthquake motions. Also, static free vibration tests were made with the original and the damaged frame to evaluate natural frequencies and stiffness degradation of the test model.

4.1 Earthquake Motion

The earthquake motions applied to the test model were scaled signals derived from the S69E Taft component of the 1952 Kern County earthquake, and the S00E El Centro component of the 1940 Imperial Valley earthquake. The API proposed scaled earthquakes, as well as the motions actually applied by the shaking table at various intensities, are listed in Table 4.1. It is important to note that the long period components were filtered out of the actual earthquake records so that relatively high acceleration intensities could be achieved without exceeding the displacement limits of the table.

To produce inelastic behavior in the test frame, the signals suggested by API were these El Centro and Taft motions scaled in two stages. First, the basic El Centro and Taft earthquakes were scaled to approximate the API Ductility-Level earthquake spectrum for seismic Zone 4 and soil type C for the prototype structure. In this stage the basic motions were scaled to a peak ground acceleration of about 0.5 g and a peak ground velocity of 25 to 30 in./sec. (see Columns 1 and 2 in Table 4.1). Then, the intensity scaled motions of the prototype structure were time scaled appropriately for the 5/48 size test model. To produce the elastic strength level tests, these ductility-level motions were reduced by one-half.

Also, to investigate the frame behavior subjected to extreme destructive earthquakes, the basic motions were intensity scaled first to provide a prototype input acceleration of 1.0 g, and a peak velocity of 4 fps; then the time scaling was adjusted for the test model according to the similitude factors.

Table 4.1 shows that the scaled earthquake motions produced at the Earthquake Simulator Laboratory of the University of California, Berkeley, exceed the API specified acceleration values, but are quite low with regard to peak API displacement values. This is the consequence of filtering out the long period components of the earthquake record, but is thought to have had little effect on the observed damage behavior.

4.2 Sequence of Test Runs

A total of ten earthquake excitation tests were performed with the model on the shaking table, but only the seven tests shown in Table 4.2 are considered significant. The other three tests had very low intensities and served only to check out the instrumentation. The factors indicated before the name of each signal represent the time scaling, i.e., the factors by which the basic signals were speeded up. The "Span Setting" indicates the control console dial setting that governs the amplitude of the input displacements.

The low intensity El Centro and Taft earthquakes with a peak acceleration of about 0.28 g were the first two significant tests performed; these were intended to indicate which motion had the greater effect on the test structure at the linear elastic response level. Following these two tests was the Taft Span 180 Test, chosen to cause inelastic response equivalent to the API Ductility-Level. The peak table acceleration and displacement during this test was 0.58 g and 0.854 in. (2.17 cm), respectively. Next, the intensity of the Taft signal was further increased to a peak acceleration of

1.23 g and a peak displacement of 1.689 in. (4.29 cm) for the purpose of evaluating the survivability of the offshore frame subjected to a maximum credible destructive earthquake.

Then two identical low intensity tests essentially equivalent to the original El Centro signal were performed. These served to demonstrate the effects of stiffness deterioration of the test frame resulting from damage in previous tests, and to investigate whether such deterioration continued. Finally an intense Taft signal, essentially equivalent to the previous maximum test, was applied to evaluate the ability of the damaged frame to survive a major aftershock.

4.3 Frequency Measurement

The fundamental natural frequencies of the test model were evaluated by vibration tests performed before and after completion of the dynamic tests. The measured frequencies and corresponding vibration decay provide useful information about the stiffness degradation associated with the structural damage and the resulting changes in modal damping. The two methods used to measure the natural frequencies are described here.

The basic vibration test was carried out by blocking the shaking table so that it would not move, and then pulling the test model at the platform level with a static load applied through a cable. The response resulting from suddenly releasing the load was monitored by an accelerometer mounted on the platform of the test model and the response signal was input to a spectrum analyzer; the natural frequencies were indicated by the sharp peaks in the plotted spectrum. As a check, the same response data were also processed by a Fast Fourier Transform program available on the NOVA mini computer that controls the earthquake simulator. The natural frequencies again were evident on the resulting spectrum plots.

In addition, frequencies of the test model were determined at the end of each dynamic test by feeding the response decay portion of the deck acceleration record to the spectrum analyzer, after the table motion had terminated. Frequencies measured under this condition are the real frequencies of the test model on the actual "soft" foundation provided by the shaking table. This soft condition results from the shaking table hydraulic actuators, passive stabilizers, and air cushion, and tends to reduce the natural frequencies of the test model as compared with the blocked foundation condition that existed in the snap tests. Results of all frequency measurements are presented in Chapter 5.

TABLE 4.1

API PROPOSED AND ACTUAL SHAKING TABLE EARTHQUAKE MOTIONS

API Seismic Zone 4 Soil Type C 5% Damping	Earthquake Signals	Prototype		5/48 Scale Model				
		Acc. Factor	Time Factor	Acc. Factor	Time Factor	Max. Acc. (cm/sec^2)	Max. Vel. (cm/sec)	Max. Displ. (cm)
API Strength Level	El Centro Taft	0.75 1.44	1.3 1.5	0.75 1.44	0.42* 0.48	256 253	10.5 12.2	1.44 3.05
Shaking Table Strength Level	El Centro Taft	0.81 1.54	1.3 1.5	0.81 1.54	0.42 0.48	276.4 270.5	~	0.59 1.08
API Ductility Level; 0.5 g, 25-30 in./sec	El Centro Taft	1.5 2.88	1.3 1.5	1.5 2.88	0.42 0.48	512 506	21.0 24.4	2.88 6.10
Shaking Table Ductility Level	Taft	3.24	1.5	3.24	0.48	569.4	~	2.17
API Max. Credible 1.0 g, 4 fps	El Centro Taft	2.87 5.57	1.27 1.23	2.87 5.57	0.41 0.40	980 980	39.3 39.3	5.26 8.13
Shaking Table Max. Credible	Taft	6.84	1.5	6.84	0.48	1203.4	~	4.29

* $0.42 = 1.3 \sqrt{5/48}$

TABLE 4.2

TEST SEQUENCE

Test No.	Earthquake Signal	Max Acc (g)	Max Displacement in. (cm)
1	2.38 * El Centro Span 50	0.282	0.234 (0.59)
2	2.08 * Taft Span 90	0.276	0.426 (1.08)
3	2.08 * Taft Span 180	0.581	0.854 (2.17)
4	2.08 * Taft Span 360 I	1.228	1.689 (4.29)
5	2.38 * El Centro Span 50	0.288	0.241 (0.61)
6	2.38 * El Centro Span 50	0.288	0.239 (0.61)
7	2.08 * Taft Span 360 II	1.241	1.693 (4.30)

5. EXPERIMENTAL RESULTS

In performing the shaking table tests, the test model described in Chapter 2 was loaded by 9 concrete blocks attached to the 6 x 20 ft steel platform bolted to the deck module of the frame. The total superimposed dead weight was 40.4 kips, 6.3 percent larger than the 38 kip load suggested by API. The measured natural frequencies of the frame with this load, as well as the dynamic response behavior of the test structure subjected to shaking table motions applied with three different intensity levels, are presented and described in this chapter.

Following a discussion of the measured natural frequencies and of the pitching interaction motion of the shaking table in Sections 5.1 and 5.2, the global response behavior of the structure observed in various tests is described in Sections 5.3 to 5.7. Data presented for each test includes time history plots of the table motions and of the relative displacements and shear forces developed in the frame together with hysteresis plots of these shear force-displacement results. Extreme values of the various response quantities are tabulated, and comments are made on the amount of stiffness degradation and other damage effects noted in each test.

The next sections of the chapter (5.8 to 5.10) present data on the local behavior of the frame as indicated by force and deformation histories of selected brace members as well as by the corresponding member hysteresis loops. Also included in the local response data are tables of the maximum forces measured in obvious members.

5.1 Natural Frequencies

The fundamental natural frequencies of the model structure measured at various stages of the test program are listed in Table 5.1. The first

frequency measurement was obtained by applying a "snap" test at the deck level, while the shaking table was resting on its support jacks and blocked against any movements. The frequency measured with this fixed foundation was 2.75 Hz, corresponding to a lateral stiffness of 31.2 kips/in. This stiffness matches within 2% the scaled stiffness calculated from Popov's test Frame I (5/8 x 51 = 31.8 kips/in.). The modal damping ratio obtained from the free-vibration response was 1.5% of critical.

Frequencies of the test model measured from the response decay portion of the deck acceleration in the first "strength level" dynamic tests 1 and 2 are listed next. The first mode frequency determined in this way was 2.125 Hz., which indicates a significant reduction (23%) with respect to the frequency obtained with the fixed foundation. As was mentioned earlier, this discrepancy is due to the shaking table - structure interaction. The table-structure interaction mechanism is very complex and varies with the type of structure on the table as well as with the intensity of input motion.

The first and second mode natural frequencies of the test model measured in the final strength level tests were 1.875 and 5.50 Hz, respectively. This 12% reduction of first mode frequency with respect to that obtained in original strength level tests, was due to the damage that occurred during application of the "maximum credible" motion. It is interesting that the second mode frequency was unchanged,indicating that distortions excited in this mode were concentrated in the undamaged portions of the frame. The modal damping ratio obtained in the final strength level tests was 2.53% of critical; showing that the damaged structure absorbs more energy due to continued local yielding in the damage zones.

5.2 Table Pitching-Motion

The 20-ft square shaking table is driven vertically by four 20 kip hydraulic actuators. The support of the shaking table provided by these active actuators, as well as the passive vertical stabilizer units and the air cushion beneath the table, has significant flexibility. Therefore it cannot completely constrain the overturning forces induced during severe seismic tests with the result that the table has a tendency to pitch. The pitching motion of the table is very complex, but in general it varies with the weight and stiffness of the structure installed on the table and with the intensity of input signals.

The test model with its superimposed weight of 40.4 kips located 21.5 ft above the table, represented a top heavy, low frequency structure which exerted very large overturning moments on the table and therefore had significant interaction with it. The acceleration time histories of the resulting pitching motion caused by table-structure interaction during tests 1 to 4 are depicted in Fig. 5.1. As these time histories indicate, the pitch acceleration is nonlinear in nature with the pitching peaks changing drastically with the intensity of the input signal. However, the results of all tests are generally similar in appearance; that is, all of them represent a high frequency signal superimposed on a lower frequency response component that is similar to the acceleration of the test frame deck. (Compare for example the pitch acceleration for El Centro Span 50 with the shear time histories shown in Fig. 5.5.)

One of the principal objectives of this experiment was to provide actual response data which could be used in computer correlations to verify the accuracy of available analysis techniques. To formulate a successful analytical model capable of predicting the experimental results, the

table-structure interaction must be accounted for. Two analytical models that might be used for representing such interaction are described here.

Model 1 - In this approach, both the horizontal and the pitch motions measured from the table are included as input signals applied to the test model. To include the pitching motion, one can either specify angular pitch acceleration directly, or transfer the pitch acceleration into equivalent vertical couple accelerations applied at the base nodes. Although this approach seems simple, in principle, it has the basic shortcoming that most available computer programs are capable of dealing only with translational input ground motions.

Model 2 - In this model, the interaction of the shaking table in the dynamic response analysis is accounted for by providing vertical spring supports under the table to simulate the oil column flexibility of the hydraulic actuators, while the table input motion is defined as simple translation. The table itself, with a rotational mass of 1245 kips-sec-in., is modeled as a rigid beam connected between two base nodes of the test frame and is allowed to rotate freely on these spring supports. The required stiffness of the spring supports depends on the type of structure and the intensity of input ground motion, and is determined by frequency analysis of the table-structure mathematical model, treating it as the unknown parameter. In this process, the stiffness properties of the test model determined from a fixed base test are kept unchanged. Then, by varying the stiffness of support springs, a trial and error procedure is used until a close match is obtained between the frequency of the analytical model and that of the actual structure observed during the dynamic tests. This type of model, shown in Fig. 5.2, has been used successfully in several previous studies[14,15,16,17].

5.3 Global Response to "Strength Level" Input

In the strength level tests, the larger horizontal component of the El Centro and Taft earthquake signals was applied to the test model with a peak acceleration of 0.28 g. These shaking table motions had a peak acceleration 12% higher than the API strength level requirement (0.25 g), but they caused only essentially elastic structural response with the x-brace members of the upper panel stressed just to the yield point. The yielding of these braces was minor and was limited to critical regions near the jacket connections. The maximum brace member loads calculated from the load cell strain data, extreme values of the total frame loads, and peak accelerations and displacements of the deck for each dynamic test are given in Table 5.2.

The overall dynamic response of the test model and table motions are graphically displayed in Figs. 5.3 to 5.8. Table motion data in Figs. 5.3 and 5.4 depict the acceleration and displacement time histories, along with the corresponding response spectra for the El Centro and Taft motion, respectively. The response spectra were obtained for five damping ratios using a program developed by Nigam and Jennings[18].

The time histories of deck displacement and of gross shear obtained from the deck acceleration, shown in Figs. 5.5 and 5.6 for the two earthquakes indicate a dominant first mode vibration as was expected. They also, particularly in the Taft test, present a peculiar large amplitude response after the 6th second of motion which does not correspond to any significant large input horizontal acceleration. It is believed that this behavior is due to the table-structure interaction mechanism as can be observed in the corresponding table pitch accelerations in Fig. 5.1.

Hysteresis loops of the gross frame shear versus deck displacement presented in intervals of four seconds, are shown in Figs. 5.5 and 5.8.

During the El Centro test (Fig. 5.7), the force-displacement relation remained essentially linear, except for the first four seconds of the response when local yielding of the upper x-braces was initiated. Clearly, these hysteresis loops do not indicate any stiffness degradation; the stiffness measured during the linear response of the last four seconds was 17.44 kips/in.

Hysteresis load-displacement loops of the Taft test (Fig. 5.8) performed after the El Centro motion, are also narrow and indicate only minor nonlinear behavior; but the load at which yielding of the braces was initiated was lower. The stiffness of the frame measured in the last four second portion of the response for this test also was 17.44 kips/in. Thus, the local yielding of braces that occurred in the stress concentration region near the jacket joints was not severe enough to produce global stiffness deterioration in the frame.

5.4 Global Response to "Ductility Level" Input

After the strength level tests, the Taft Span 180 earthquake motion was applied to the test model with a peak acceleration of 0.58 g (two times the strength level test). The general response of the frame in this test resembled that of the Taft Span 90 Test with no visible brace buckling. The compression and tension yielding of x-braces in the upper panel continued, but energy dissipation of the frame was not significant. The results of this test are depicted in Figs. 5.9 to Fig. 5.11, with the table motions (Fig. 5.9) in the same format as for the strength level tests. The time histories of the deck displacement and frame shear load (Fig. 5.10) similarly to the previous Taft test, indicate a dominant first mode vibration with significant table-structure interaction. Also, a reduction in response frequency due to brace yielding is evident, especially in the 4 to 6 second portion of the response (compare Fig. 5.10 with Fig. 5.6). The maximum deck displacement during this test reached 1.18 in. which is twice the amplitude in the previous Taft strength

level test, but the frame load was magnified only 1.7 times.

The force-displacement hysteresis loops, shown in Fig. 5.11, exhibit only three relatively open loops, indicating only a small amount of energy dissipation during this rather intense test. The stiffness of the frame measured during the final portion of the response was 15.34 kips/in. This 12% stiffness reduction with respect to the previous tests demonstrates that some damage was incurred, but with no significant loss in structural integrity.

The maximum average transverse acceleration measured at the deck level was 0.023 g, corresponding to a 930 lb transverse frame load. Of course this lateral load was resisted by the test fixture, and is not significant in the test frame responses.

5.5 Global Response to "Maximum Credible" Input

The "maximum credible" earthquake motion applied to the test model was the Taft Span 360 signal having a peak table acceleration of 1.228 g and peak table displacement of 1.689 in. (Fig. 5.12). The application of this very strong table motion caused major inelastic frame response with significant compression buckling and tension yielding in the upper panel x-braces. The buckling, which occurred in the out-of-plane direction, was observed in braces 2 and 4; that is, in the lower segment of the x-braces.

A graphical display of the results from this test is presented in Figs. 5.13 and 5.14 in the same sequence as those of the earlier tests. The maximum frame shear force and relative deck displacement were 28.52 kips and 2.42 in., respectively. The time histories of these quantities (Fig. 5.13) show that a significant portion of the nonlinear frame response took place during the first 6.5 seconds of the test, while the larger amplitudes of the input acceleration were being applied. Overall force-displacement hysteresis loops of the test frame during intervals of 4 seconds are shown in Fig. 5.14. The hysteresis loops

in the upper left graph clearly show when the initial buckling of the x-braces occurred. The first buckling occurred in brace 2 when the table acceleration reached its first peak at time 2.18 seconds. No buckling occurred during the next two response cycles, but as the table acceleration reached another peak at 3.38 seconds, significant buckling developed again in brace 4. After these initial bucklings, braces 2 and 4 went through three more cycles of compression buckling and tension yielding. During the last eight seconds, the response of the frame was linear, and the stiffness of the frame calculated from the slope of the hysteresis loops was 11.25 kips/in., only 73% of the stiffness calculated at the end of the previous test. The overall stiffness reduction with respect to original elastic stiffness was 36%.

5.6 Post-Damage Global Strength Level Response

The maximum credible test (Test 4 TAFT-360 I) was followed by two tests using the same strength level El Centro Earthquake signal used earlier. The purpose of these tests was to assess the effect of stiffness degradation of the test frame due to the damage caused in the previous tests. The table motion and overall response of the test frame during the first of these repeat tests (having a peak acceleration of 0.288 g) are shown in Figs. 5.15 to 5.17. Time histories of the frame load and deck displacement (Fig. 5.16) differ noticeably from those of the initial strength level test (Fig. 5.4) and their lower response frequency indicates the substantial stiffness loss from the condition during the previous tests. The maximum resulting frame load was only 6.34 kips, only 52% of that obtained in the initial strength level test. Thus it is evident that the damage has reduced the strength demanded of the frame. The load imposed on the upper panel x-braces is seen in Table 5.2 to be only 2.26 kips, compared to the 6.55 kips developed in the previous strength level test. Hysteresis loops of the frame load versus deck

displacement (Fig. 5.17) are generally wider compared with the previous test (Fig. 5.7), with some minor pinching during the first four second interval of the response. The stiffness of the test frame determined from the free vibrations at the end of the response is 13.34 kips/in. compared to the 17.44 kip/in. found during the initial strength level test, a stiffness degradation of 24%. However, the stiffness in this test, surprisingly, is higher than the stiffness determined during the maximum credible test (11.25 kips/in.). This difference is believed to have been caused by the table-structure interaction which tends to decrease the natural frequency of the frame response. In the Taft Span 360 test, the table pitching was relatively more severe compared to the pitching observed in the El Centro Span 50 test (see Fig. 5.1).

The results of the second post-damage strength level test, are shown in Figs. 5.18 to 5.20. These resemble the results of the preceding test except that the pinching of the force-displacement hysteresis loop is slightly more pronounced, suggesting a slight addition to the damage state. However, the measured frame stiffness was 13.10 kips/in. which shows that the additional stiffness degradation was only 1.8%.

5.7 Global Response to Second "Maximum Credible" Input

In order to study further how the damaged structure responded to dynamic excitation, and also to evaluate its ability to withstand a major aftershock, the same earthquake input applied in Test No. 4 (TAFT 360 I) was applied again. The table displacement and acceleration, shown in Fig. 5.21, clearly were essentially identical to the previous test input (Fig. 5.12), so comparison of the response data from the two tests demonstrates the effects of the damage caused during Test No. 4.

The most explicit comparison is given by the global shear force and displacement histories. It is evident from the plots of Fig. 5.22, showing the

response of the damaged structure, that the damage has induced some important changes from the corresponding previous graphs of Fig. 5.13, although the general character of the response is similar to the earlier test. Specifically, it may be noted that the amplitude of shear force has been reduced somewhat by the damage, while the displacements were increased; also the response frequency was slightly reduced. All of these effects are consistent with a loss of stiffness due to brace damage.

Comparison of the new shear force-displacement hysteresis loops of Fig. 5.23 with the previous results in Fig. 5.14 also supports this conclusion, especially the reduced force amplitude shown during 0-4 seconds and the broader loops during 4-8 seconds. Moreover, the free vibration stiffness during the final four seconds was only 8.45 kip/in., a reduction of 24% from the value observed in Test No. 4.

Further details of the additional damage done during this second maximum credible event is presented in Figs. 5.24 and 5.25. The upper curves of Fig. 5.24 show the time history of shear forces in the upper panel jacket legs, while the lower curves compare the total shear force in the frame with the component resisted by the diagonal braces. These figures clearly show the limited resistance capability of the bracing members, even during the first few seconds of the test. After diagonals 2 and 4 rupture, at about 6 seconds, the entire shear force is resisted by the jacket legs. Of course these shear forces are associated with reverse bending of the upper panel jacket legs, as evidenced by the end moment histories shown in Fig. 5.25.

Detailed evidence of the brace damage observed after this test is shown in the photographs of Fig. 5.26. A general view of the upper panel damage, given in (a), shows the complete rupture of brace 4 and the mid-span crumpling of brace 2. In (b) the damage to brace 2 is shown in close-up view. Careful

examination reveals that this brace also was torn, but did not fail completely. In (c) it may be seen that brace 4 suffered severe buckling damage at the lower end as well as in mid-span. Even though no buckling occurred in the stronger braces provided in the lower panel, photograph (d) shows that significant yielding occurred at the ends of some of the brace members.

The maximum forces measured in all brace members during all tests are listed in Table 5.2, together with the maximum accelerations and displacements measured at the deck level. Also listed in Table 5.2 are the total frame shear forces evaluated from the deck level accelerations. Related response information giving the maximum jacket moments observed at top and bottom panel locations during all tests is listed in Table 5.3. Corresponding maximum dynamic axial forces measured in the jacket legs during all tests are listed in Table 5.4.

5.8 Local Brace Response to "Ductility Level" Input

To give greater insight into the observed damage mechanisms, the preceding comments on the global response behavior will now be supplemented by data concerning the forces and deformations measured in the upper panel brace members, considering in this section the ductility level test which caused the first appreciable damage. Figure 5.27 presents time-history plots of the axial displacements induced in the members. The appearance of the displacement curves for brace 2, with the maximum amplitude portions being "clipped" off the cyclic response variation, suggests that this displacement gage was not performing reliably; however the cause of this problem is not known.

Axial force-displacement hysteresis loops for braces 1, 2, and 4 are presented in Figs. 5.28, 5.29, and 5.30, respectively. These all show significant cyclic yielding in tension and compression, leading to

considerable energy loss during each cycle. It should be noted that the vertical unloading segments in the hysteresis loops for brace 2 are associated with the "clipping" effect mentioned above. They demonstrate instrument malfunction, and do not describe the true brace behavior.

5.9 Local Brace Response to First "Maximum Credible" Input

Figure 5.31 presents the axial displacement records for the four upper panel braces subjected to the first severe damage test. It is interesting to note that brace 4 underwent the greatest deformation, consistent with its observed buckling and ultimate failure. The much smaller deformation of brace 3 shows that the damage was concentrated in the lower half of this complete diagonal member. The 180^{o} out-of-plane response in braces 3 and 4, however, suggest instrumentation malfunction. It seems likely that the pin to which the displacement gages were attached at the intersection joint of the "X" was undergoing significant rotation after about 3 seconds, and this apparent axial displacement due to rotation was being added to (or subtracted from) the actual axial deformation of the bracing members. This effect also may have been responsible for the "clipping" which is apparent in the brace 2 records; these records are similar to the ductility level results described above.

The out-of-plane displacements of the brace intersection joint for the upper panel are plotted in Fig. 5.32; results for the first three tests are presented in the upper curves together with the results for Test 4 shown in the lowest curve. Because displacement is evident even in the least intense motions, it is apparent that some out-of-plane eccentricity was present, however the amplitude of the displacement was not important until Test 4. It is interesting to note the significant residual displacement resulting from Test 4; this was concurrent with the residual axial distortions shown in Fig. 5.31.

Axial force vs axial displacement hysteresis loops are shown for upper panel braces 1, 2, and 4 in Figs. 5.33 to 5.35, respectively. All of these curves have the characteristic shape associated with cyclic tension yielding and compressive buckling. The compressive force is seen to reach its maximum value early in the compressive loading cycle, and then to drop off significantly as the buckling deformation develops. Also, the continuing reduction of the peak force values during successive cycles is apparent, showing the effects of cumulative damage to the brace members. Figure 5.34 shows the distortion resulting from the "clipping" of the brace 2 axial displacement records, and can only be used in a qualitative evaluation of the performance. For similar reasons, the hysteresis loop was not plotted for brace 3, because its out-of-plane character would produce a reverse direction hysteresis loop.

To provide further understanding of the buckling deformation mechanism for brace 4, plots are presented in Figs. 5.36 to 5.39 showing the variation of bending strains at the ends of the member with the axial force. The bending strains were measured by taking the difference between axial strains indicated at opposite sides of the cross-section (see Fig. 3.5). Figure 5.36 shows the strain due to out-of-plane bending at the lower end of the brace (i.e., at the jacket connection) -strain 1, while Fig. 5.37 gives the corresponding results measured at the upper (x-joint) end of the brace -strain 2. It should be noted that the positive strain direction assumed in these plots has been chosen arbitrarily; it has no real significance. However, it is interesting to note that the bending strains correspond quite closely with the axial displacements, as may be seen by comparison with Fig. 5.35. The amplitude of the strains indicated by these post-yield strain gages, listed in Table 5.5, greatly exceeds the yield limit of

this material. The corresponding results for in-plane bending of brace 4 shown in Figs. 5.38 and 5.39, strain 3 and strain 4, respectively, are of interest mainly in verifying that the dominant buckling mechanism was in the out-of-plane direction.

The final set of results from this first significant damage test are presented in Figs. 5.40 to 5.42. These show axial force vs axial displacement hysteresis loops for certain brace members of the lower panel. Because these braces were more than three times stronger than those in the upper panel, they were able to resist these intense lateral frame loads without buckling (see Table 5.2). However, some definite yielding of the brace members is evident in these hysteresis loops.

5.10 Local Brace Response to Second "Maximum Credible" Input

Further details of the damage suffered by the test frame were indicated by the results measured during the second maximum input test (TAFT 360-II). In general, the local member responses observed during this test were similar to those in the first maximum credible event, but because the braces actually ruptured during this test the behavior was modified in some significant details.

Figure 5.43 shows the axial displacement histories measured in the upper panel braces. Comparison with Fig. 5.31 shows generally similar performance, but the "clipping" phenomenon of brace 2 has disappeared (no explanation is available). However, the out-of-phase response of brace 3 relative to brace 4 is still present, and apparently is responsible for the compression direction "clipping" in the record presented for brace 4. It is interesting that no additional "drift" was observed in the axial displacements during this test (compare with Fig. 5.31).

The early history of out-of-plane displacements of the upper panel cross joint, shown in Fig. 5.44, is quite similar to those observed in the earlier tests (Fig. 5.32), except that the amplitude is approximately doubled due to the large residual eccentricity developed during test 4 (TAFT 360-I). Note that the first two curves of Fig. 5.44 were from tests essentially equal to the first curve of Fig. 5.32. The rupture of braces 2 and 4 shows up clearly in the third curve of Fig. 5.44. No out-of-plane displacements could be induced by the ruptured braces.

Similar conclusions concerning the rupture of the braces can be drawn from the axial force-axial displacement hysteresis loops presented in Figs. 5.45 to 5.47 for braces 1, 2, and 4, respectively. All of these curves have a normal appearance until rupture occurred after about 6 seconds.

To complete the record, the plots of out-of-plane and in-plane bending strain measured at the ends of brace 4 are presented in Figs. 5.48 and 5.49 (out-of-plane) and Figs. 5.50 and 5.51 (in-plane). These generally are quite comparable with the results of the Taft 360-I test, shown in Figs. 5.36 to 5.39, up to the time when rupture occurred.

TABLE 5.1

FUNDAMENTAL NATURAL FREQUENCIES

Test ID	1st Mode	2nd Mode
Static Test (table locked)	2.75 Hz	--
Initial-strength level Tests 1 and 2	2.125	5.50
Post-strength level Tests 5 and 6	1.875	5.50

TABLE 5.2

MAXIMUM LOAD OF FRAME AND BRACE MEMBERS

Test No.	Input Signal	Deck Acc. (g)	Deck Displ (in.)	Frame Load (kips)	Brace 1	Brace 2	Brace 3	Brace 4	Brace 5	Brace 6	Brace 7	Brace 8
1	EC 50	0.301	0.804	12.16	-6.65	-6.75	6.55	6.62	-10.46	-10.87	-10.56	10.81
2	TAFT 90	0.234	0.595	9.45	-5.53	-5.61	5.29	5.31	- 8.07	- 8.28	8.01	8.24
3	TAFT 180	0.398	1.180	16.08	-7.85	-7.95	7.39	7.39	-13.72	-14.17	13.88	4.10
4	TAFT 360 I	0.706	2.419	28.52	-8.98	-9.17	8.51	8.86	23.71	22.88	-24.08	-24.56
5	EC 50	0.157	0.517	6.34	2.15	2.27	2.29	2.34	- 6.36	- 6.46	6.16	6.21
6	EC 50	0.158	0.511	6.42	2.11							
7	TAFT 360 II	0.595	3.319	24.04	7.00	7.28	7.43	7.63	-24.73	-25.32	-25.29	-25.63

$\overline{P}_y$ = 6.95 kips Brace 1 to 4.

$\overline{P}_y$ = 24.35 kips Brace 5 to 8.

TABLE 5.3

MAXIMUM BENDING MOMENTS OF THE FRAME JACKETS AT LOCATIONS SHOWN IN FIG. 3.6

Test No.	Input Signal	Top-End UPJ1	Bottom-End UPJ1	Top-End UPJ2	Bottom-End UPJ2	Top-End LPJ1	Bottom-End LPJ1	Top-End LPJ2	Bottom-End LPJ2	Top-End BPJ1	Top-End BPJ2
1	EC 50	-33.004	-39.175	-33.809	-36.760	48.298	93.645	46.152	85.059	-97.938	-94.450
2	TAFT 90	-22.539	-24.149	-15.294	-22.539	29.516	72.716	28.979	68.423	-76.204	-72.447
3	TAFT 180	-77.277	-79.961	-73.252	-76.472	91.230	123.429	88.547	-110.818	-127.990	-117.526
4	TAFT 360 I	-232.905	194.803	-201.243	194.803	217.342	194.535	-227.270	-183.534	-189.168	-159.116
5	EC 50	-56.348	-55.275	-56.080	-53.933	58.495	44.273	58.763	-44.005	-53.128	48.835
6	EC 50	-58.763	54.738	54.470	-52.592	57.690	43.468	57.421	-47.762	-50.445	47.762
7	TAFT 360 II		323.062	332.722	-317.964	-395.241	-150.261	-355.529	-149.456	-194.803	164.483

$S = 9.065\ in.^3$ Section Modulus

$\sigma_y = 48$ ksi

$M_y = \sigma_y S = 435.15$ kips-in.

TABLE 5.4

MAXIMUM DYNAMIC AXIAL FORCES OF THE JACKET LEGS AT THE LOCATIONS SHOWN IN FIG. 3.6 (kips)

Test No.	Input Signal	UPJ1	UPJ2	LPJ1	LPJ2	BPJ1	BPJ2
1	EC 50	20.842	-20.701	32.248	-31.544	41.120	42.669
2	TAFT 90	17.462	-17.180	25.770	-25.489	33.234	34.501
3	TAFT 180	29.291	-28.164	42.669	-41.543	52.104	56.188
4	TAFT 360 I	43.514	42.669	63.229	64.356	65.905	85.338
5	EC 50	11.266	-11.688	15.913	15.490	19.856	22.250
6	EC 50	10.984	-11.266	15.631	-15.350	19.997	21.827
7	TAFT 360 II	35.769	36.755	56.892	57.033	59.709	69.285

$A = \pi t(D-t) = \pi(.194)(8-.194) = 4.7575$ in^2, E = 29,600 ksi.

$P_y = \sigma_y A = 48 \times 4.7575 = 228.361$ kips.

TABLE 5.5

MAXIMUM BENDING STRAINS MEASURED AT LOCATIONS 1, 2, 3, AND 4 IN BRACE 4 (milli in./in.)

Test No.	Input Signal	Bending Strain 1	Bending Strain 2	Bending Strain 3	Bending Strain 4
1	EC 50	-0.305	0.789	-0.148	-0.182
2	TAFT 90	-0.079	0.207	-0.111	-0.074
3	TAFT 180	-3.318	1.173	-0.351	0.484
4	TAFT 360 I	-10.676	5.285	-8.420	-15.616
5	EC 50	0.303	0.646	-0.208	-0.408
6	EC 50	0.283	0.606	-0.227	-0.385
7	TAFT 360 II	3.423	-10.396	-2.350	-3.800

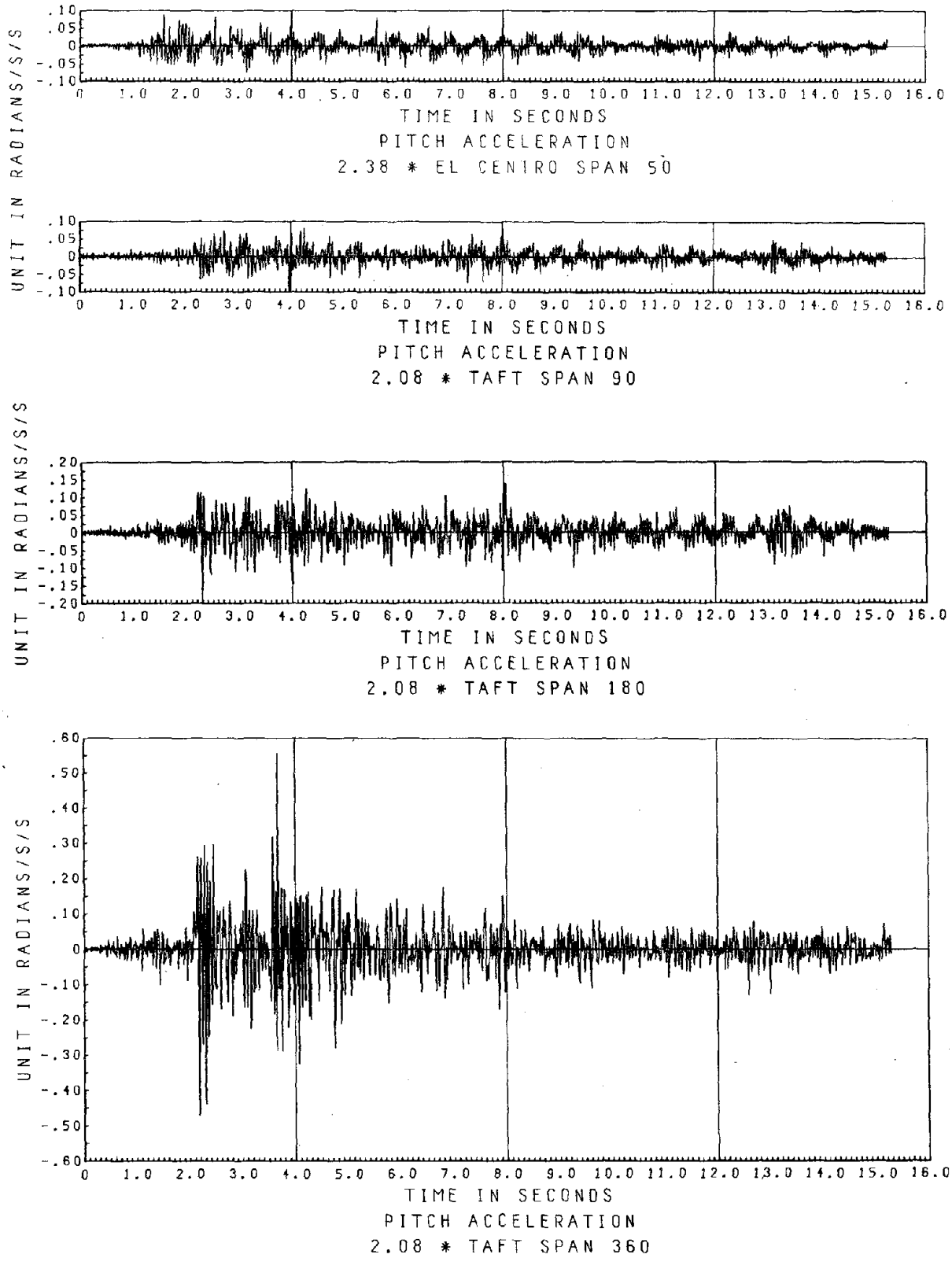

Fig. 5.1 Table Pitch Acceleration Time Histories.

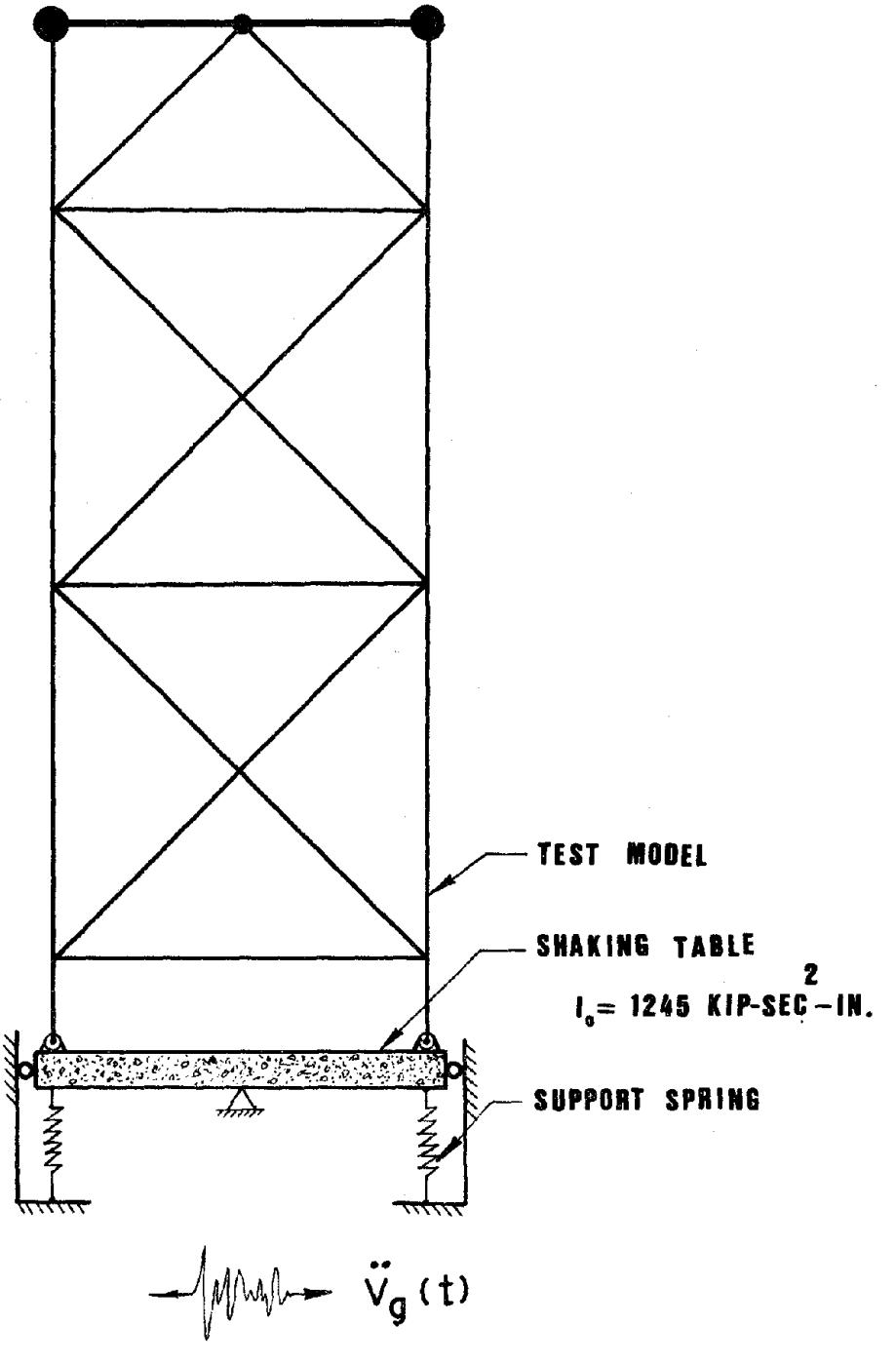

Fig. 5.2 Mathematical Model including Table Interaction

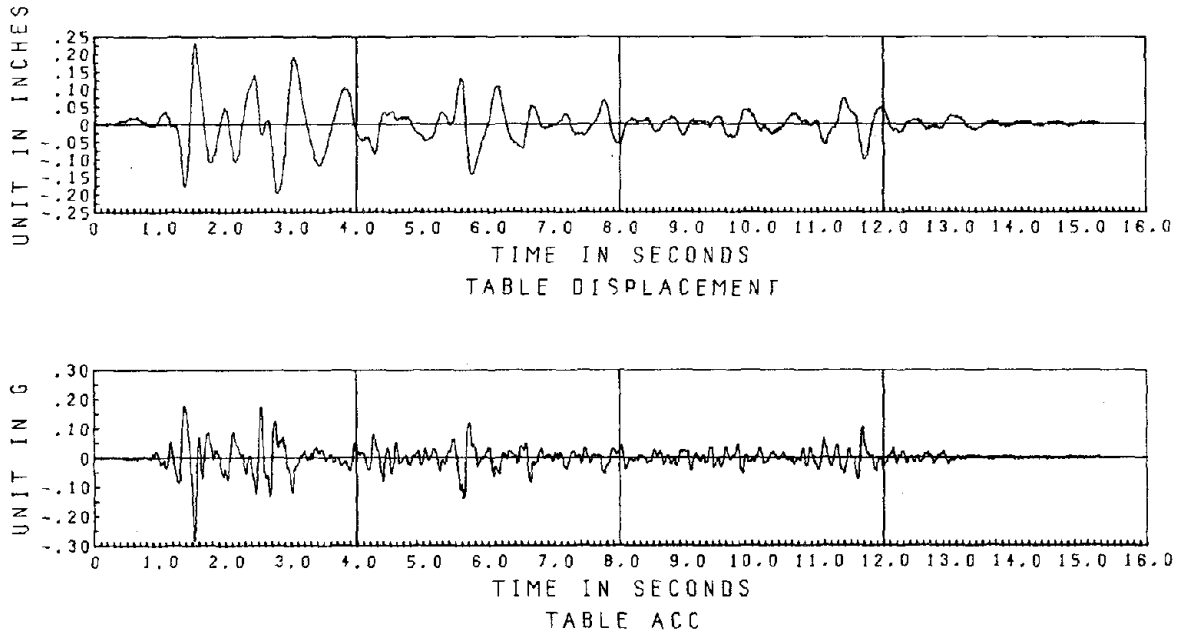

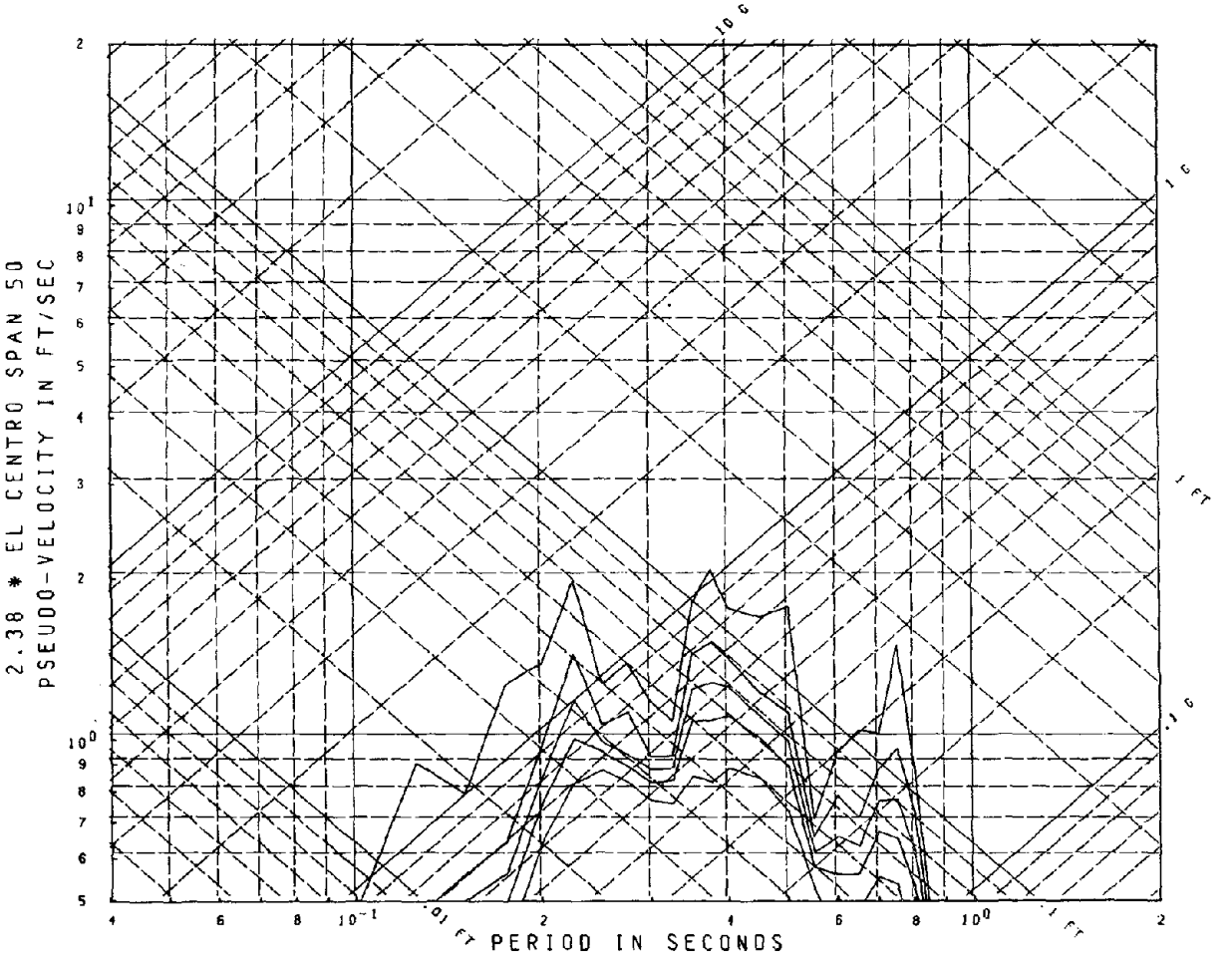

Damping Ratios: 0.0, 0.01, 0.02, 0.03, 0.05

Fig. 5.3 2.38 * El Centro Span 50 Horizontal Table Motion.

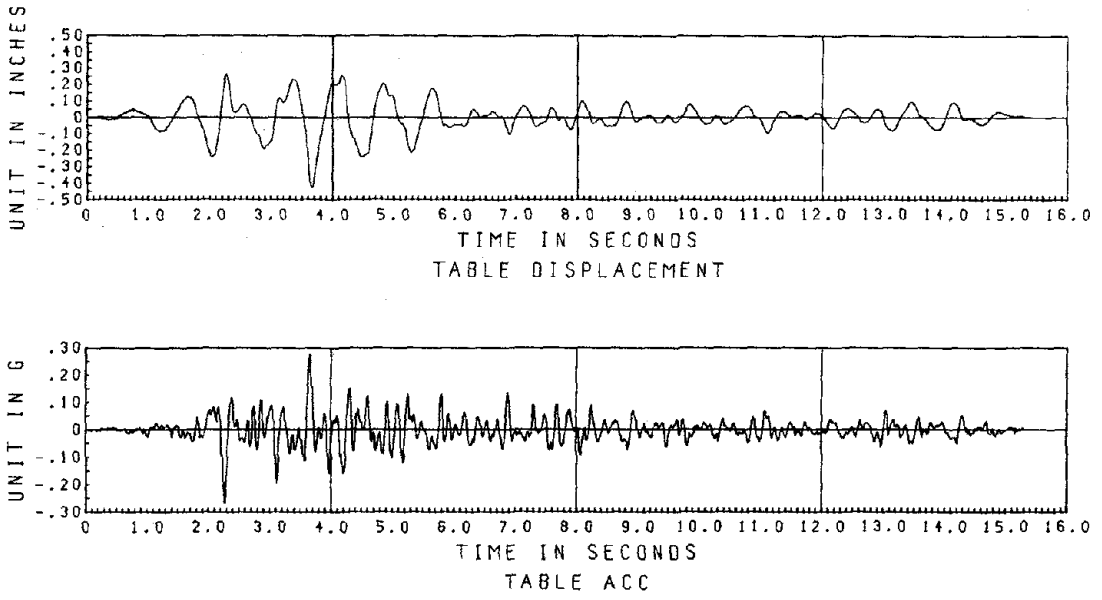

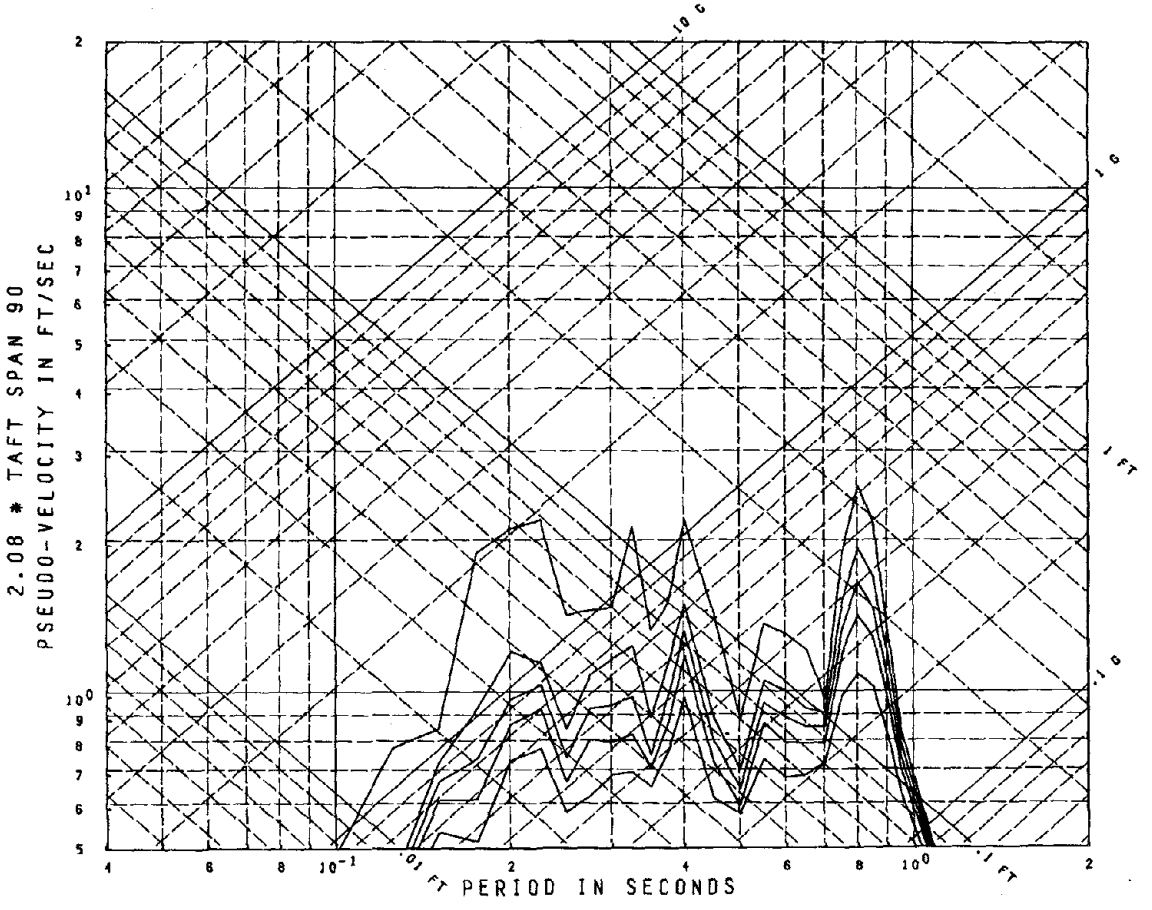

Damping Ratios: 0.0, 0.01, 0.02, 0.03, 0.05

Fig. 5.4 2.08 * Taft Span 90 Horizontal Table Motion.

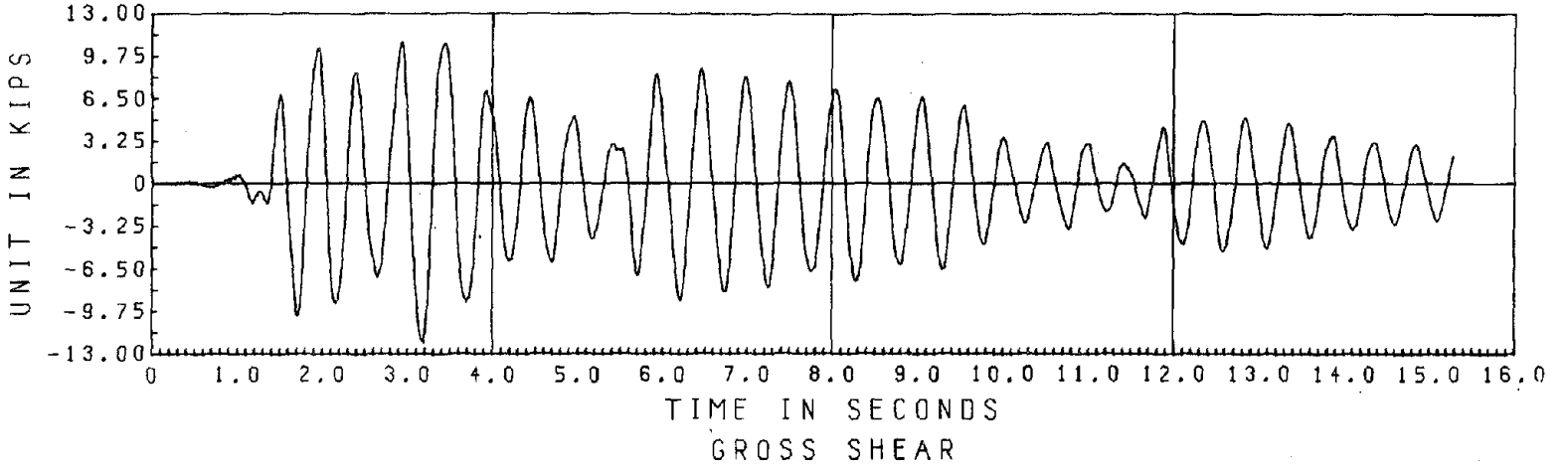

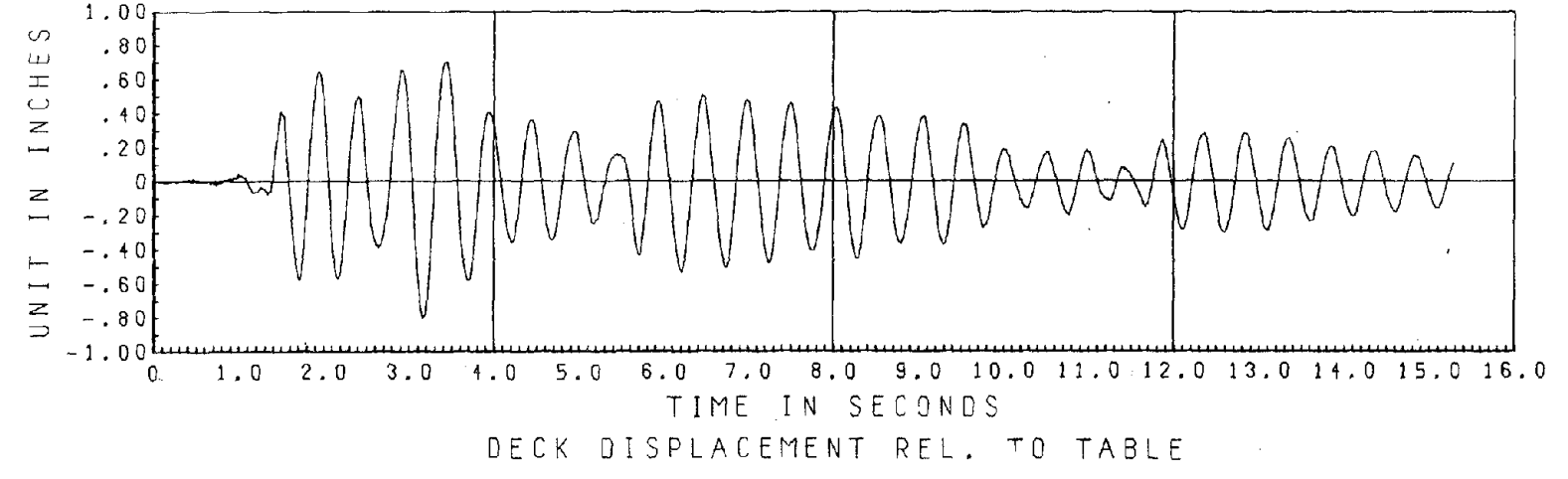

2.38 * EL CENTRO SPAN 50

Fig. 5.5 Time History of Gross Shear and of Deck Displacement.

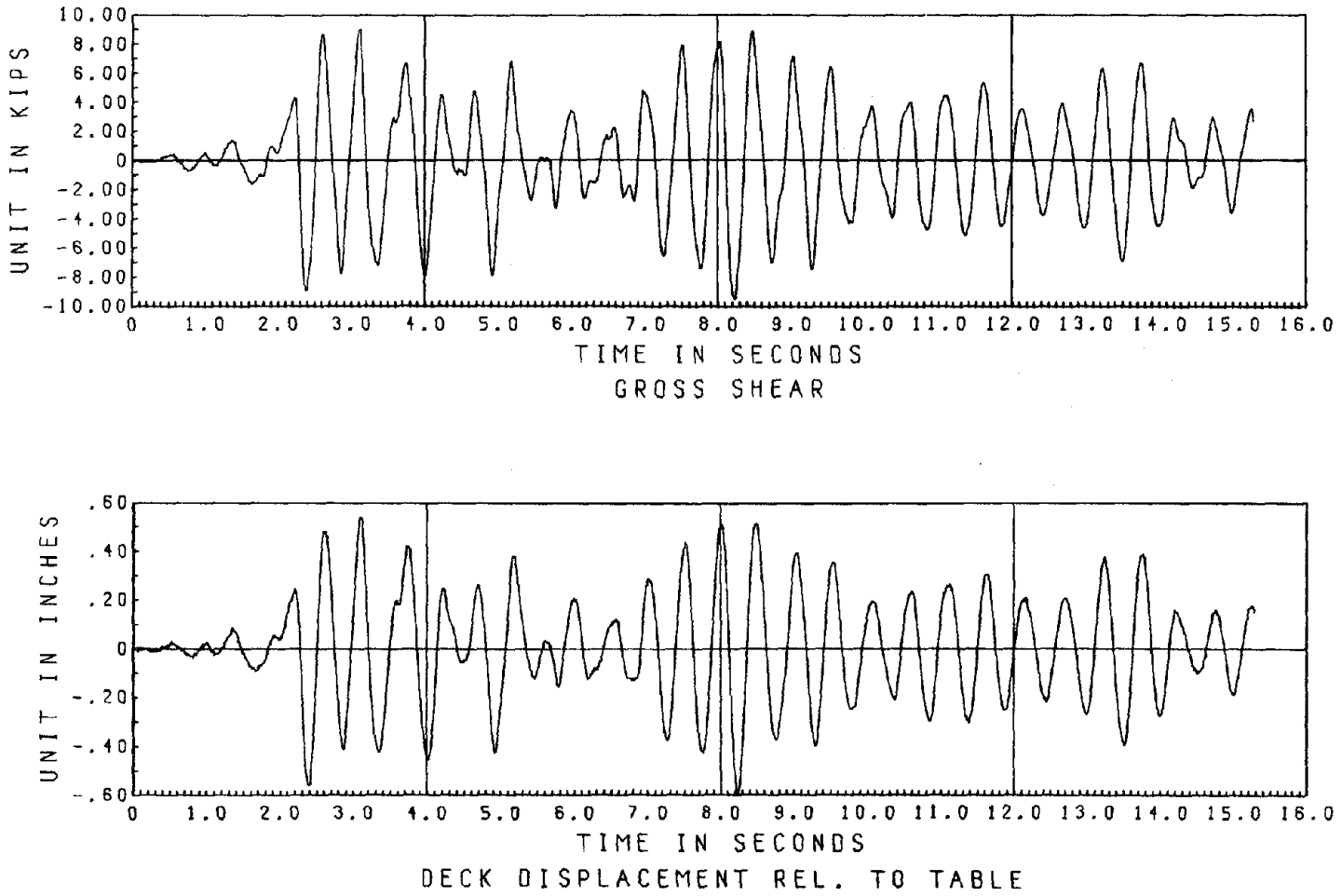

Fig. 5.6 Time History of Gross Shear and of Deck Displacement.

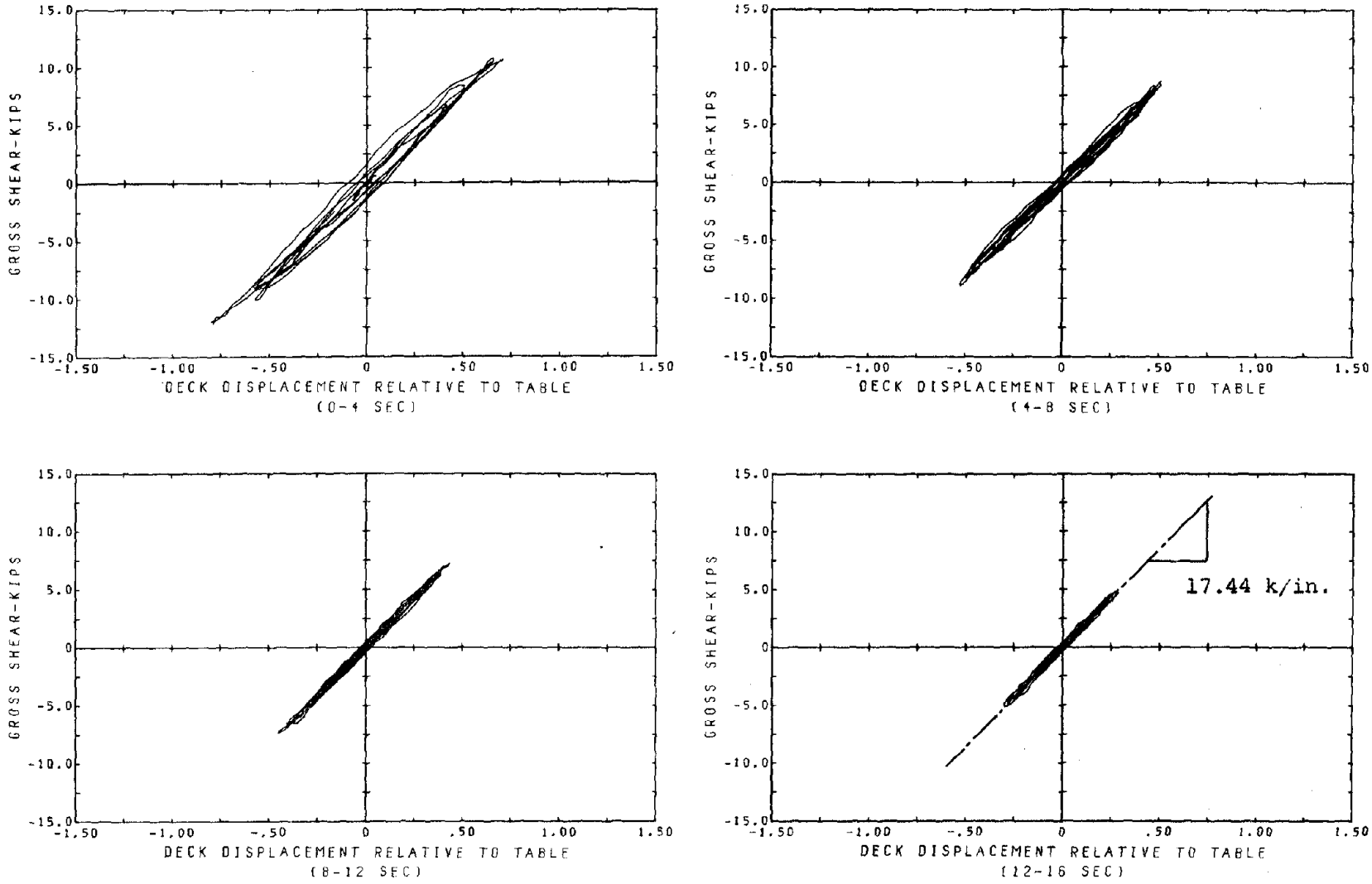

2.38 * EL CENTRO SPAN 50
TEST RESULTS OF THE OFFSHORE TUBULAR FRAME

Fig. 5.7 Hysteresis Loops of Gross Shear vs. Deck Displacement.

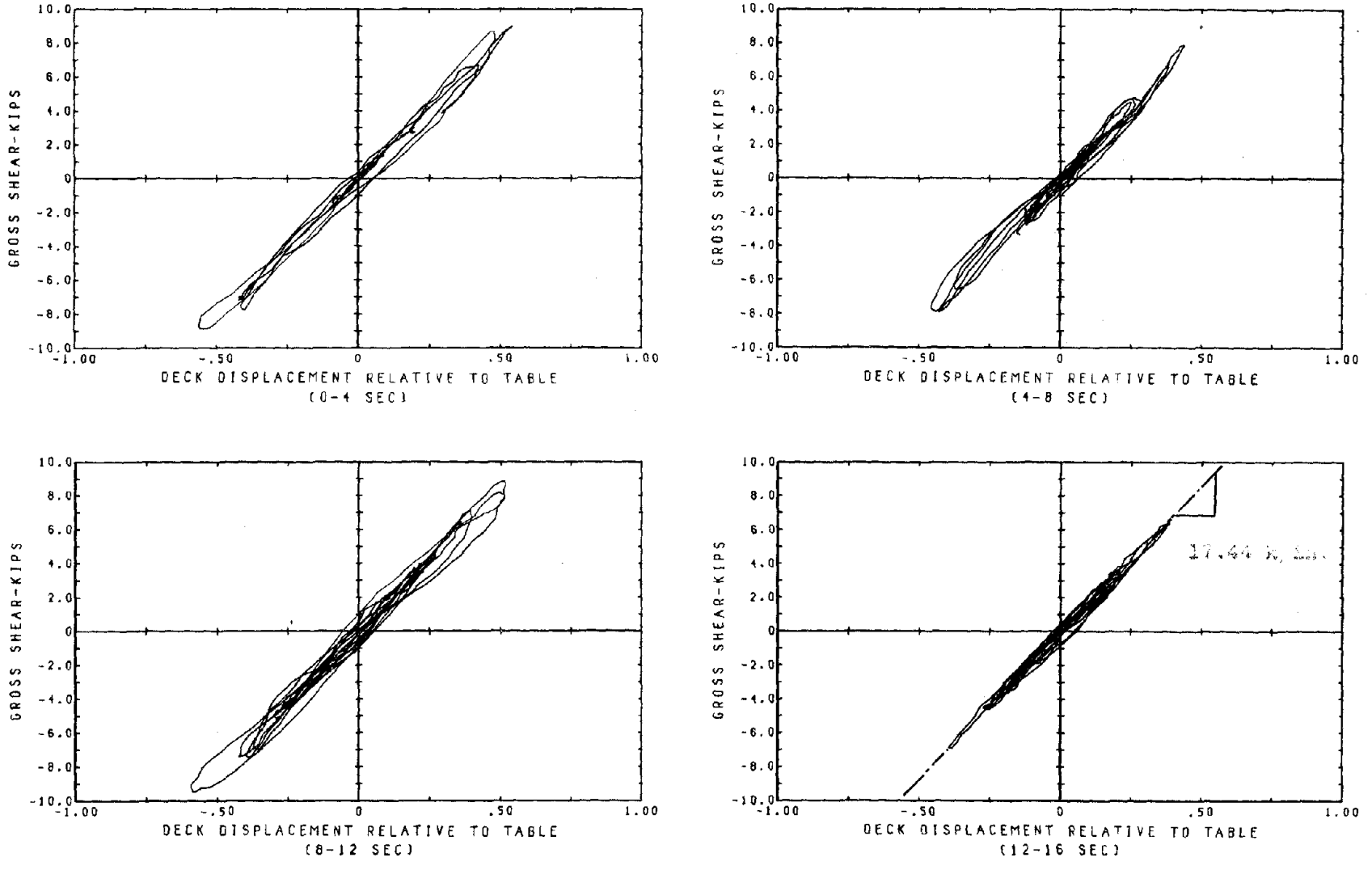

2.08 * TAFT SPAN 90

Fig. 5.8 Hysteresis Loops of Gross Shear vs. Deck Displacement.

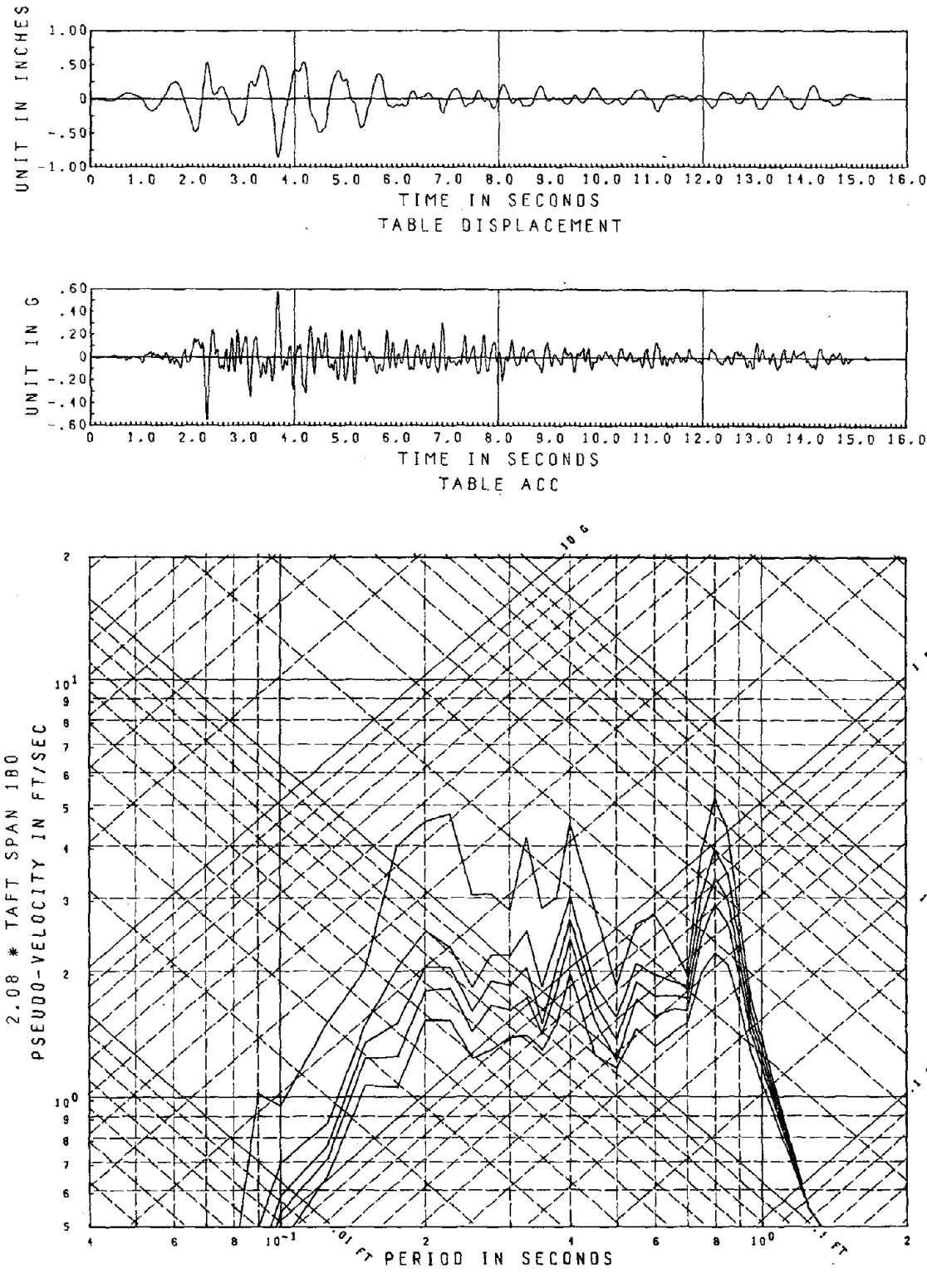

Damping Ratios: 0.0, 0.01, 0.02, 0.03, 0.05

Fig. 5.9 2.08 * Taft Span 180 Horizontal Table Motion.

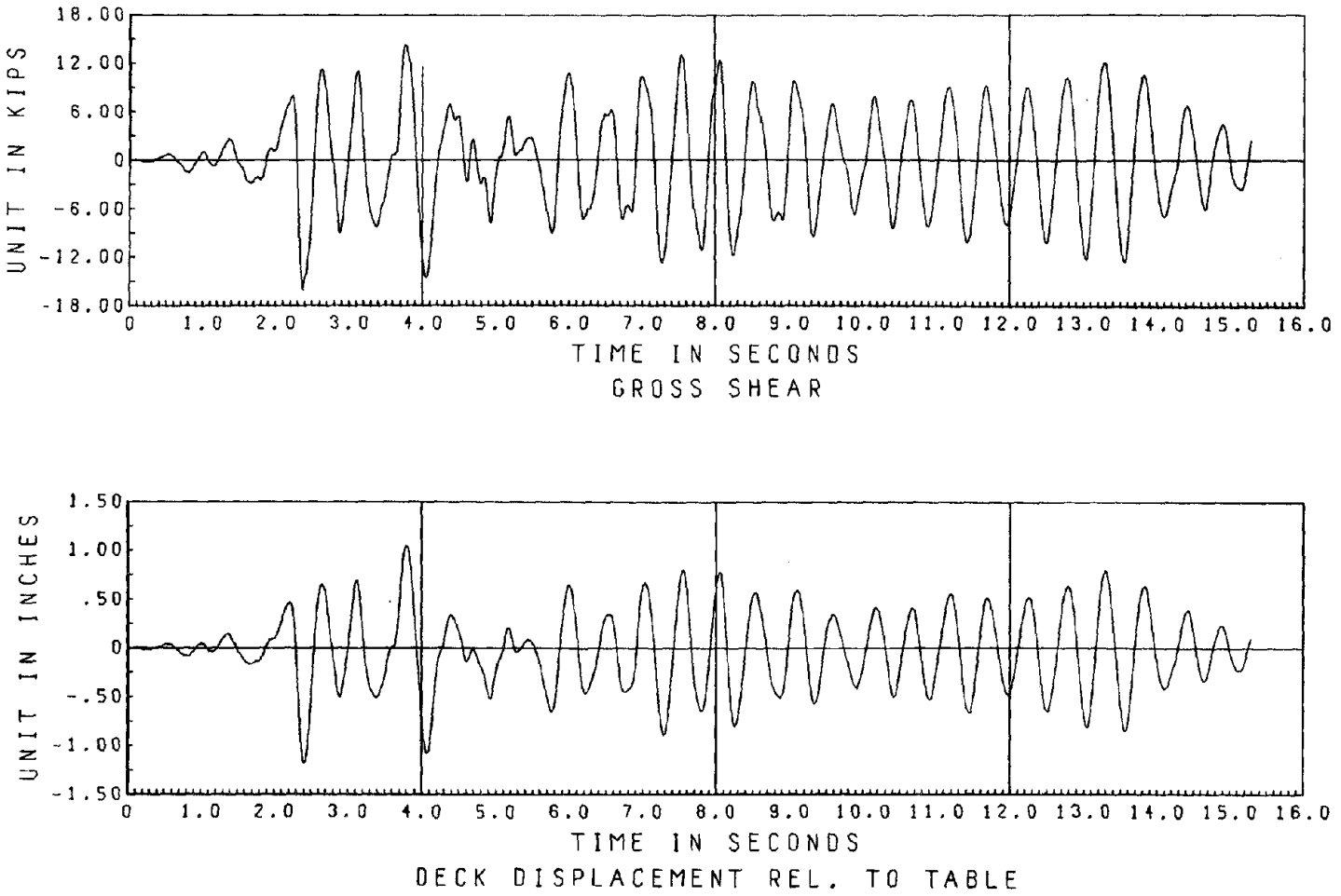

2.08 * TAFT SPAN 180

Fig. 5.10 Time History of Gross Shear and of Deck Displacement.

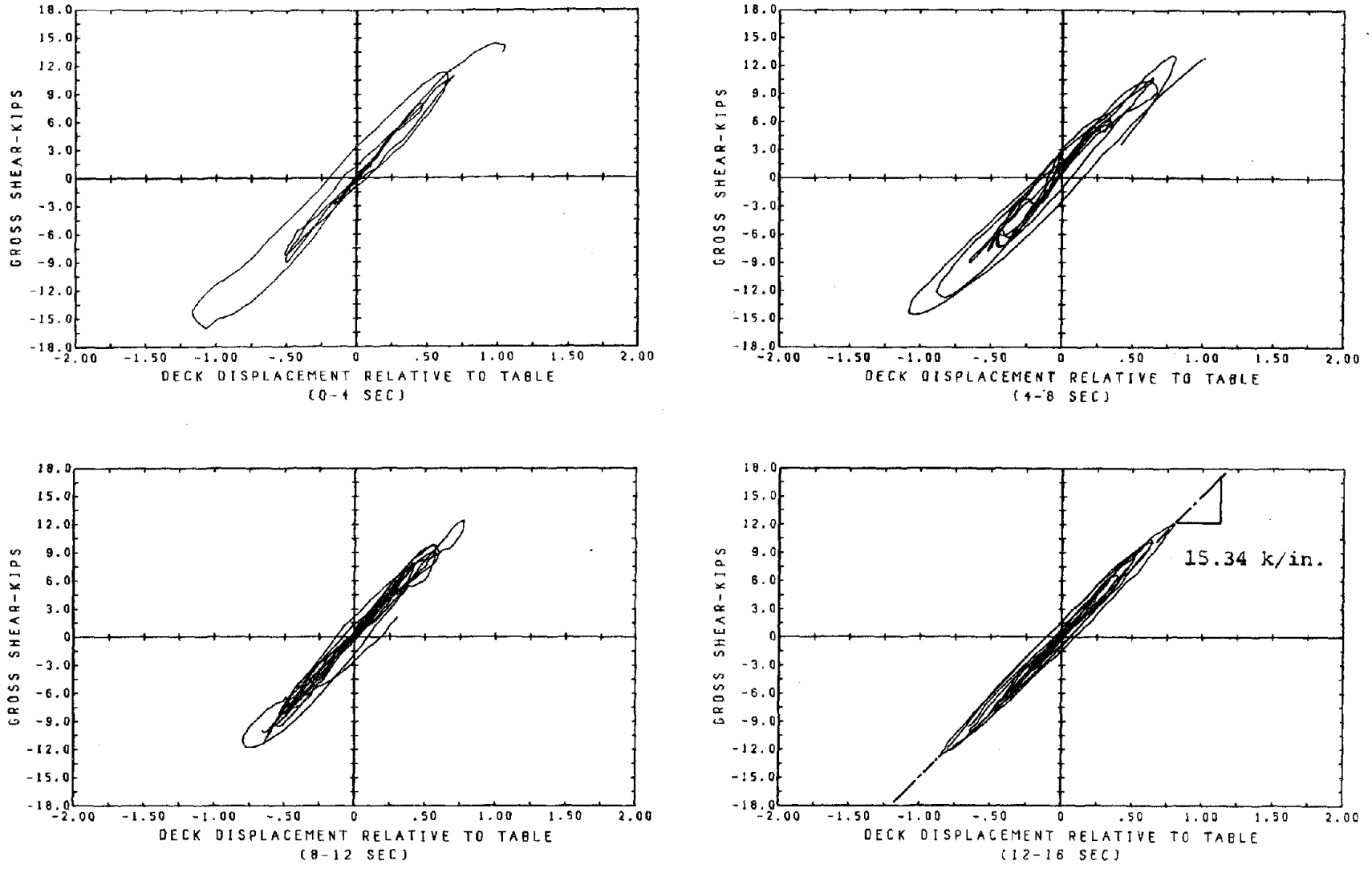

2.08 * TAFT SPAN 180

Fig. 5.11 Hysteresis Loops of Gross Shear vs. Deck Displacement.

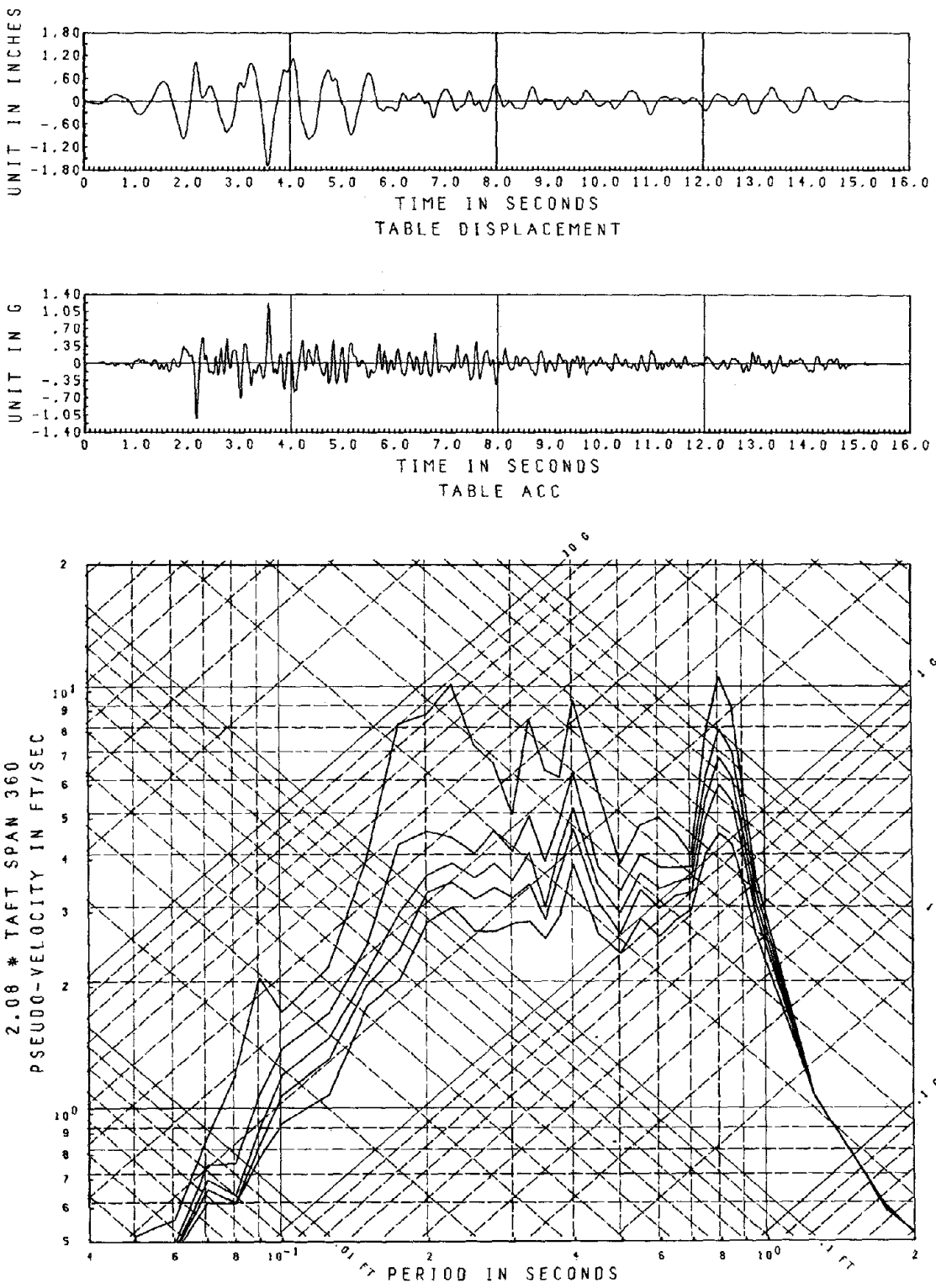

Damping Ratios: 0.0, 0.01, 0.02, 0.03, 0.05

Fig. 5.12 2.08 * Taft Span 360 (I) Horizontal Table Motion.

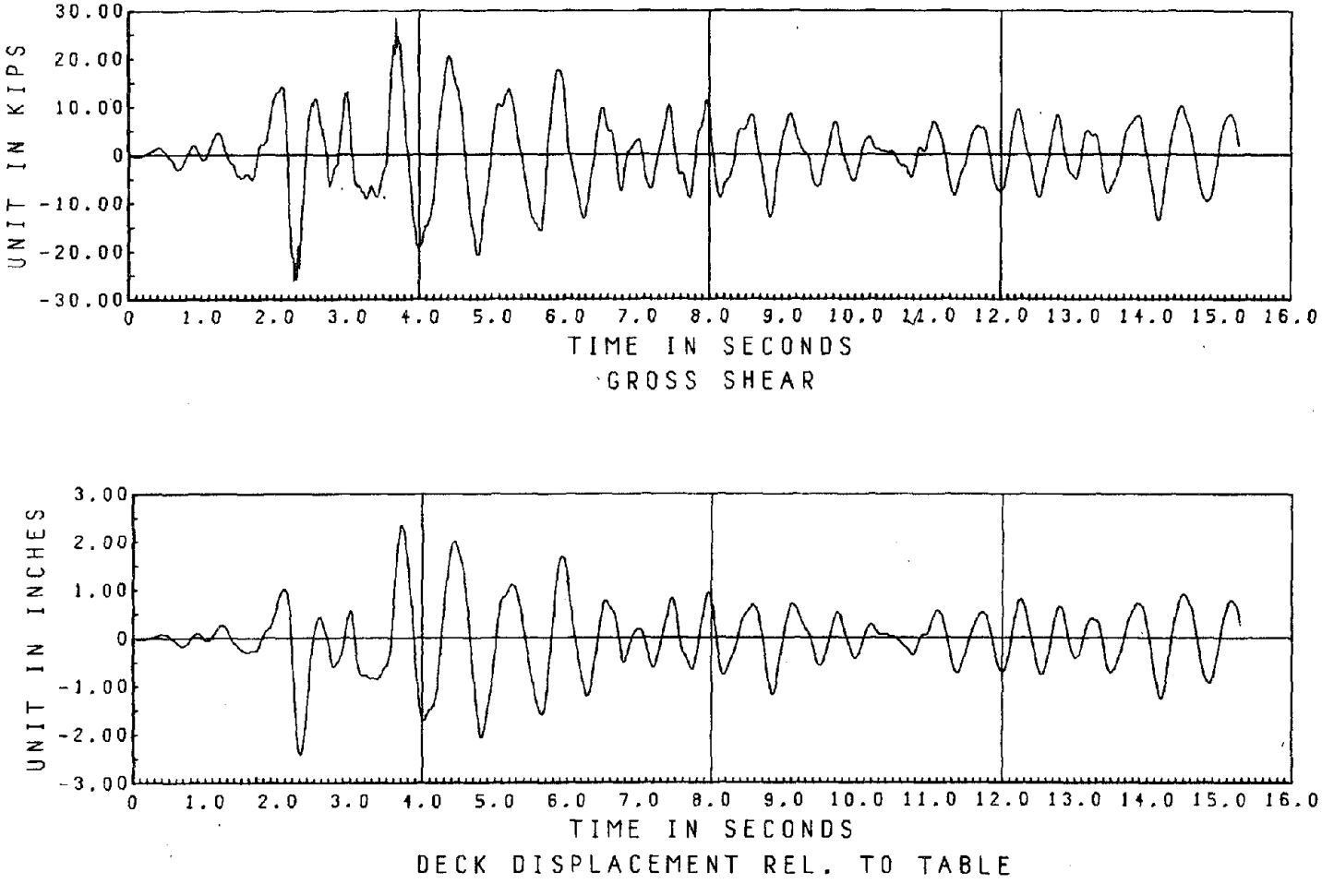

Fig. 5.13 Time History of Gross Shear and of Deck Displacement.

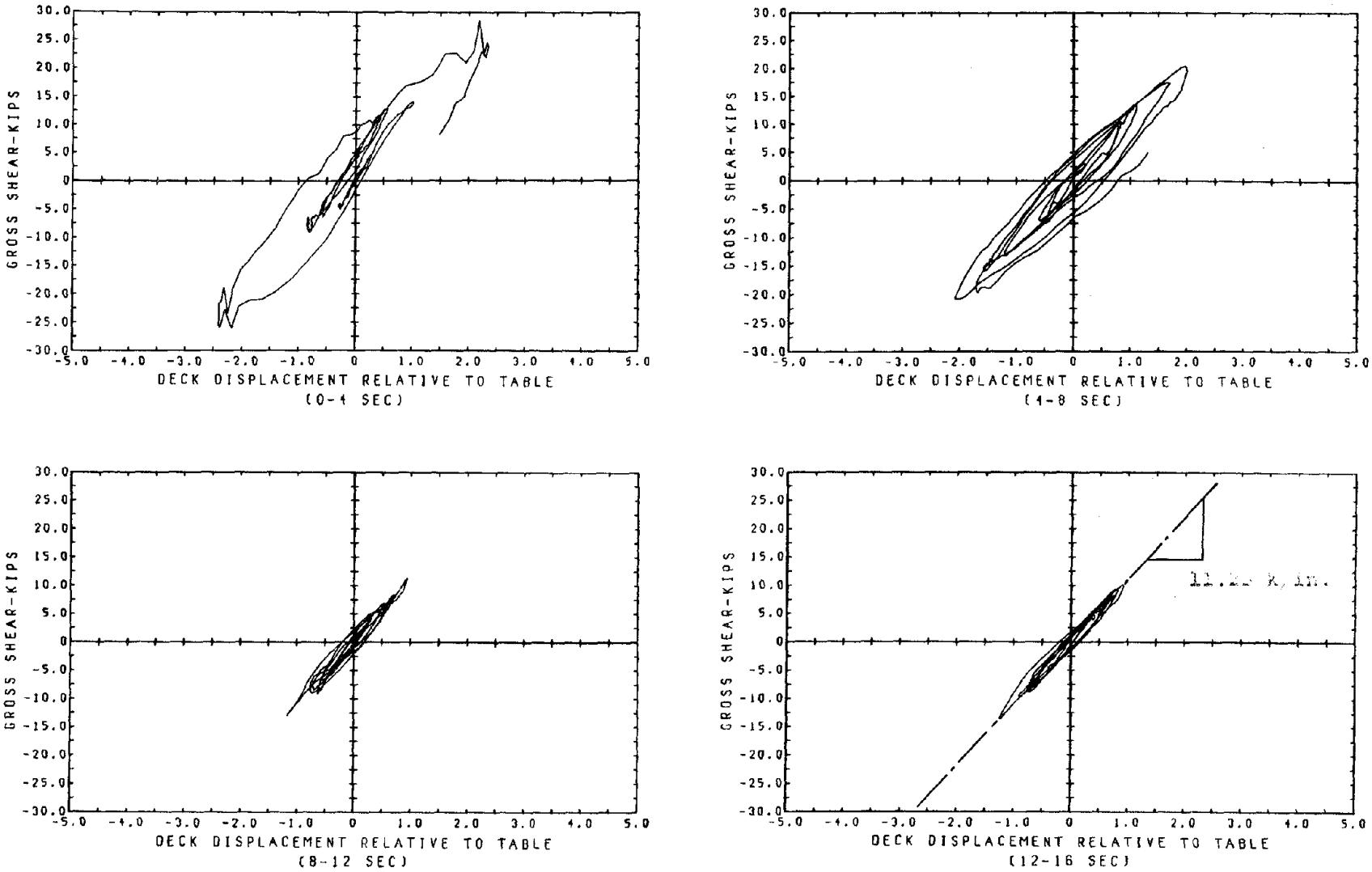

2.08 * TAFT SPAN 360 I

Fig. 5.14 Hysteresis Loops of Gross Shear vs. Deck Displacement.

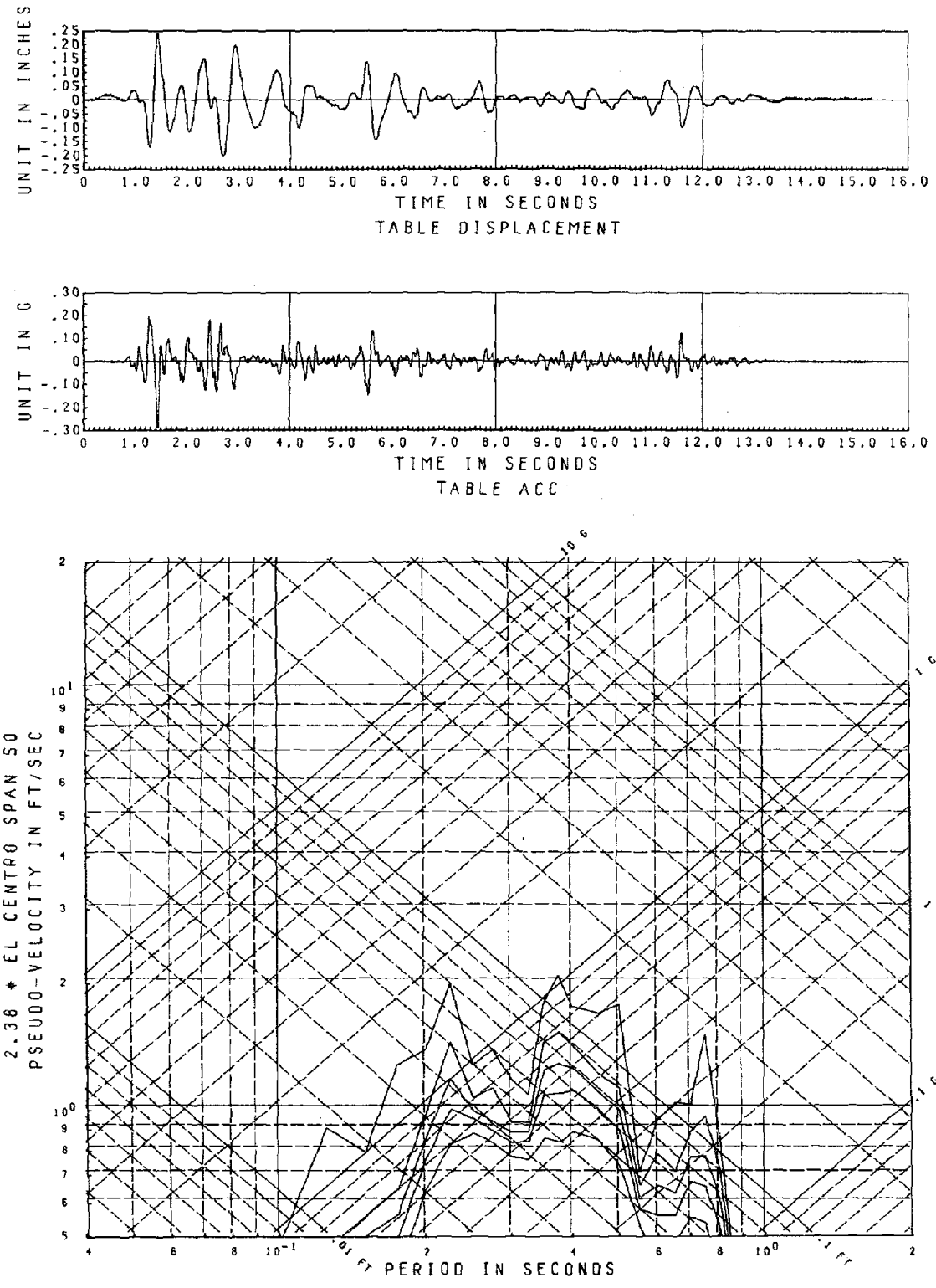

Damping Ratios: 0.0, 0.01, 0.02, 0.03, 0.05

Fig. 5.15 2.38 * El Centro Span 50 Horizontal Table Motion.

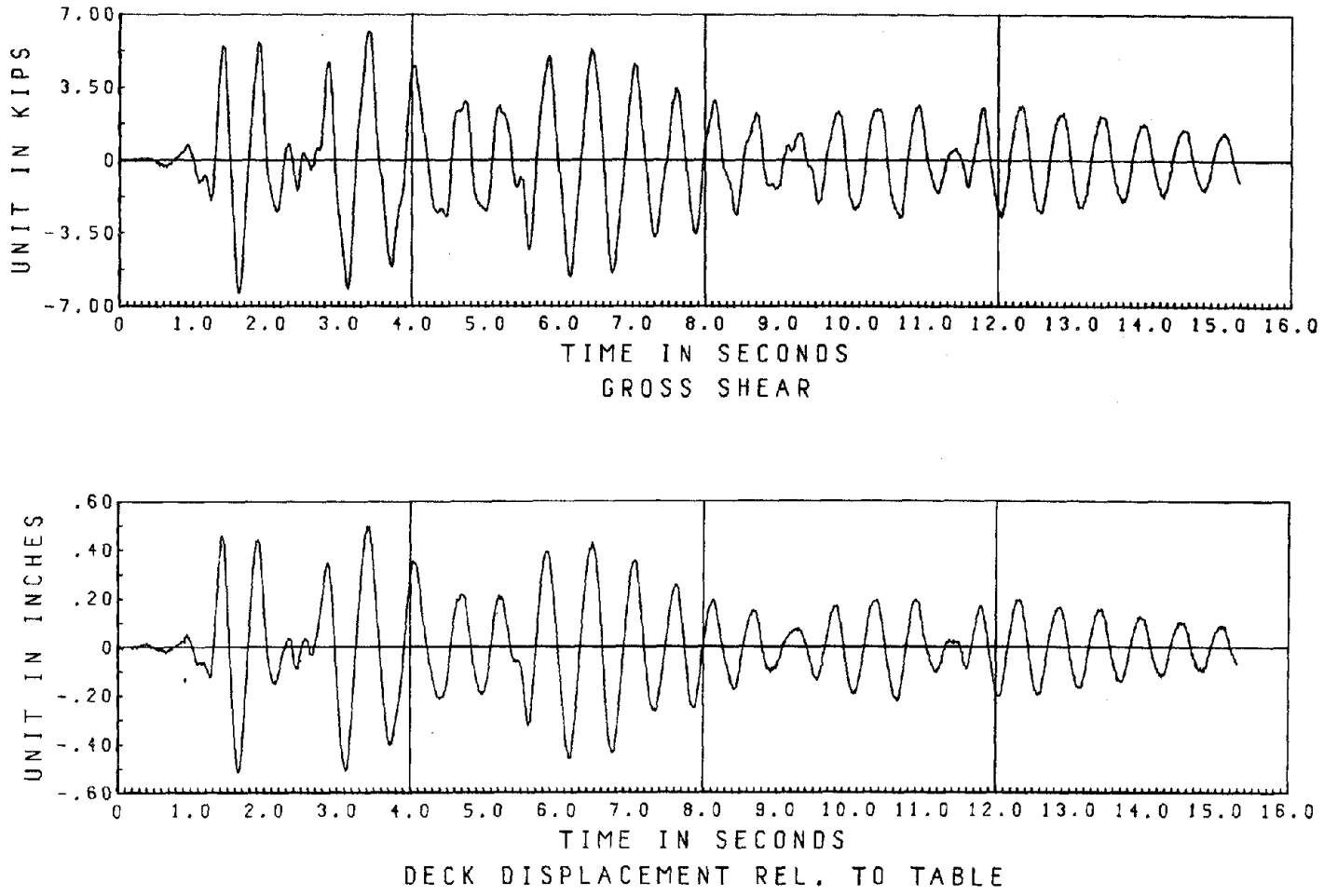

Fig. 5.16 Time History of Gross Shear and of Deck Displacement. (post-strength level 1)

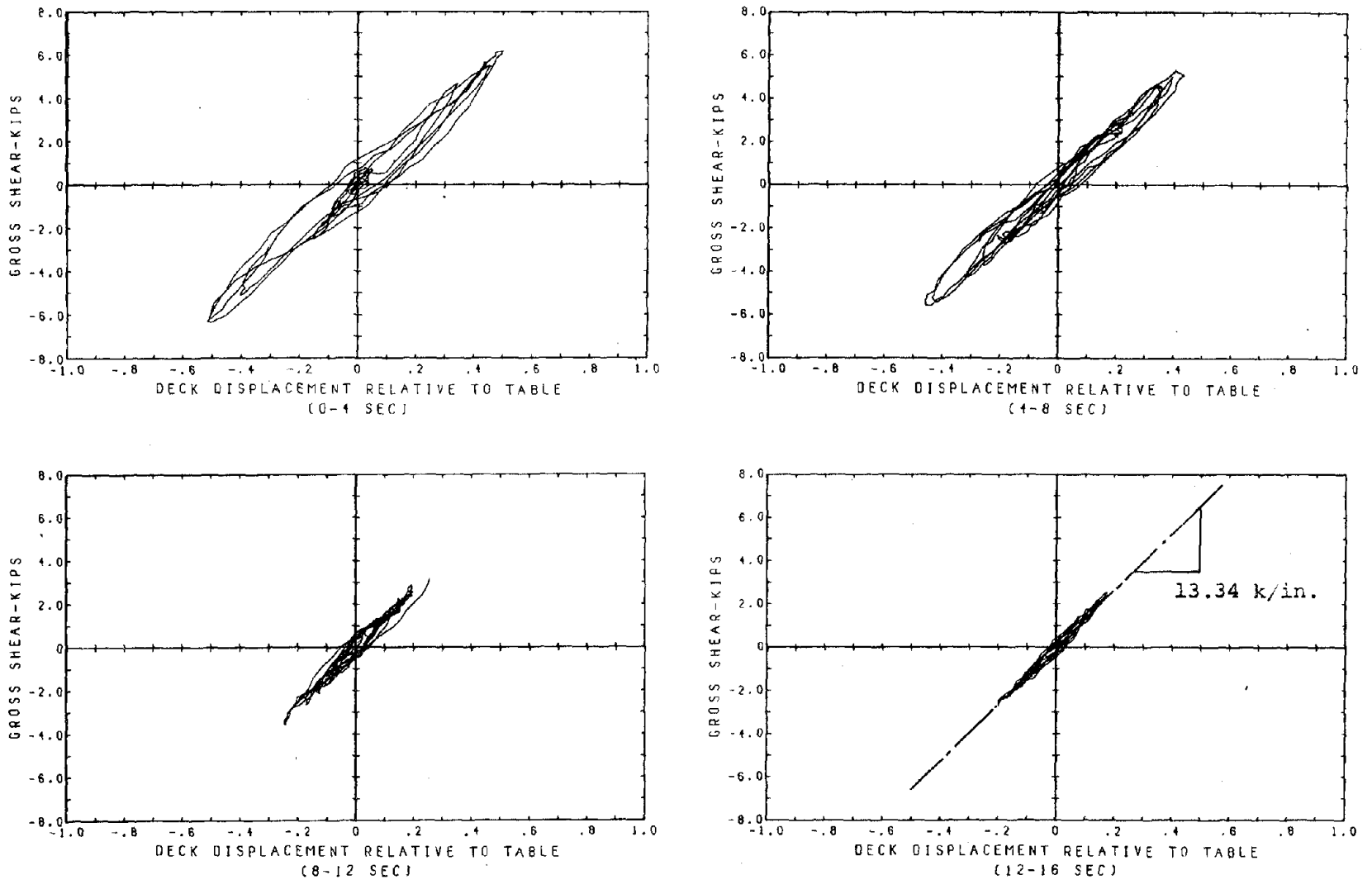

2.38 * EL CENTRO SPAN 50

Fig. 5.17 Hysteresis Loops of Gross Shear vs. Deck Displacement. (post-strength level 1)

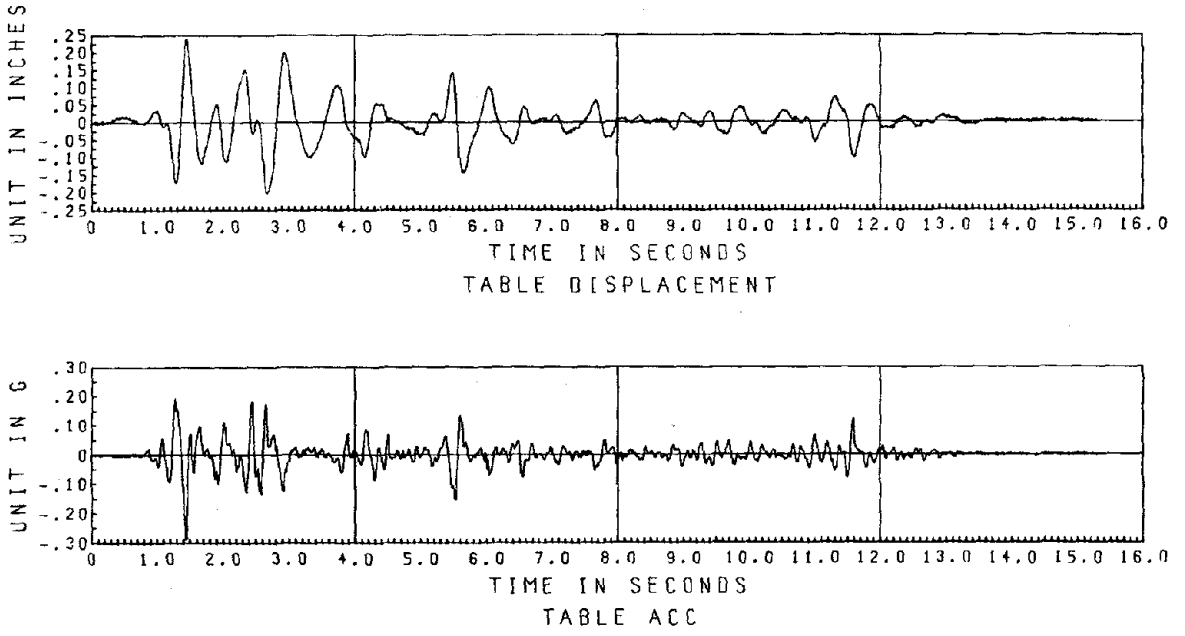

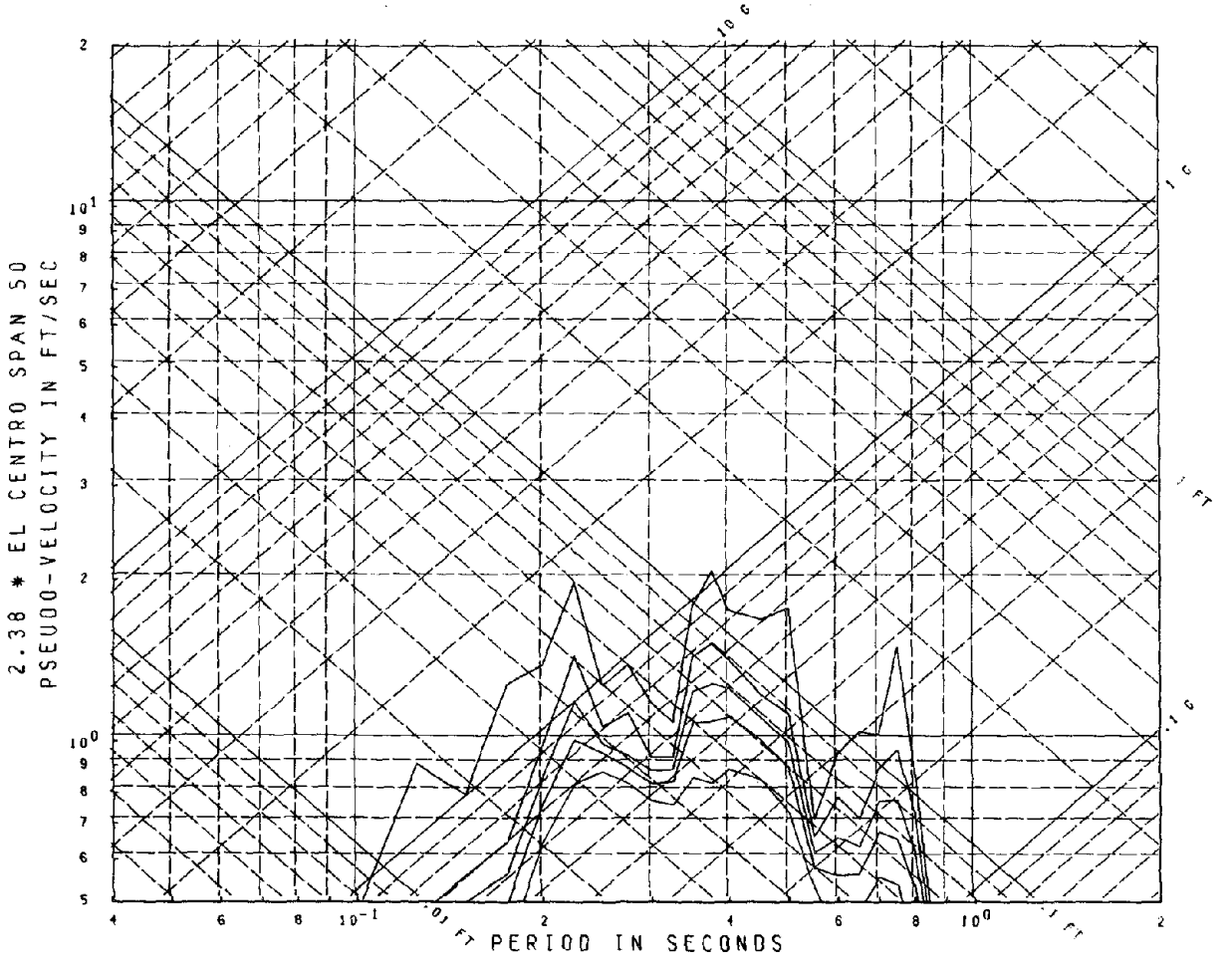

Damping Ratios: 0.0, 0.01, 0.02, 0.03, 0.05

Fig. 5.18 2.38 * El Centro Span 50 Horizontal Table Motion.

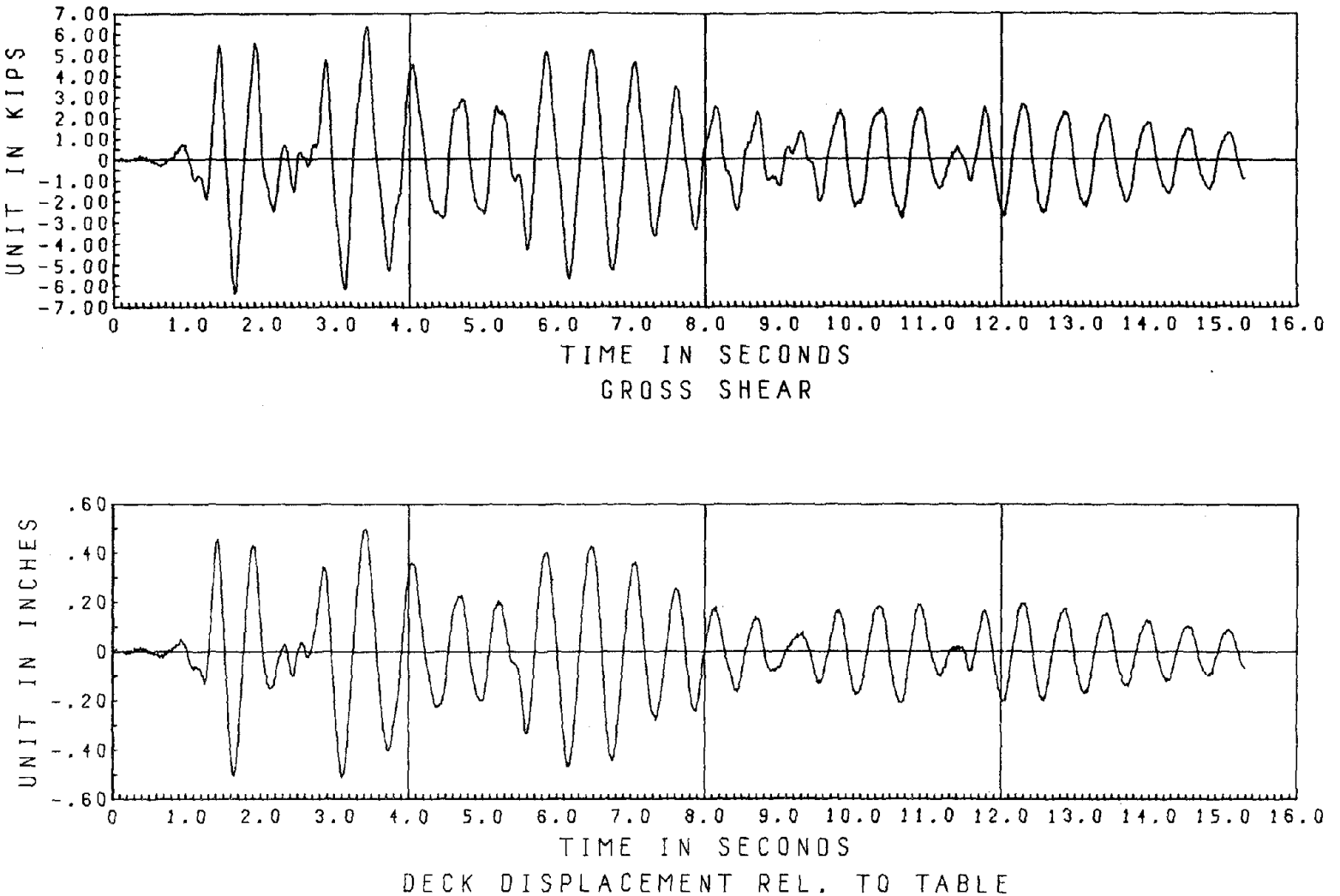

Fig. 5.19 Time History of Gross Shear and of Deck Displacement.
(post-strength level 2)

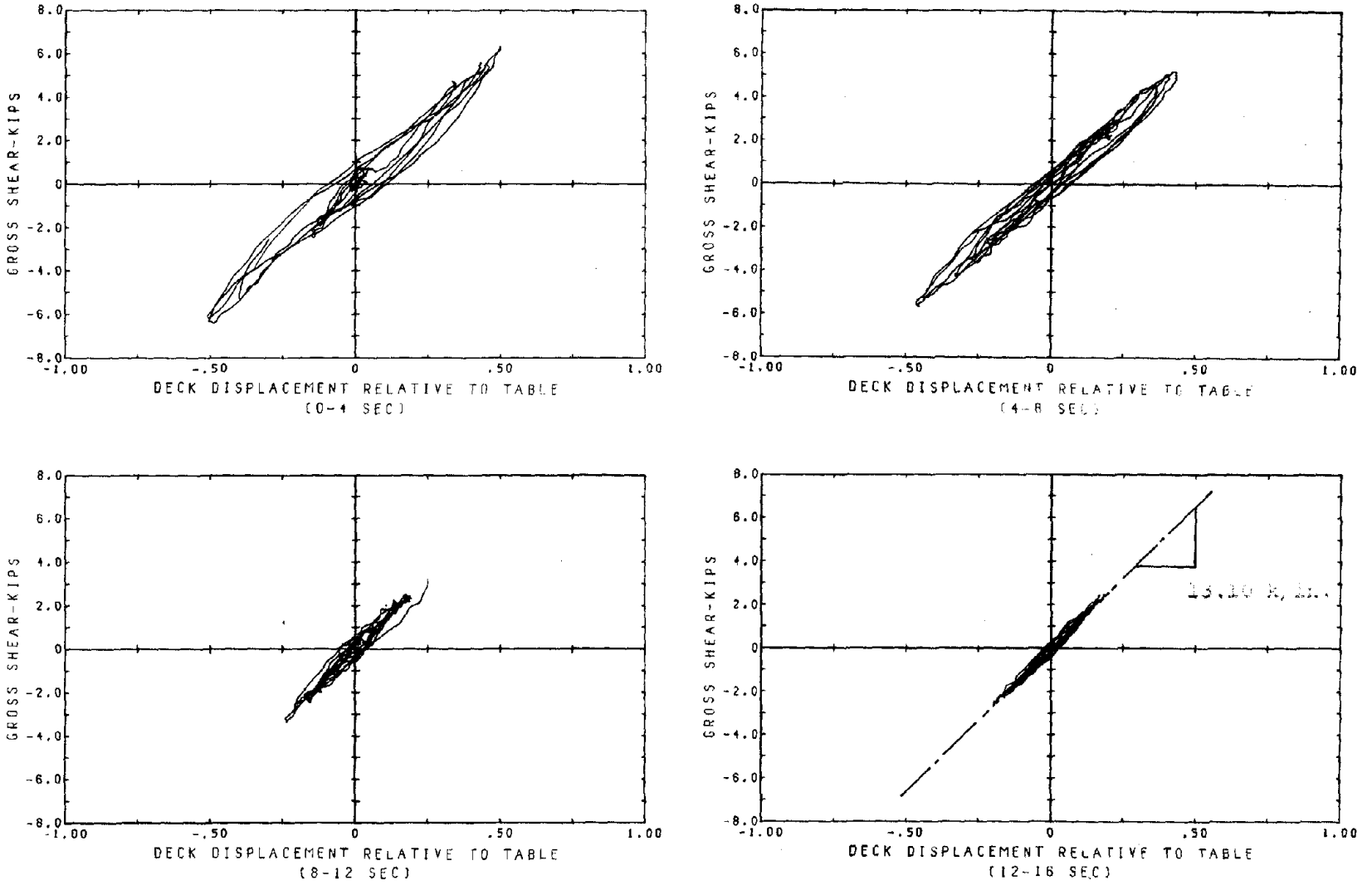

2.38 * EL CENTRO SPAN 50

Fig. 5.20 Hysteresis Loops of Gross Shear vs. Deck Displacement. (post-strength level 2)

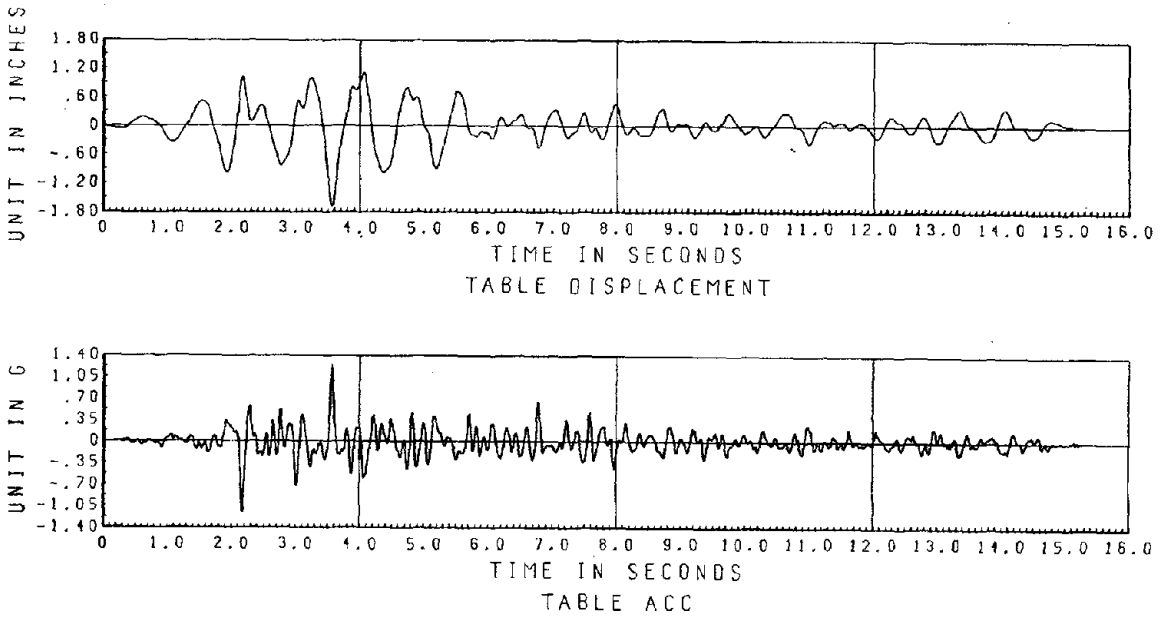

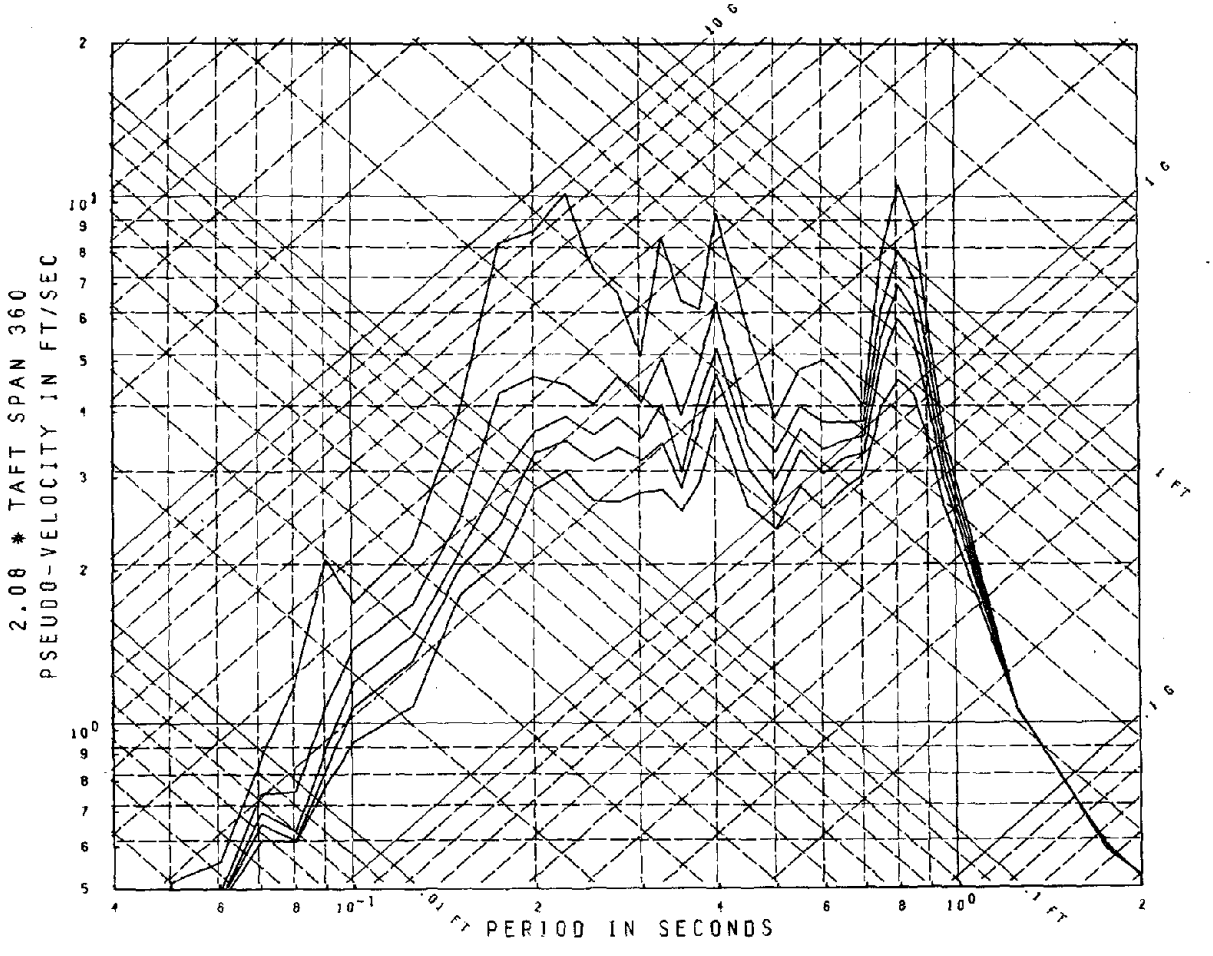

Damping Ratios: 0.0, 0.01, 0.02, 0.03, 0.05

Fig. 5.21 2.08 * Taft Span 360 (II) Horizontal Table Motion.

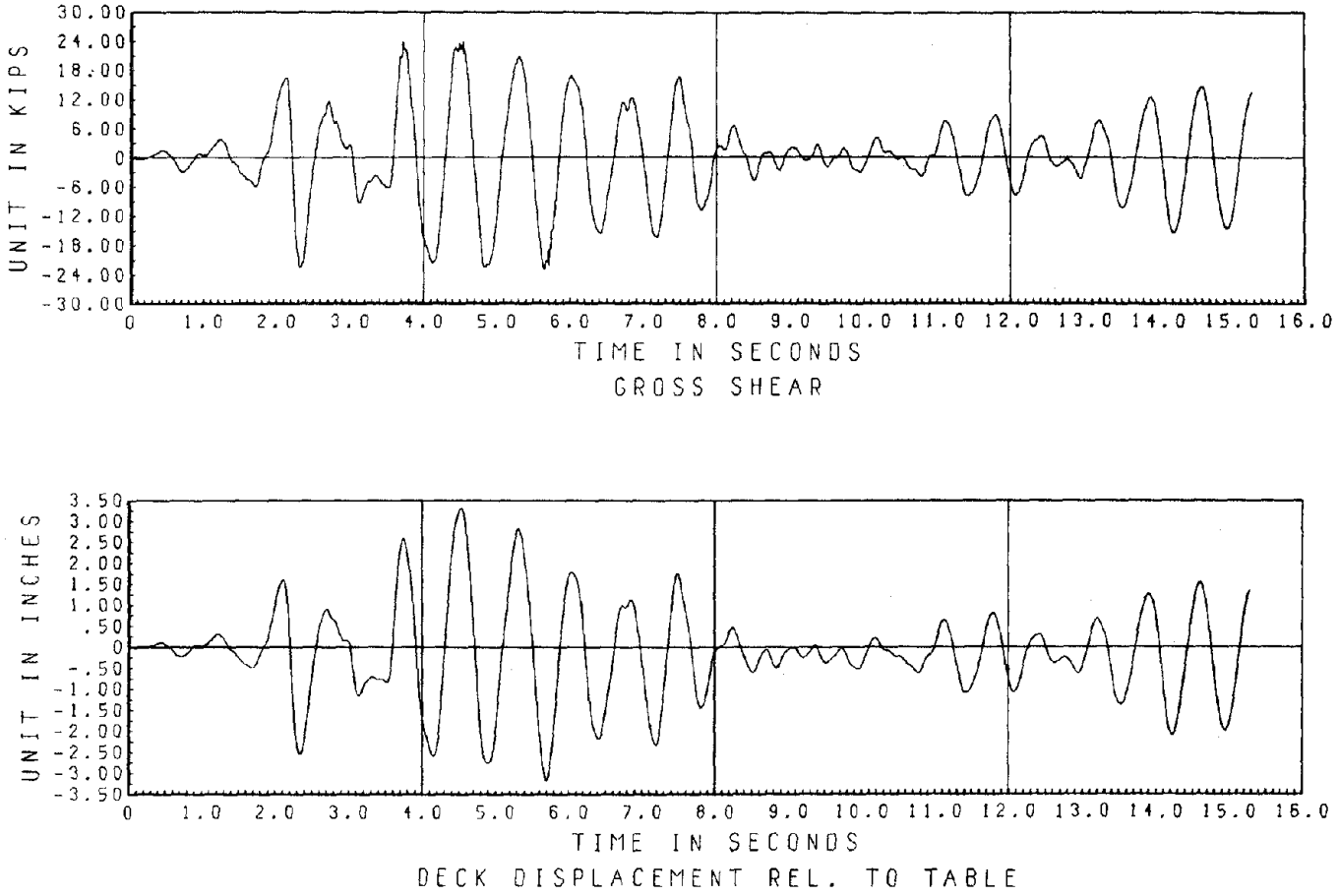

2.08 * TAFT SPAN 360 II

Fig. 5.22 Time History of Global Shear and of Relative Deck Displacement.

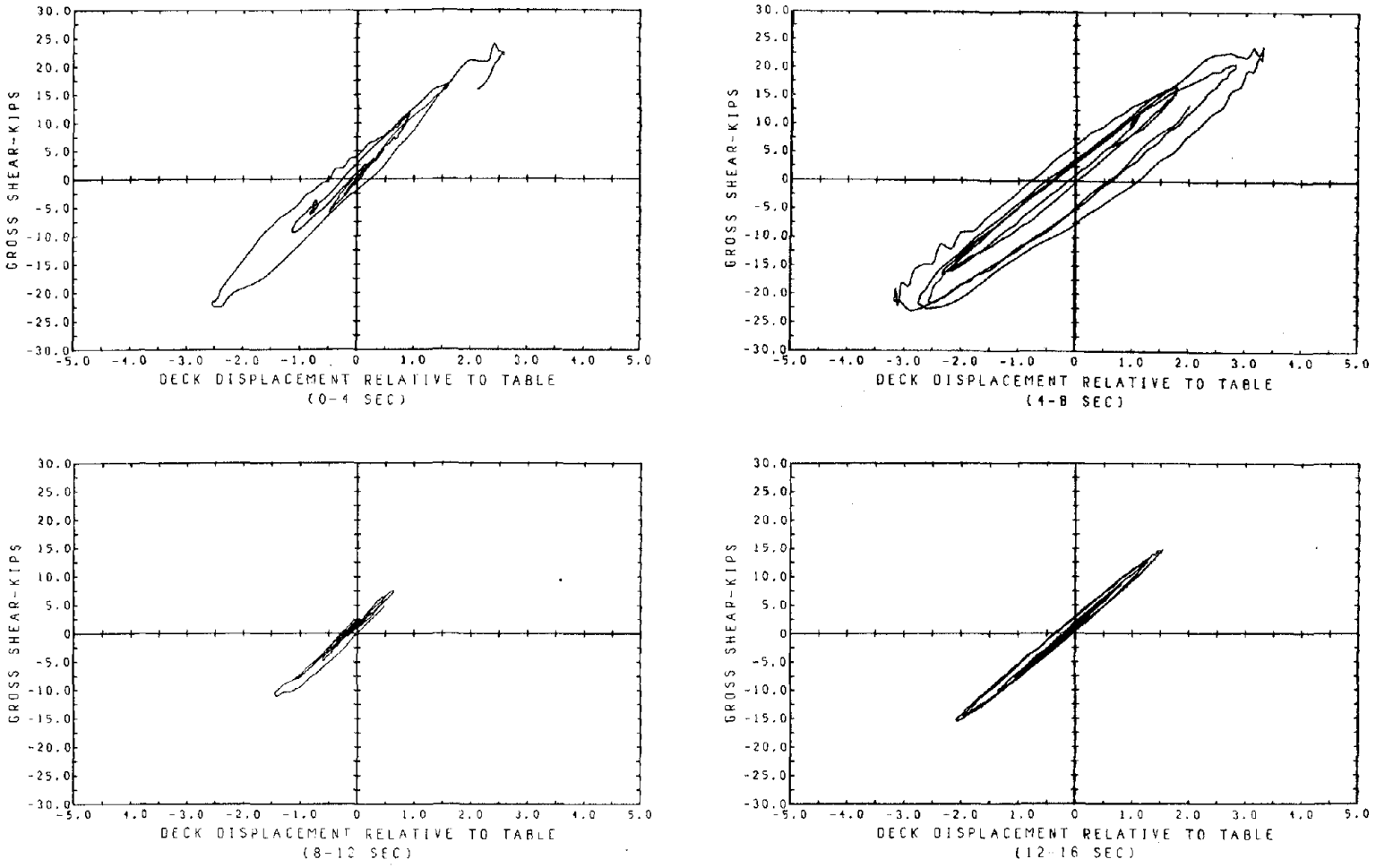

Fig. 5.23 Hysteresis Loops of Gross Shear vs. Deck Displacement. Taft Span 360 (II)

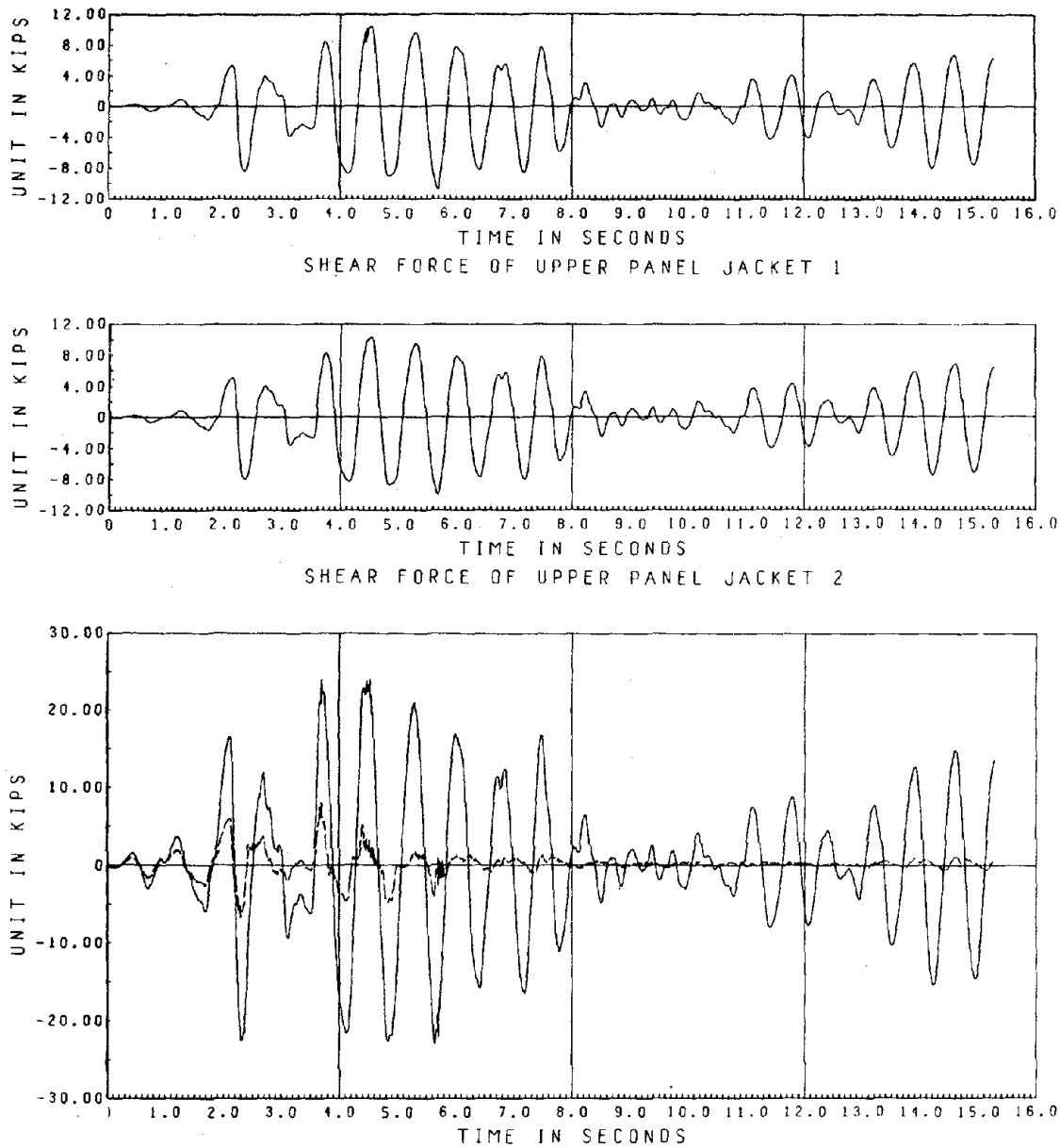

Fig. 5.24 Time History Plots of Shear Resisted by Upper Panel Jackets, Diagonals, and the Frame. (Taft 360 II)

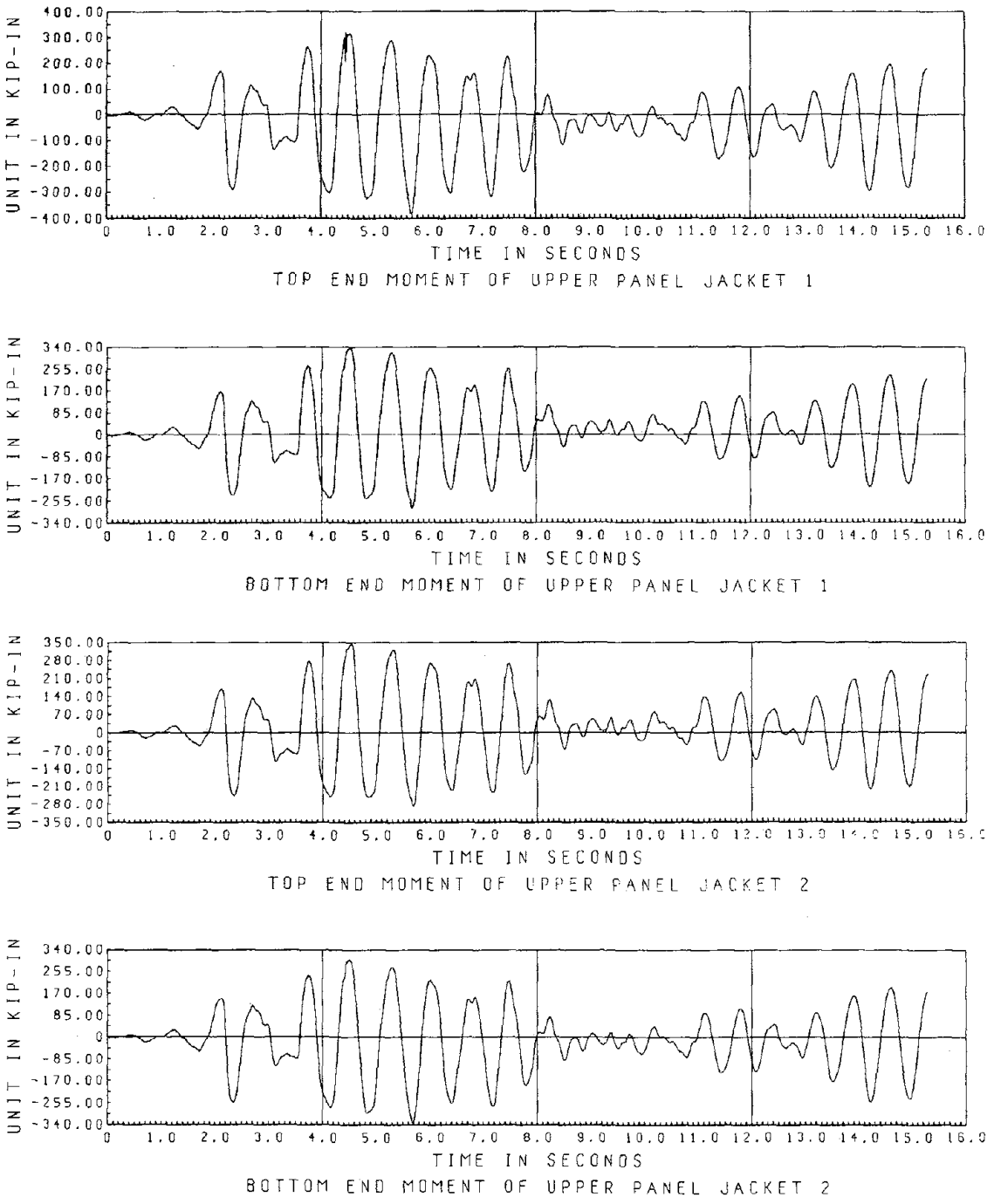

Fig. 5.25 Time History Plots of Bending Moment of the Upper Panel Jackets.
(Taft 360 II)

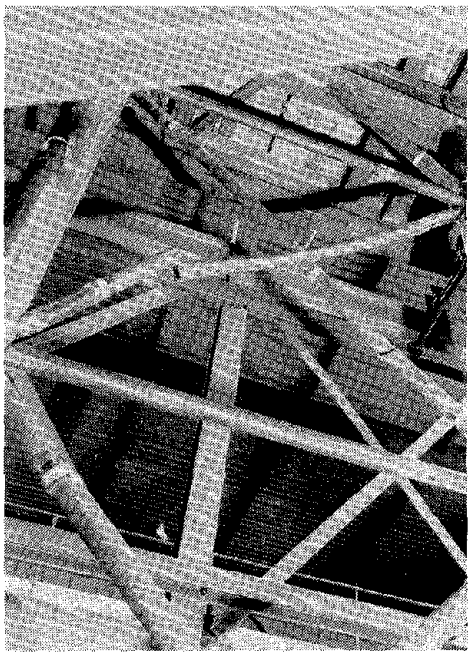

(a) Damaged Upper Panel X-Braces

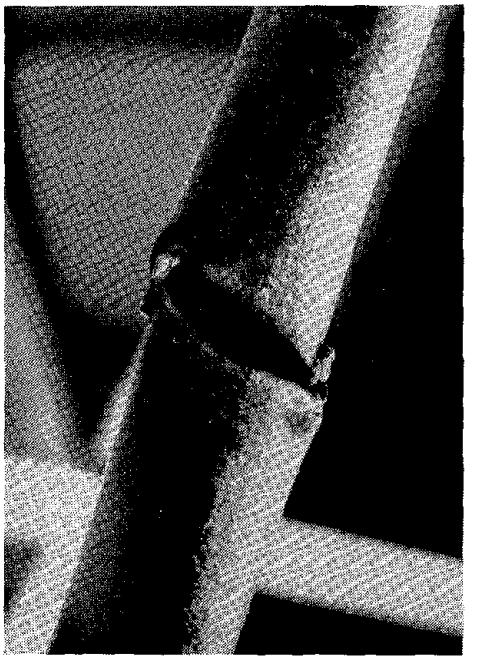

(b) Brace 2, Mid-span Damage

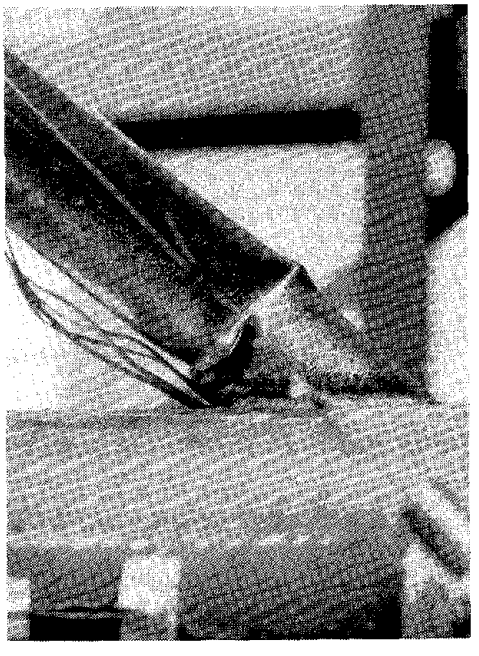

(c) Brace 4, End-Connection Damage

(d) Yielding of the Lower Diagonal & Horizontal Braces

Fig. 5.26 Photographs of Brace Damage.

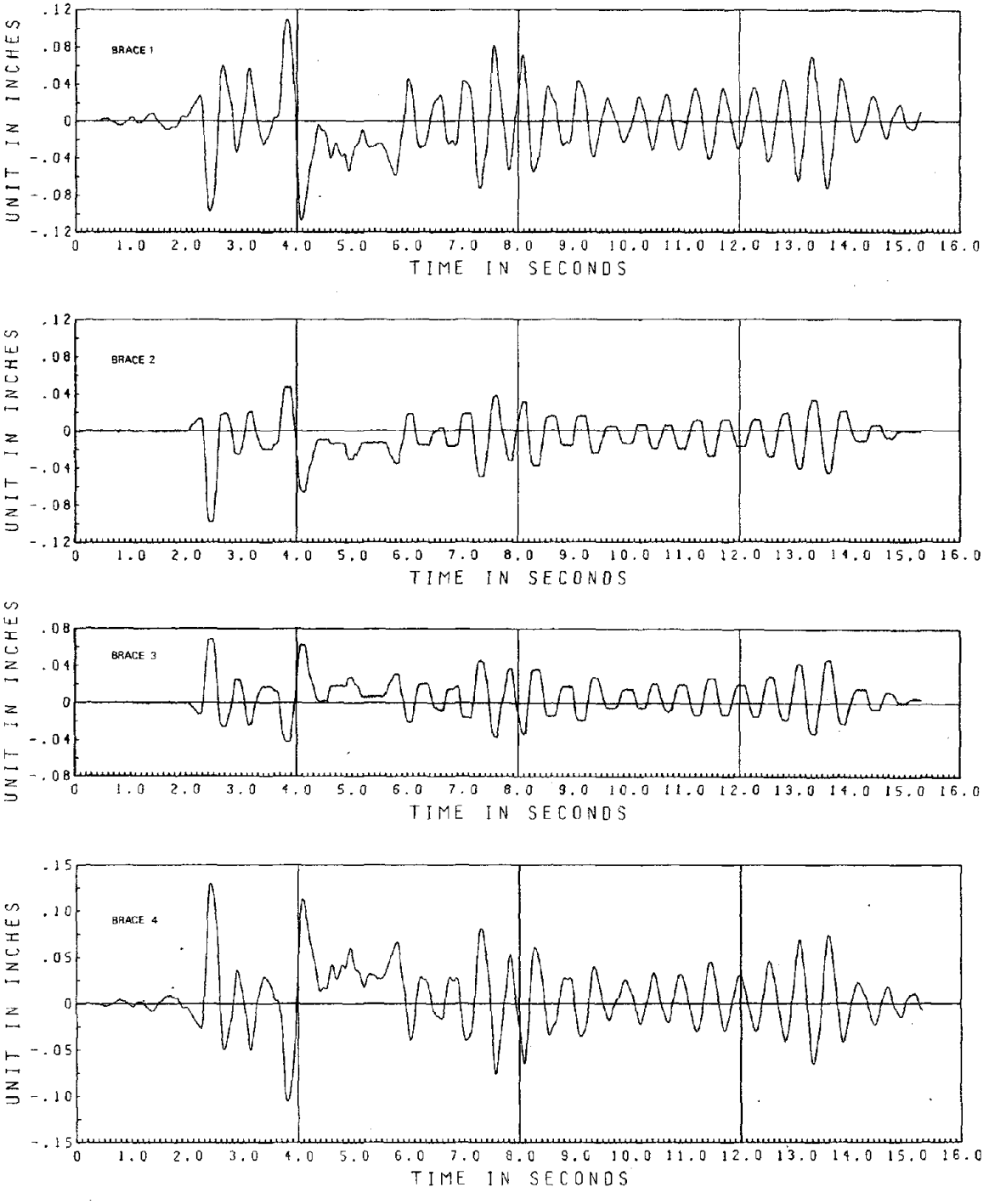

Fig. 5.27 Axial Displacement Time Histories of the Upper Panel Diagonals.

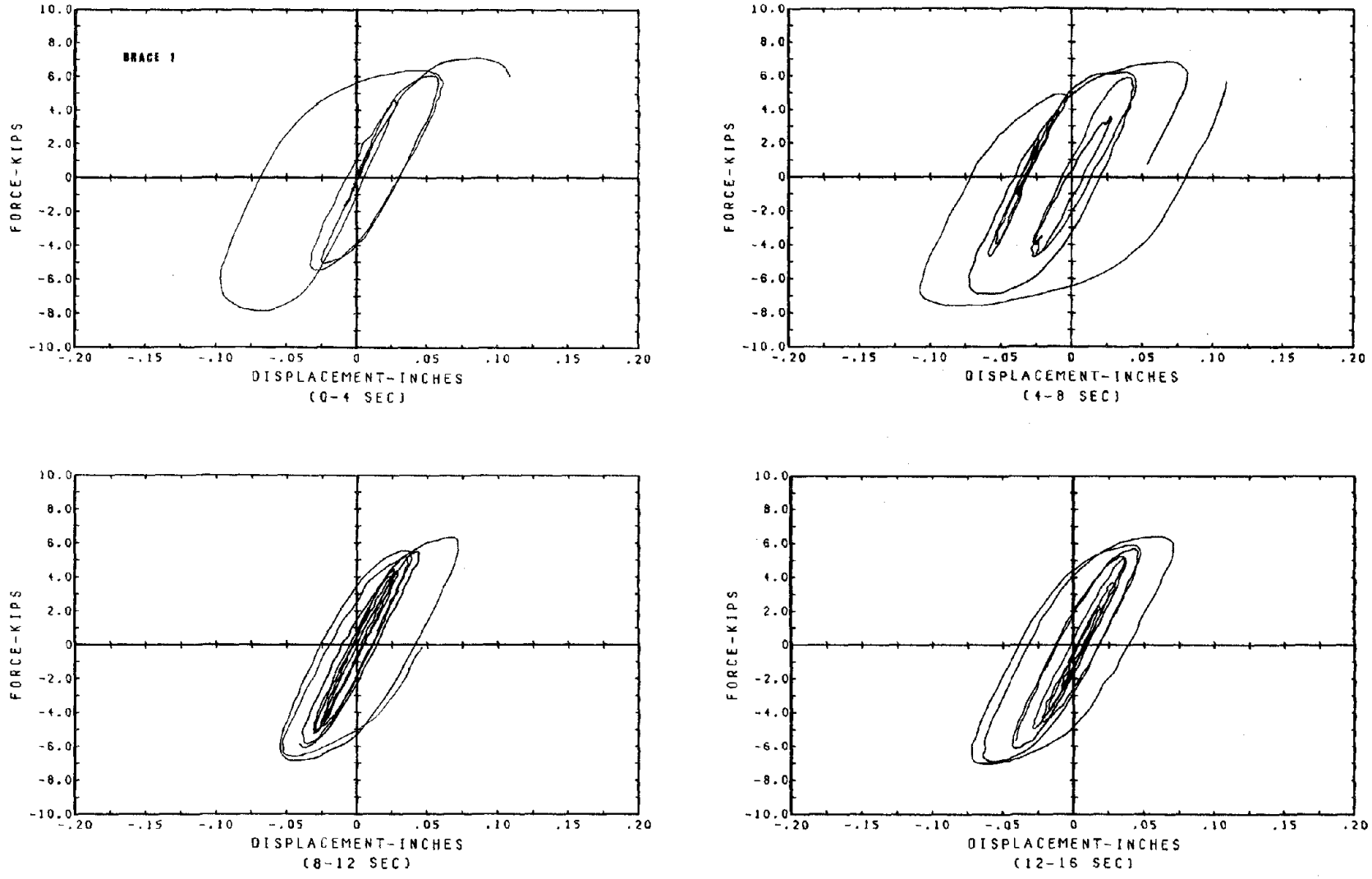

5/48 SCALED MODEL
OFFSHORE PLATFORM TUBULAR FRAME
2.08 * TAFT SPAN 180

Fig. 5.28 Axial Force - Axial Displacement Hysteresis Loops of Brace 1.

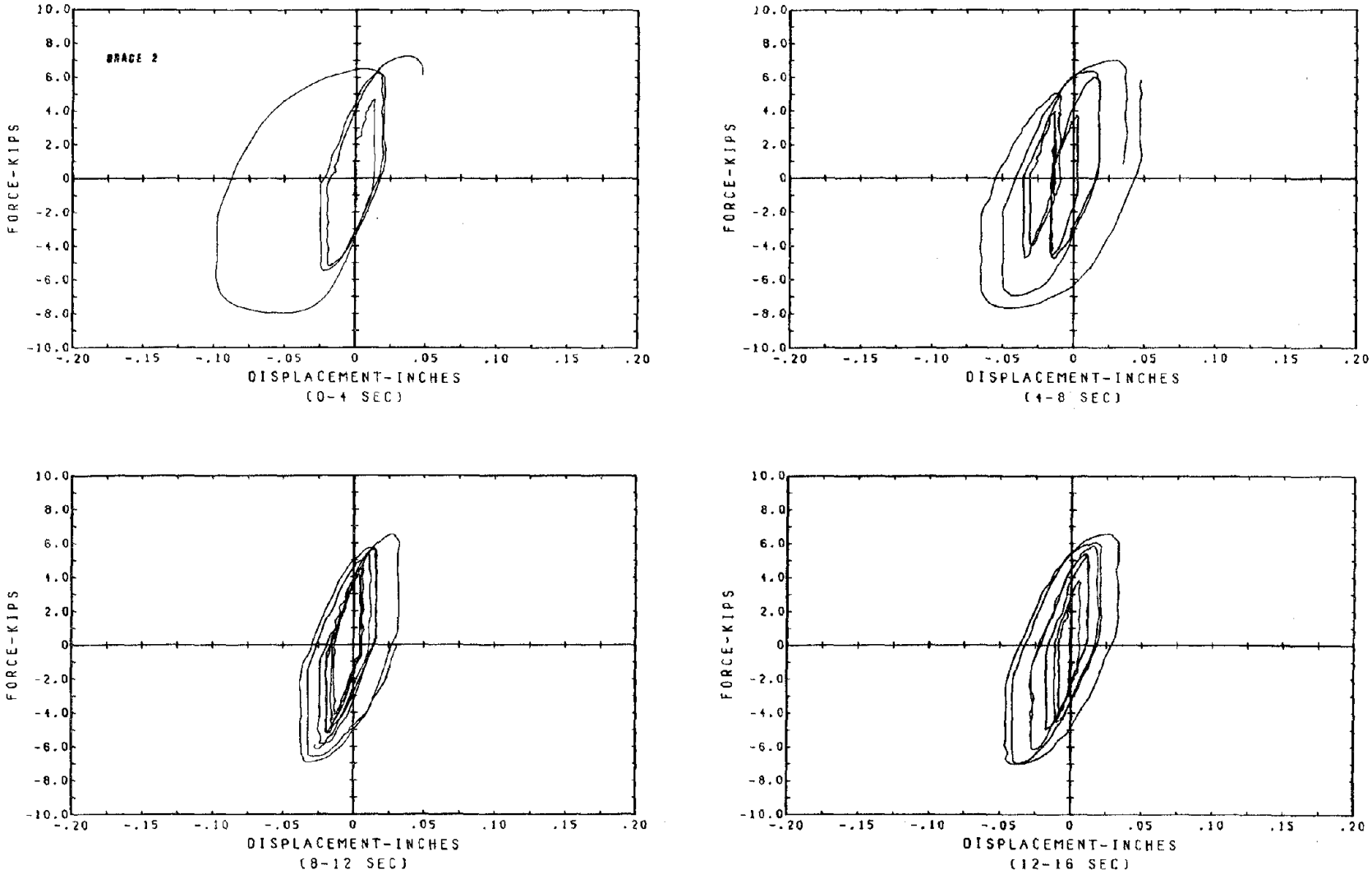

5/48 SCALED MODEL
OFFSHORE PLATFORM TUBULAR FRAME
2.08 * TAFT SPAN 180

Fig. 5.29 Axial Force - Axial Displacement Hysteresis Loops of Brace 2.

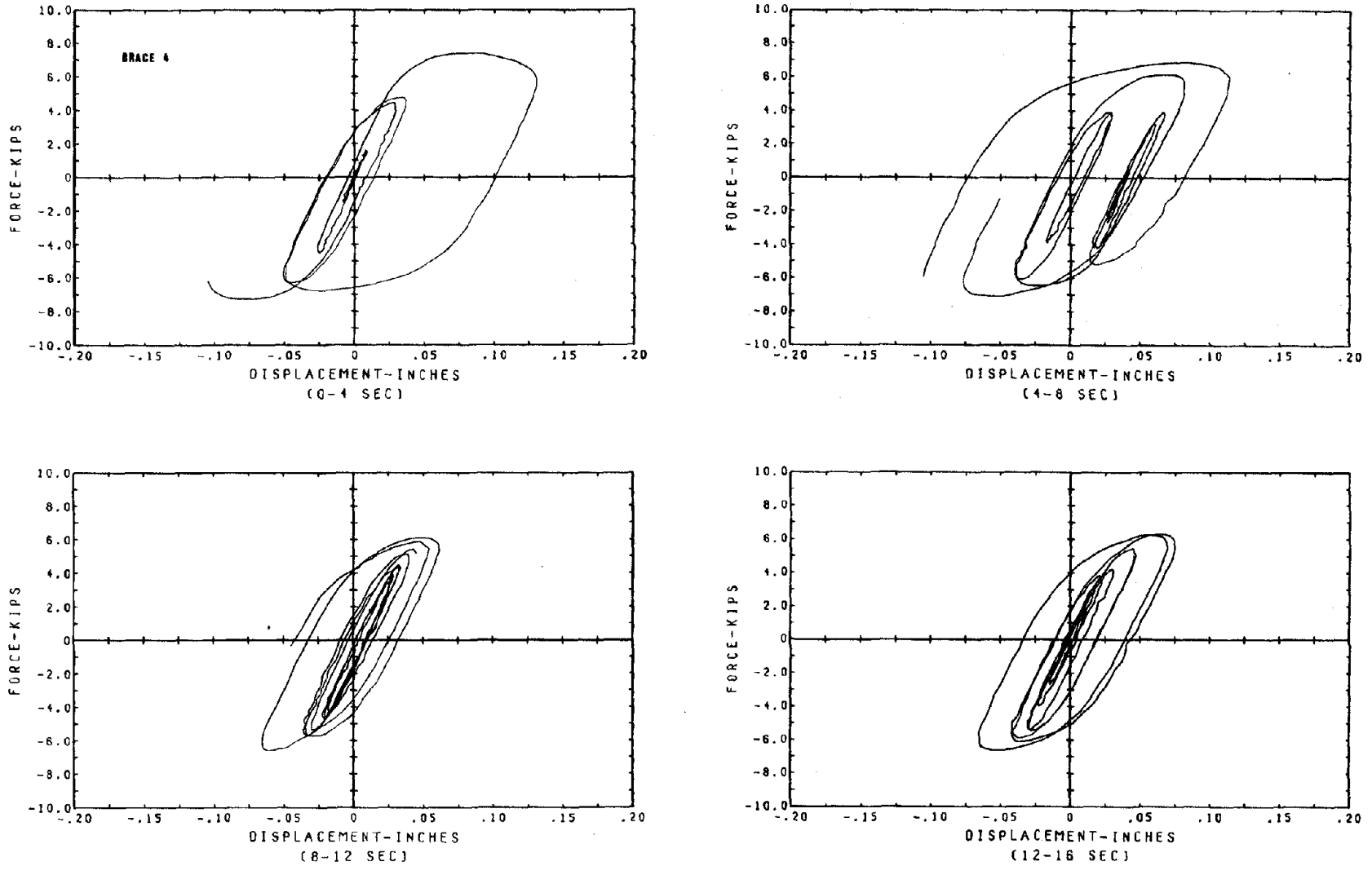

5/48 SCALED MODEL
OFFSHORE PLATFORM TUBULAR FRAME
2.08 * TAFT SPAN 180

Fig. 5.30 Axial Force - Axial Displacement Hysteresis Loops of Brace 4.

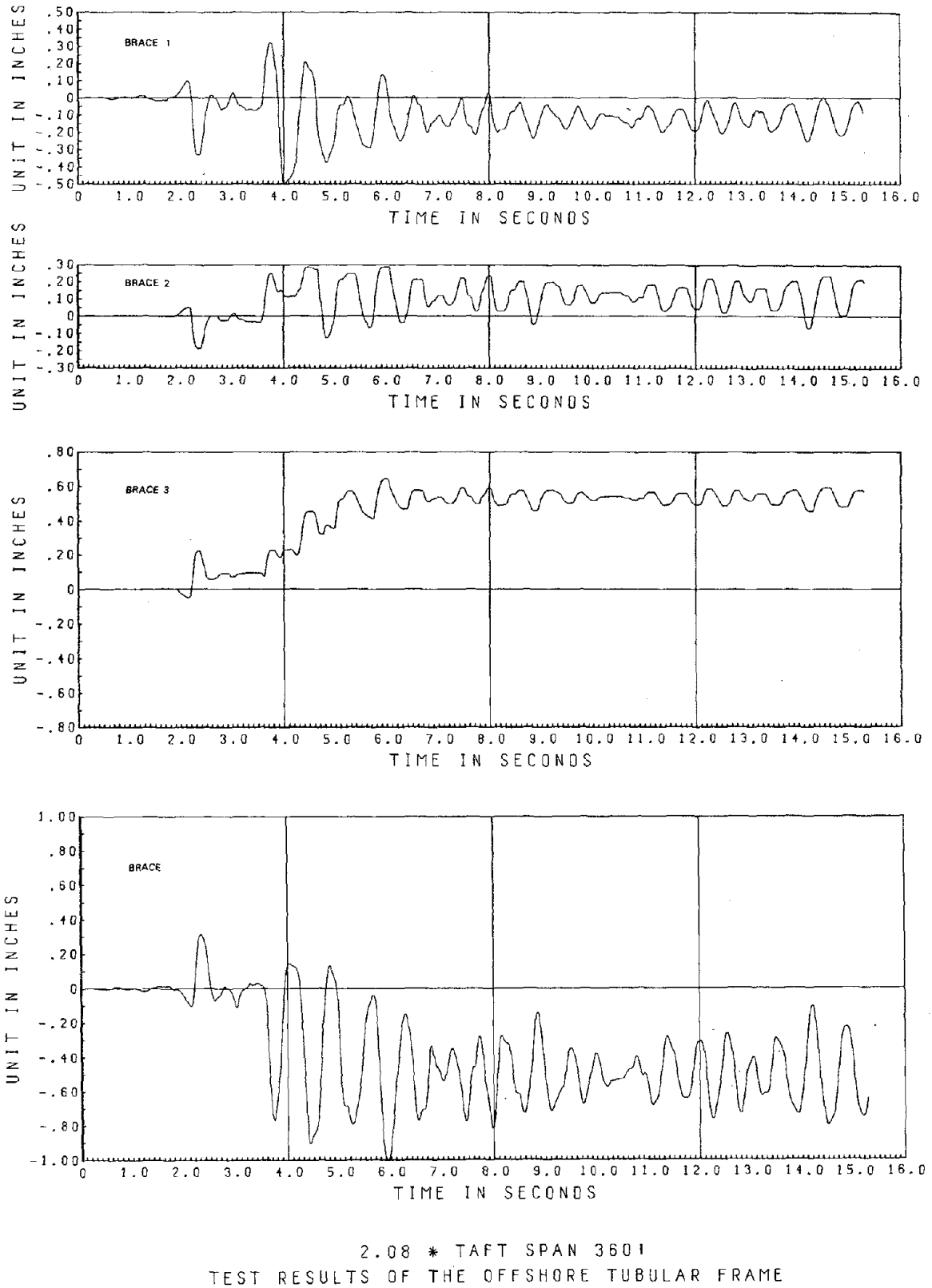

Fig. 5.31 Axial Displacement Time Histories of the Upper Panel Diagonals.

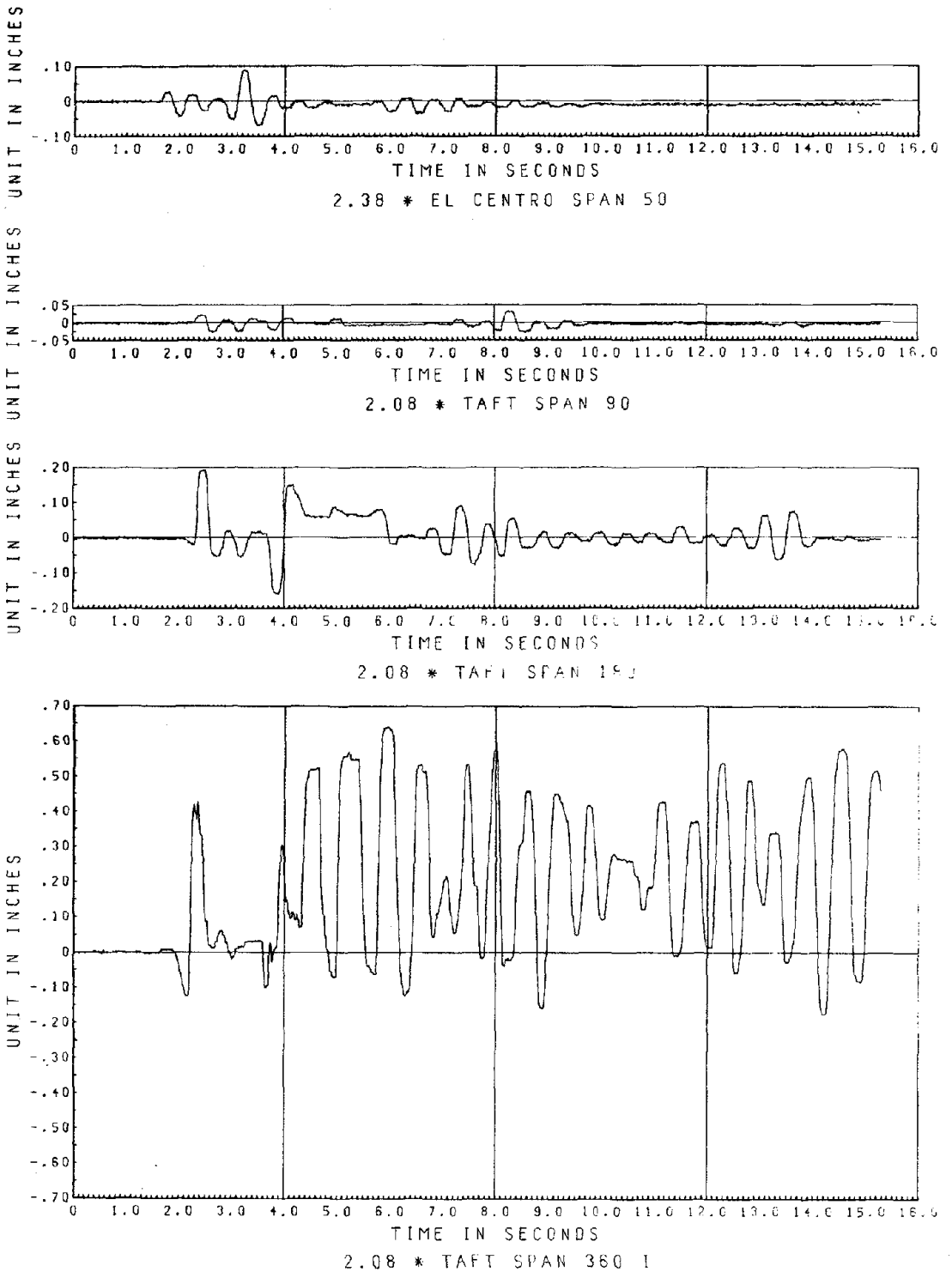

Fig. 5.32 Time History of Out-of-Plane Deflection of the Upper Cross Joint. (Tests 1, 2, 3, 4).

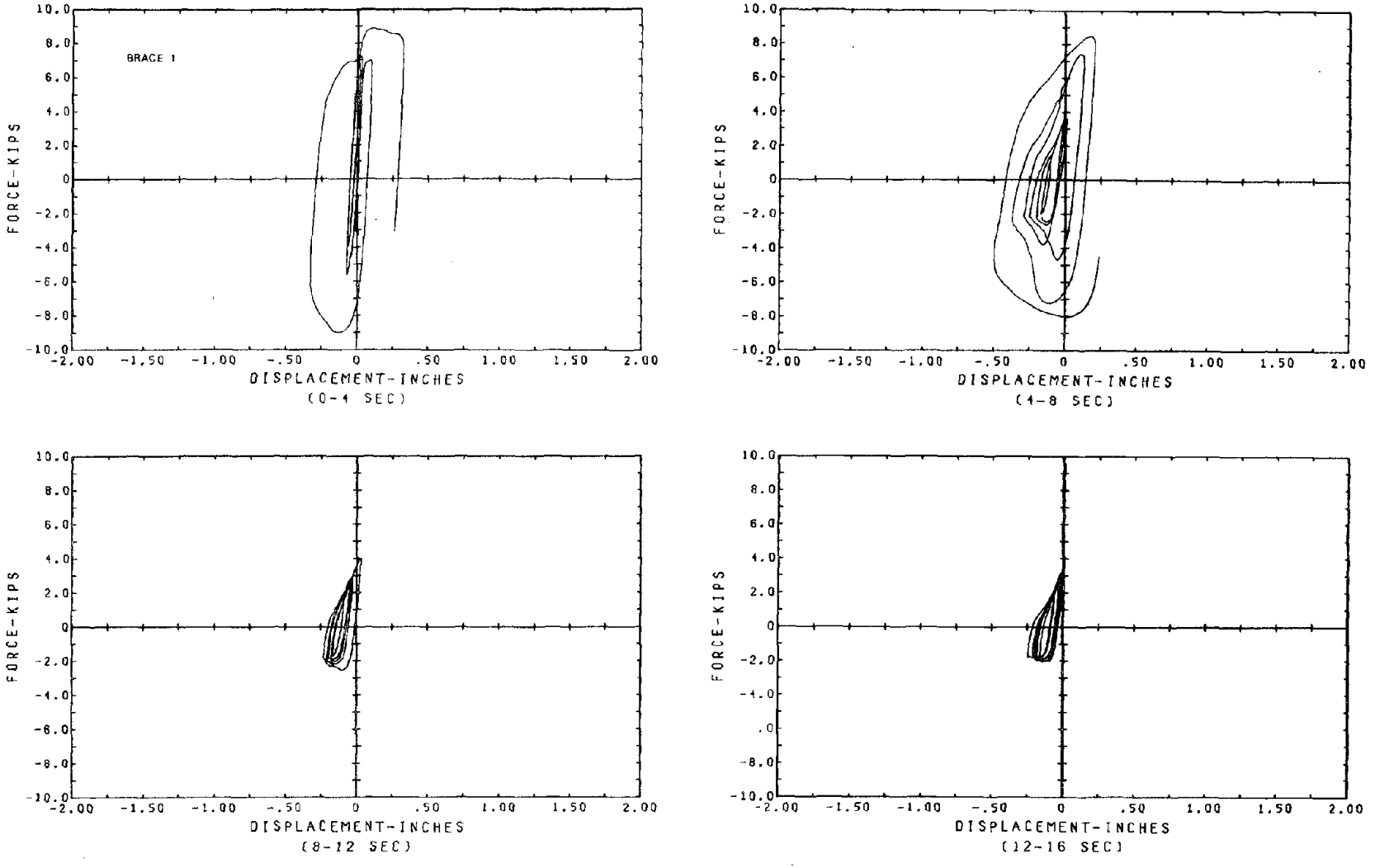

BRACE 1, FORCE VS. DISPLACEMENT
5/48 SCALED MODEL
OFFSHORE PLATFORM TUBULAR FRAME
2.08 * TAFT SPAN 360I

Fig. 5.33 Axial Force - Axial Displacement Hysteresis Loops of Brace 1. (Taft 360 I)

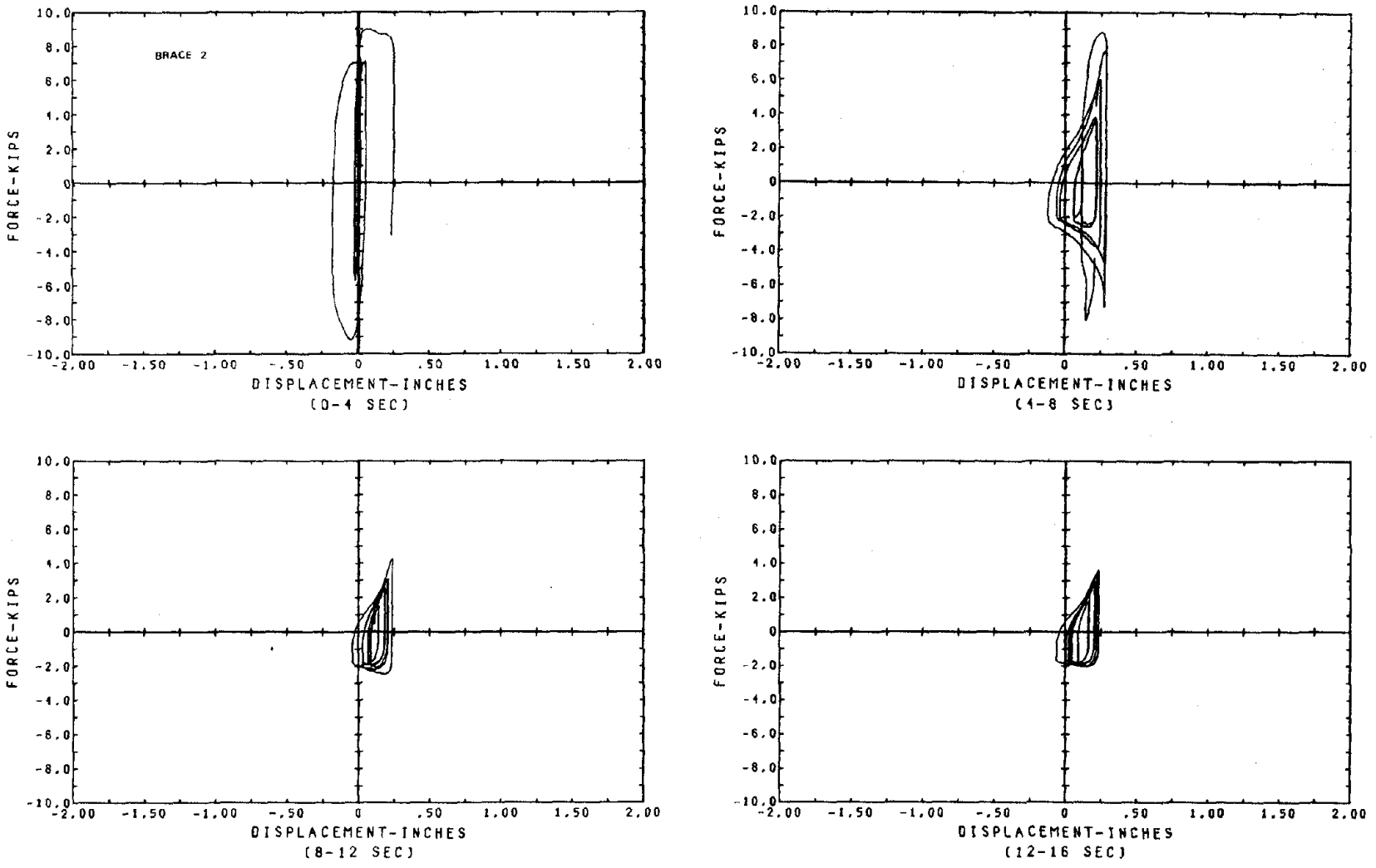

Fig. 5.34 Axial Force - Axial Displacement Hysteresis Loops of Brace 2. (Taft 360 I)

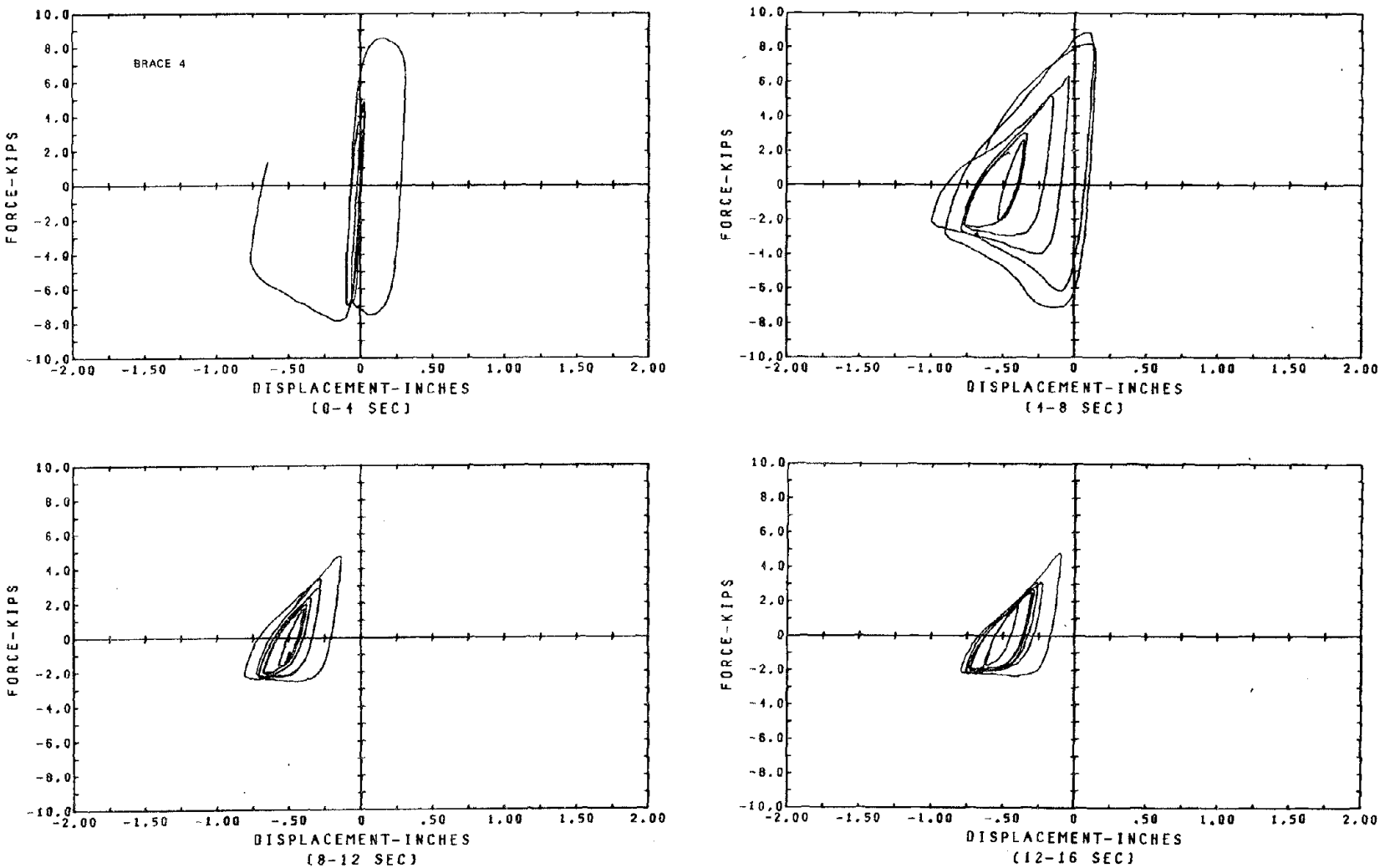

BRACE 4, FORCE VS. DISPLACEMENT
5/48 SCALED MODEL
OFFSHORE PLATFORM TUBULAR FRAME
2.08 * TAFT SPAN 360 I

Fig. 5.35 Axial Force - Axial Displacement Hysteresis Loops of Brace 4. (Taft 360 I)

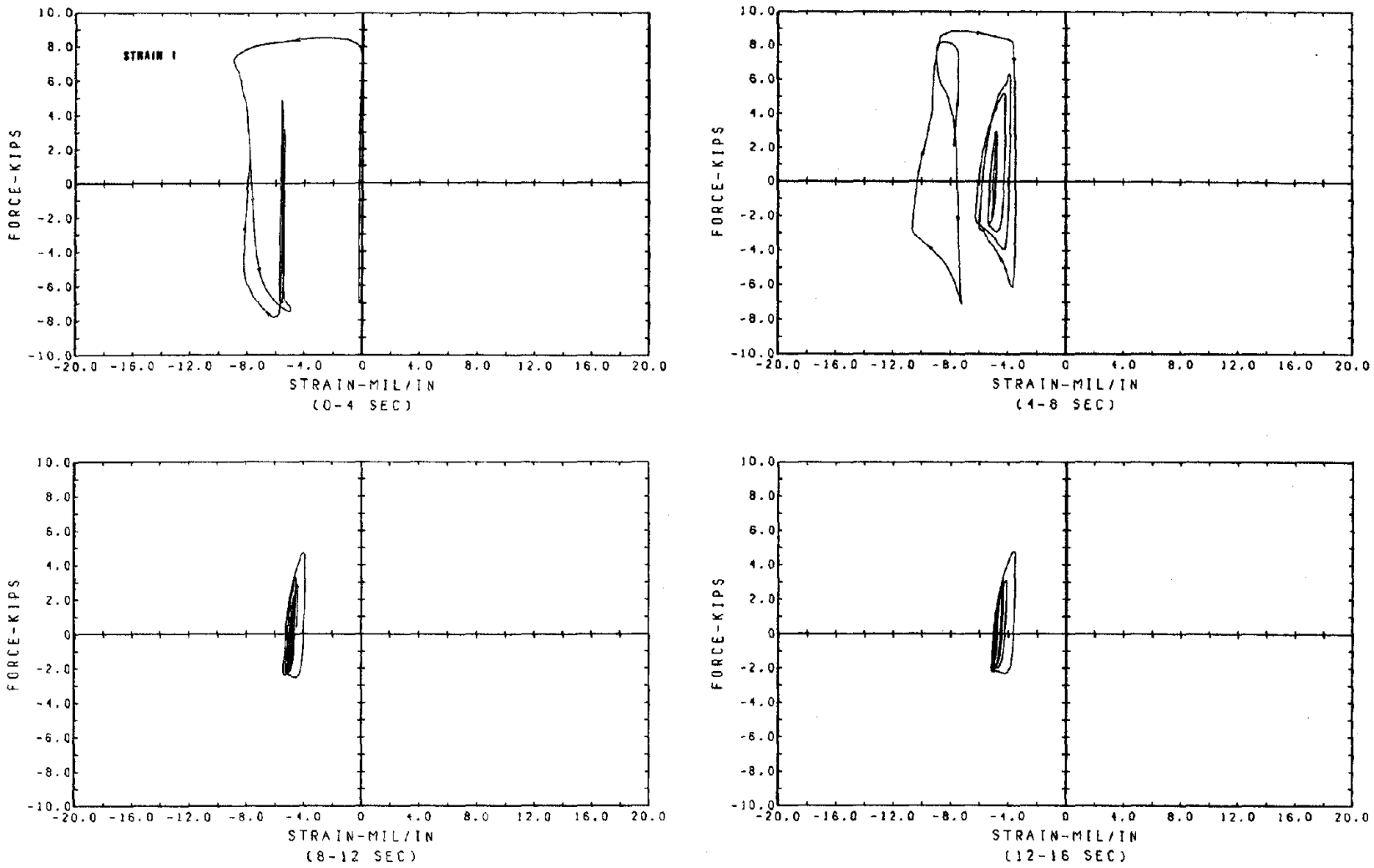

Fig. 5.36 Axial Force vs. Out-of-Plane Bending Strain of Brace 4 at the Brace-to-Jacket Connection End.

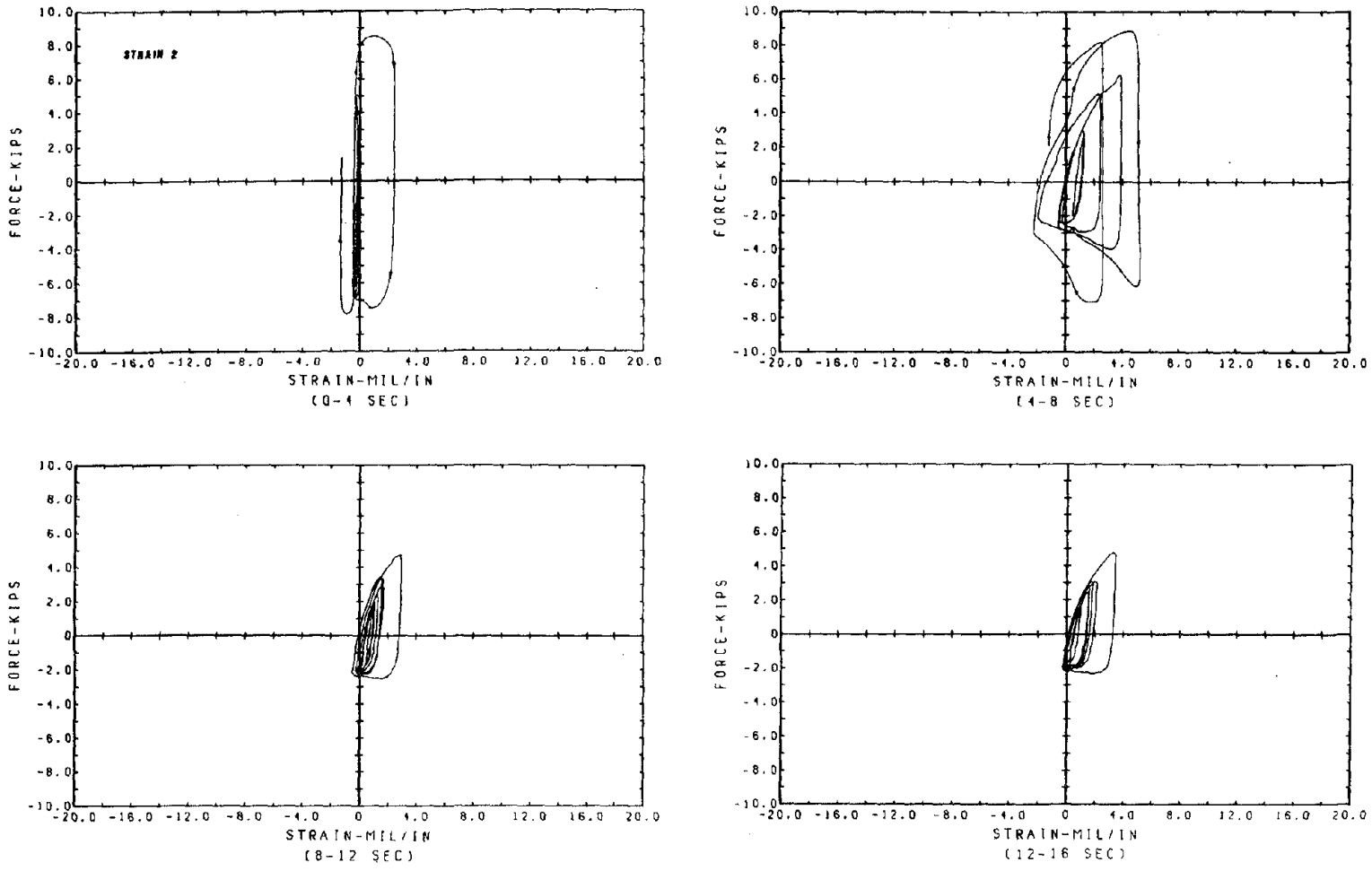

Fig. 5.37 Axial Force vs. Out-of-Plane Bending Strain of Brace 4 at the Diagonal Cross-Joint End.

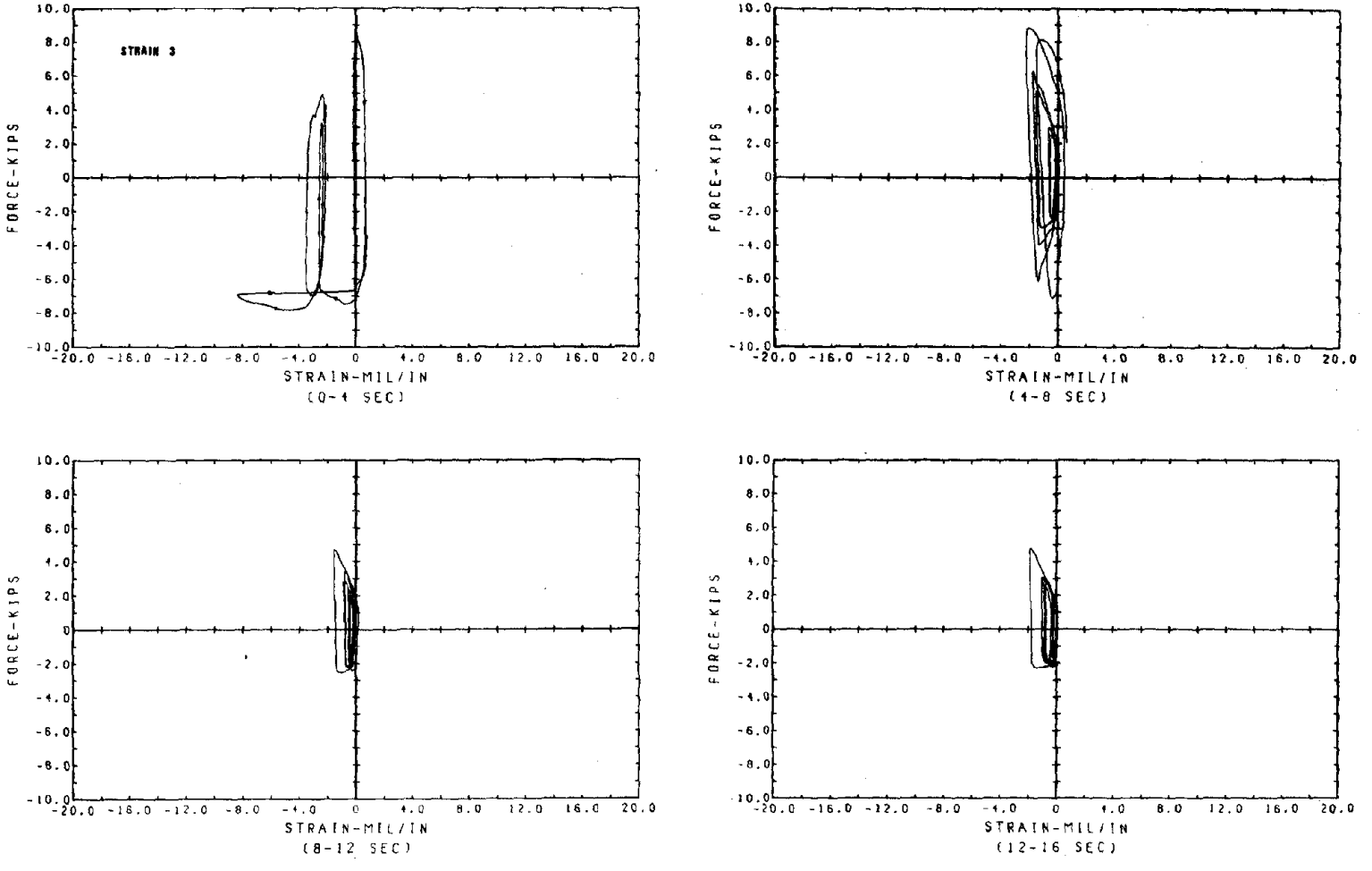

Fig. 5.38 Axial Force vs. In-Plane Bending Strain of Brace 4 at the Brace-to-Jacket Connection End. (Taft 360 I)

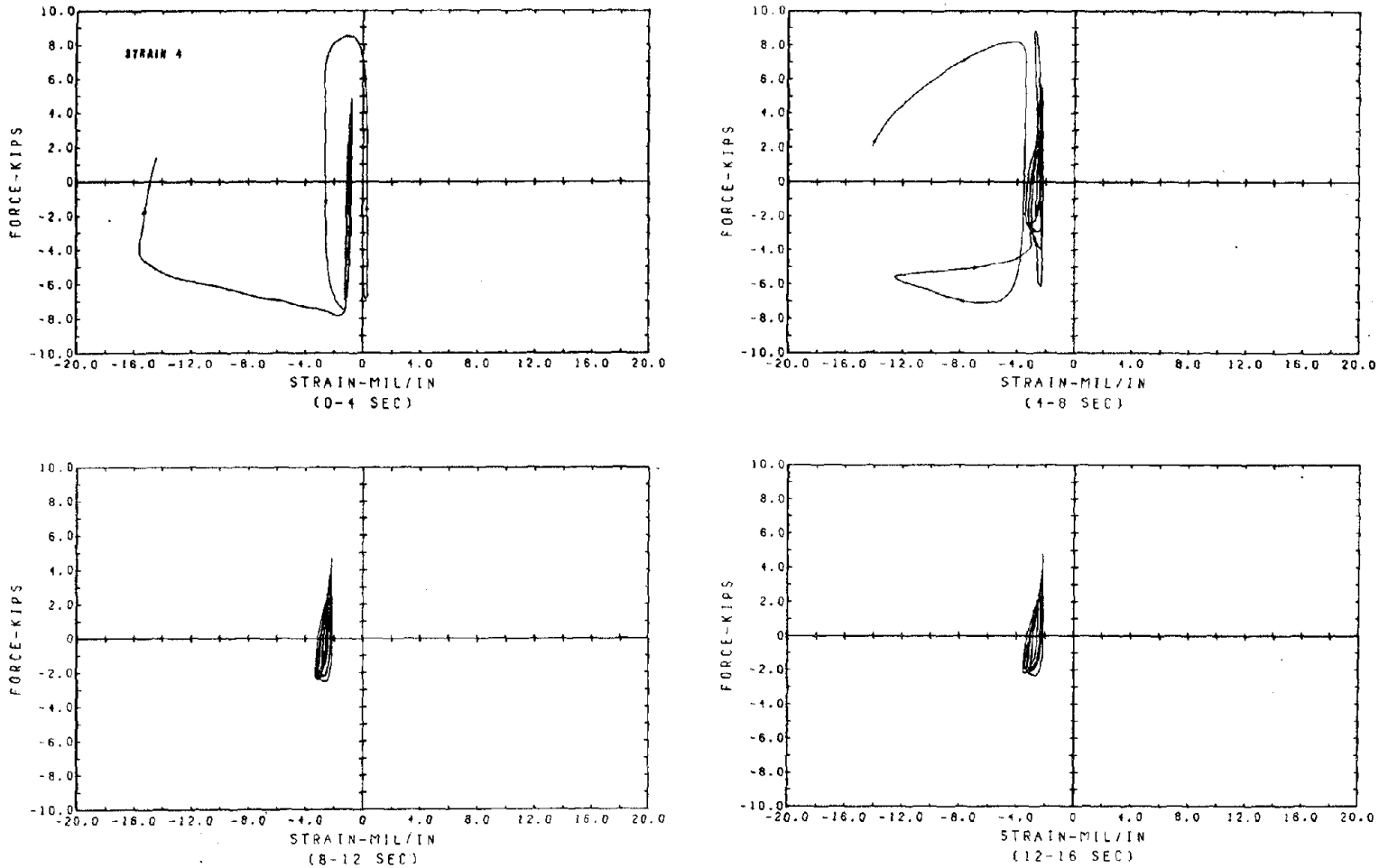

Fig. 5.39 Axial Force vs. In-Plane Bending Strain of Brace 4 at the Diagonal Cross-Joint End. (Taft 360 I)

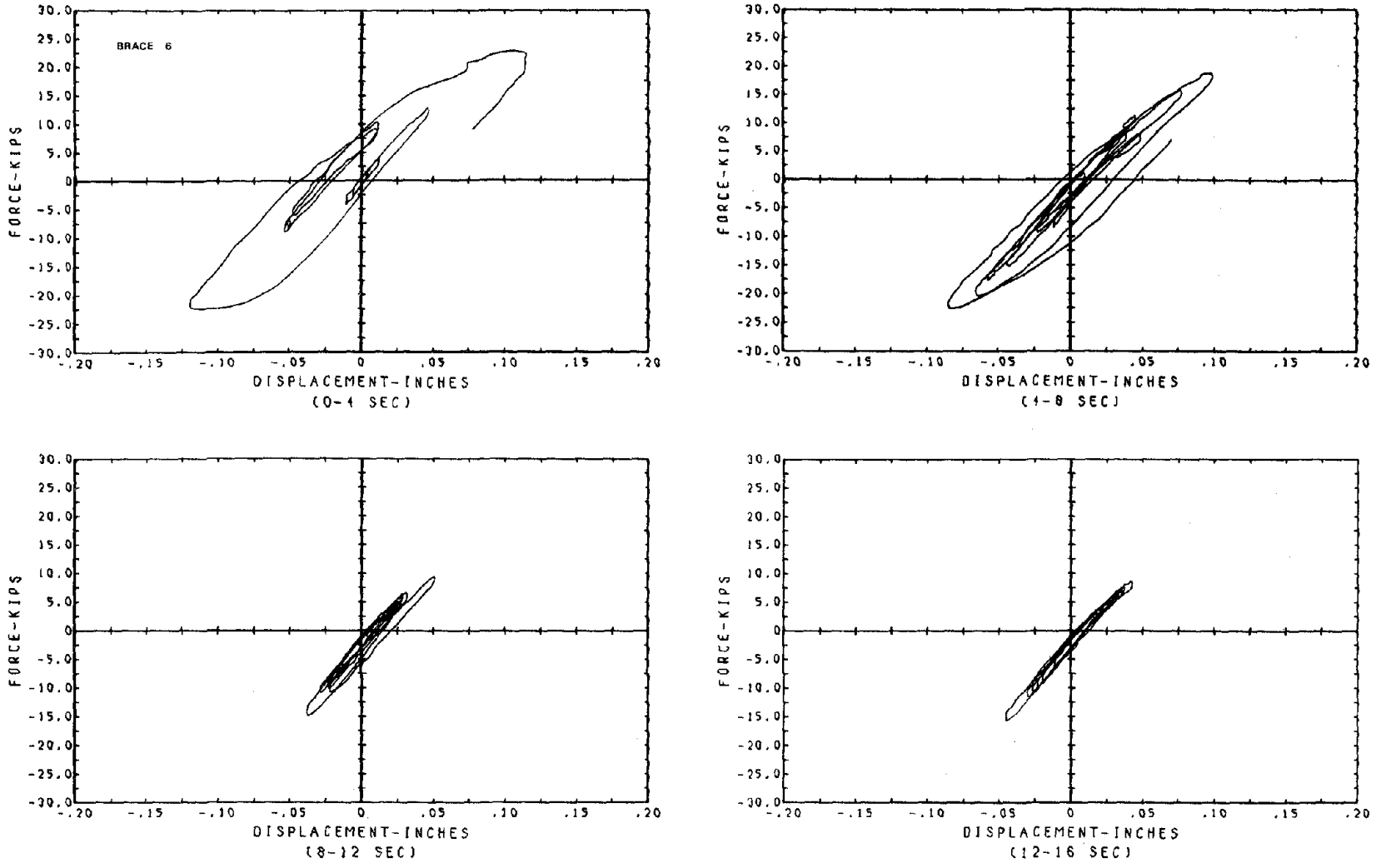

5/48 SCALED MODEL
OFFSHORE PLATFORM TUBULAR FRAME
2.08 * TAFT SPAN 360I

Fig. 5.40 Axial Force - Axial Displacement Hysteresis Loops of Brace 6. (Taft 360 I)

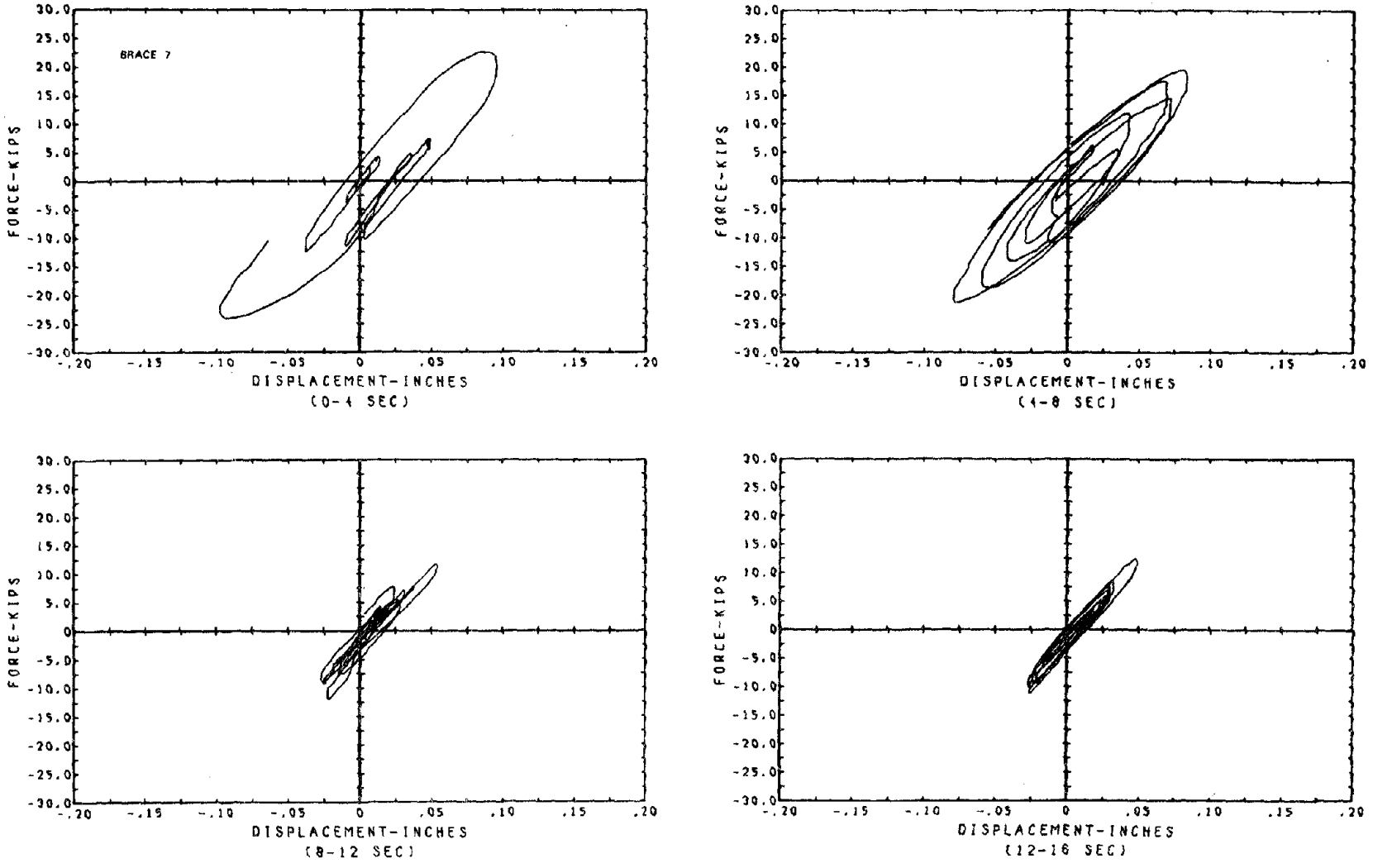

Fig. 5.41 Axial Force - Axial Displacement Hysteresis Loops of Brace 7. (Taft 360 I)

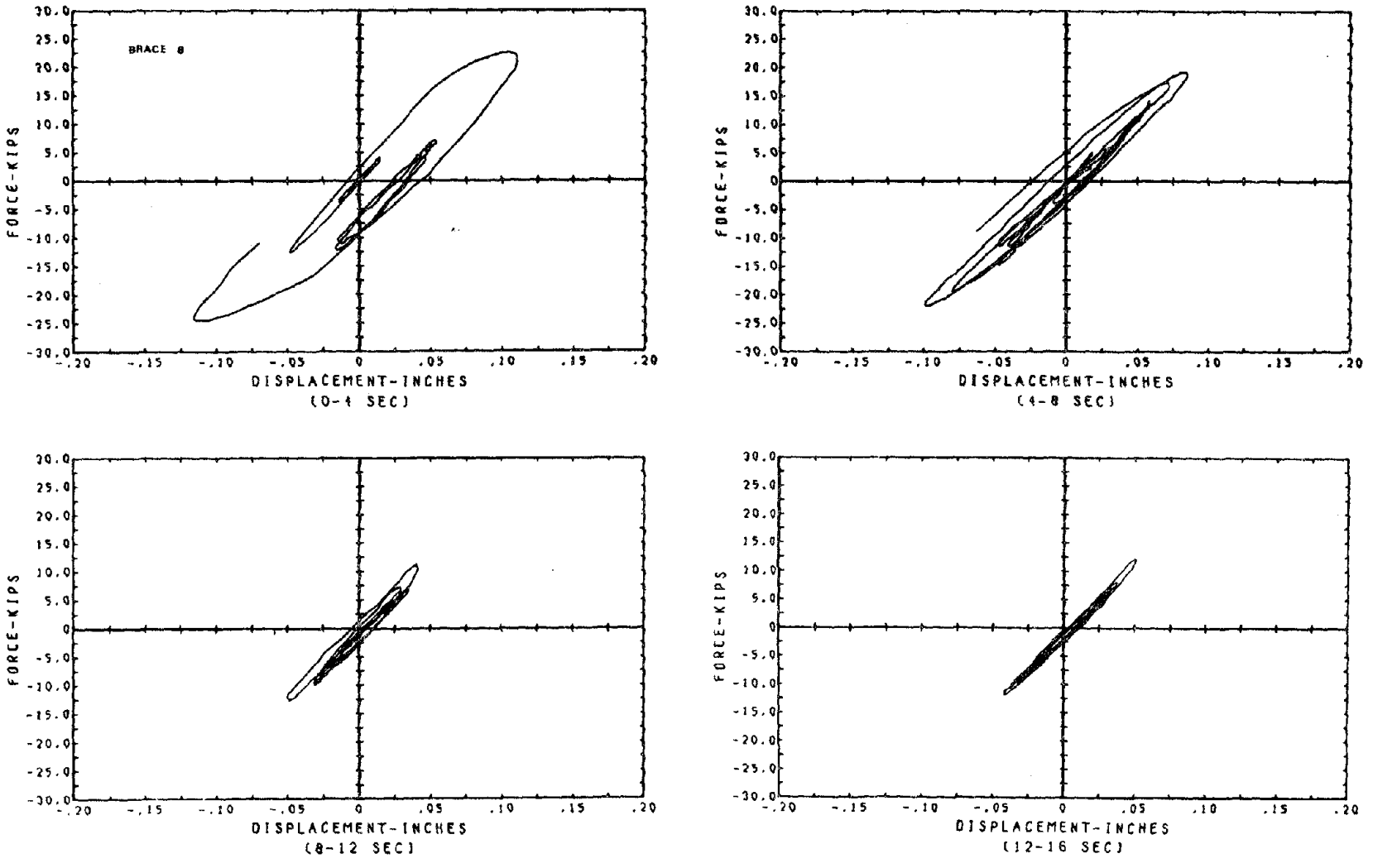

5/48 SCALED MODEL
OFFSHORE PLATFORM TUBULAR FRAME
2.08 * TAFT SPAN 360I

Fig. 5.42 Axial Force - Axial Displacement Hysteresis Loops of Brace 8. (Taft 360 I)

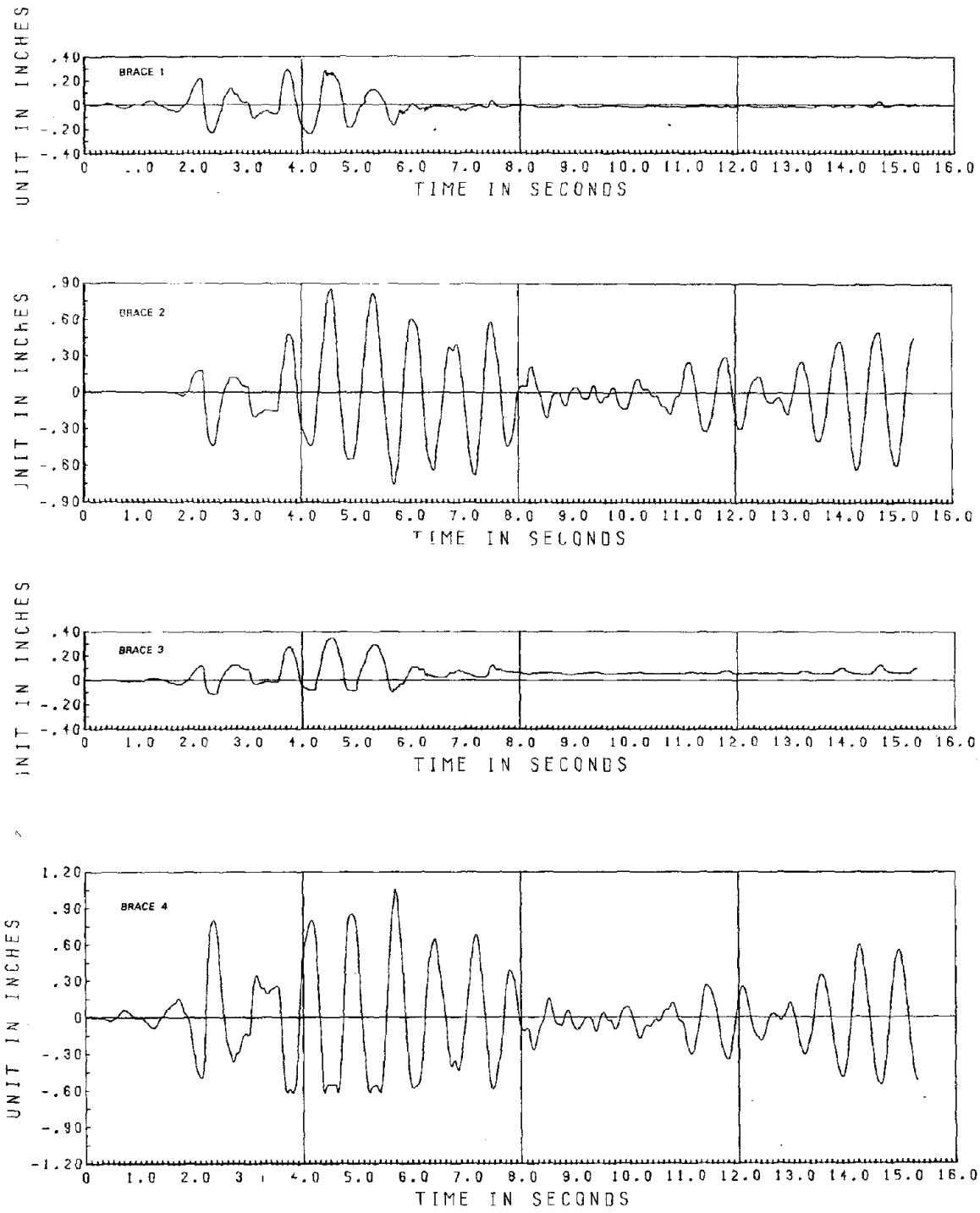

Fig. 5.43 Axial Displacement Time Histories of the Upper Panel Diagonals. (Taft 360 II)

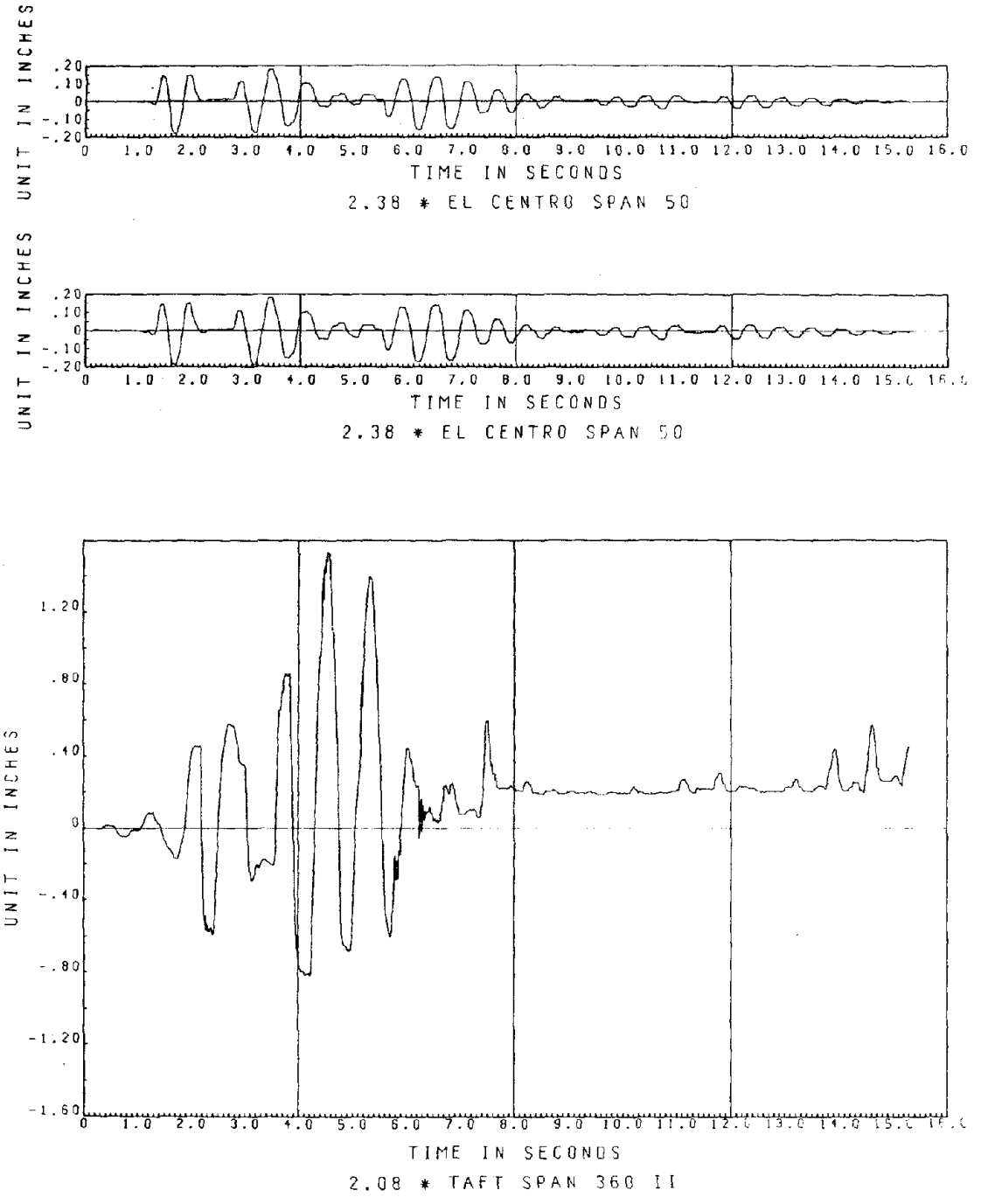

Fig. 5.44 Time History of Out-of-Plane Deflection of Upper Cross Joint. (Tests 5, 6, 7)

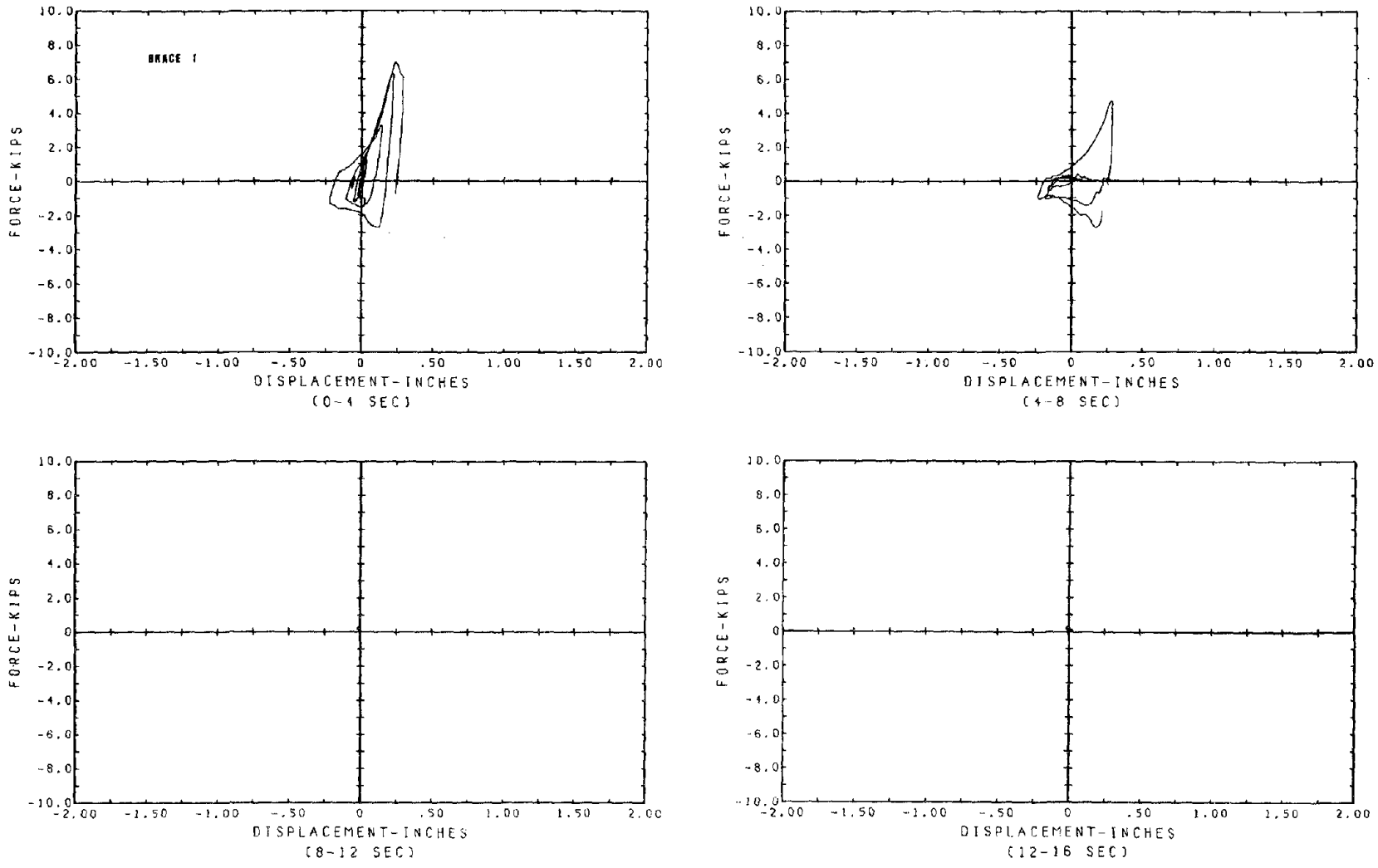

Fig. 5.45 Axial Force - Axial Displacement Hysteresis Loops of Brace 1. (Taft 360 II)

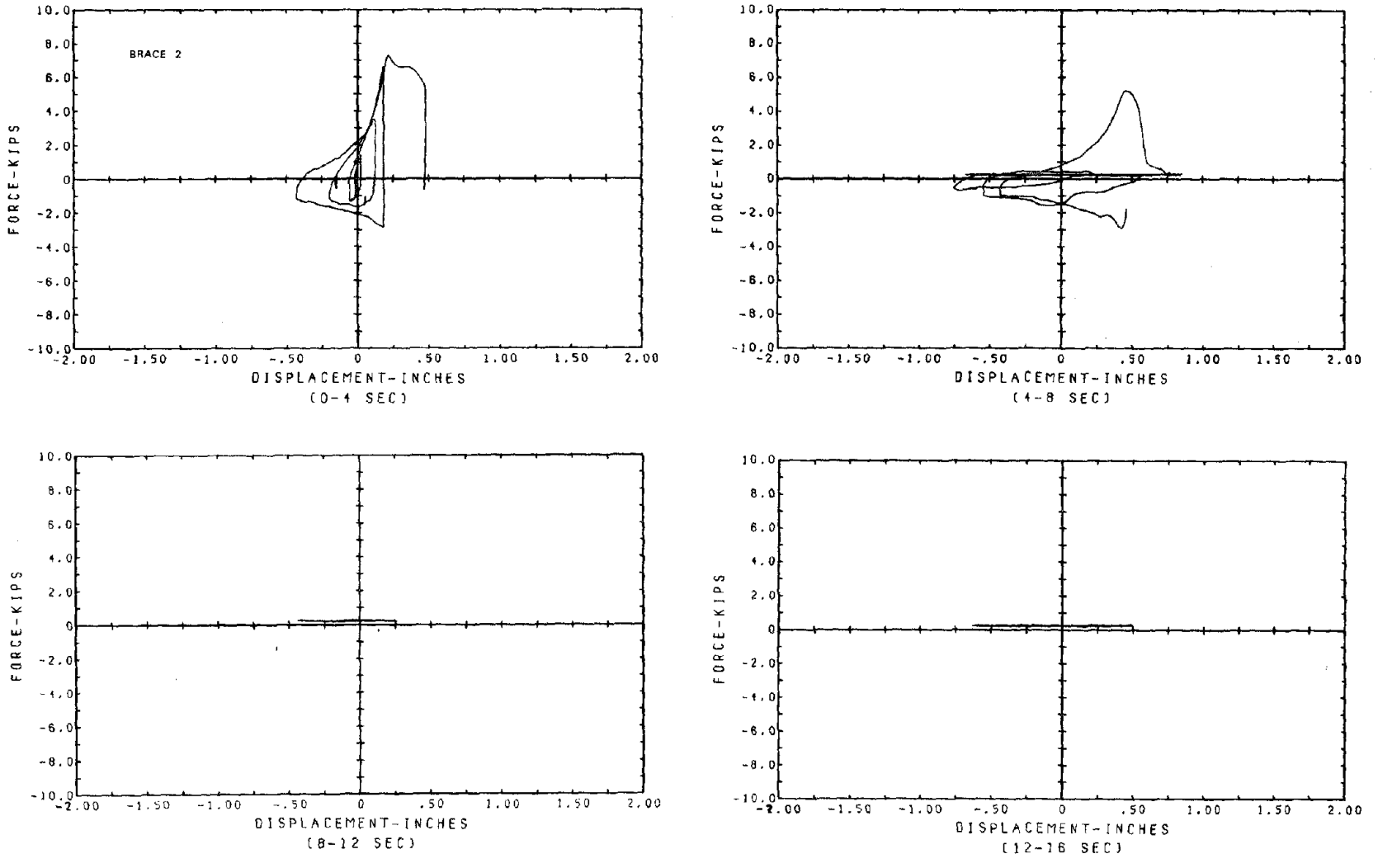

Fig. 5.46 Axial Force - Axial Displacement Hysteresis Loops of Brace 2. (Taft 360 II)

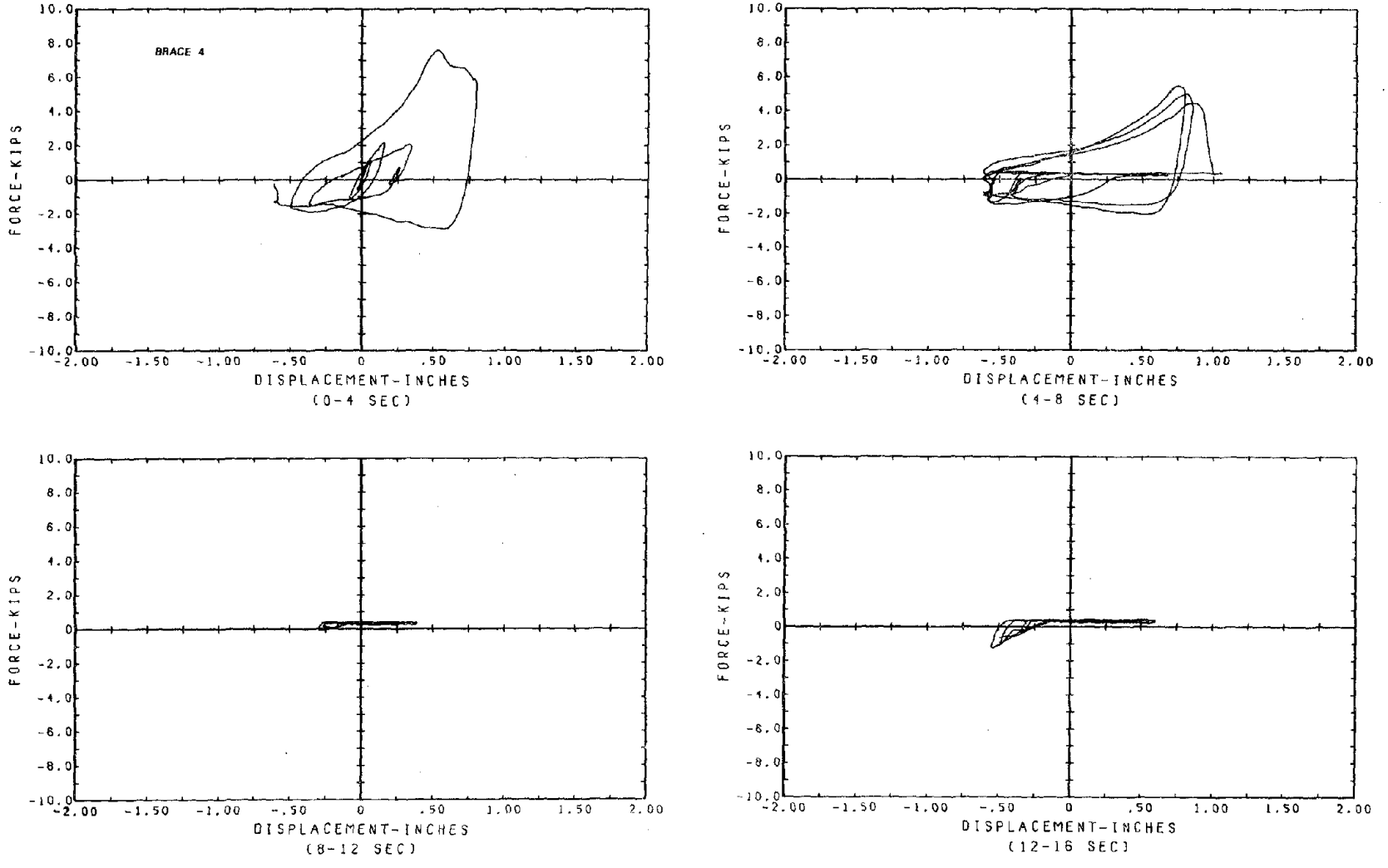

Fig. 5.47 Axial Force - Axial Displacement Hysteresis Loops of Brace 4. (Taft 360 II)

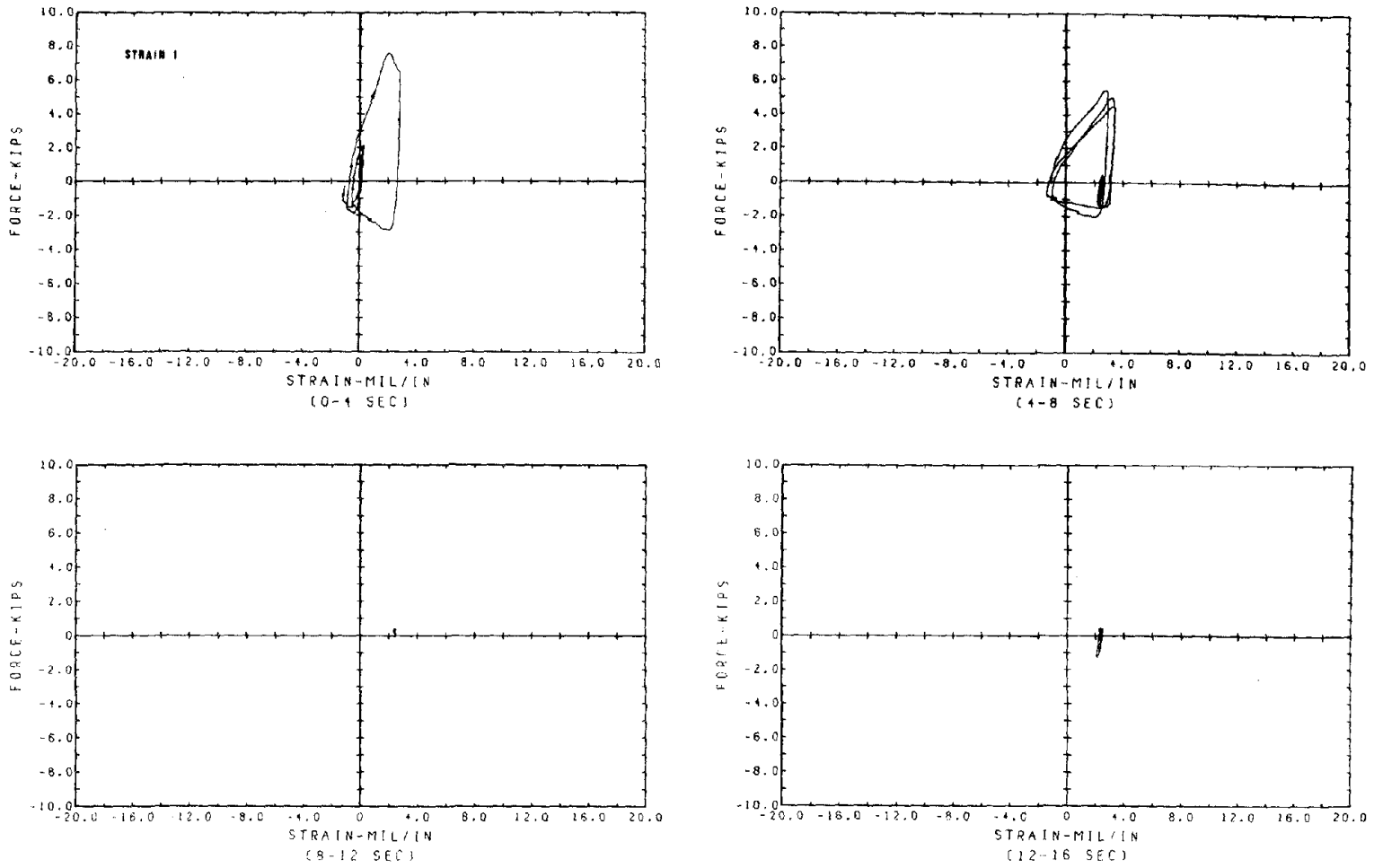

Fig. 5.48 Axial Force vs. Out-of-Plane Bending Strain of Brace 4 at the Brace-to-Jacket Connection End. (Taft 360 II)

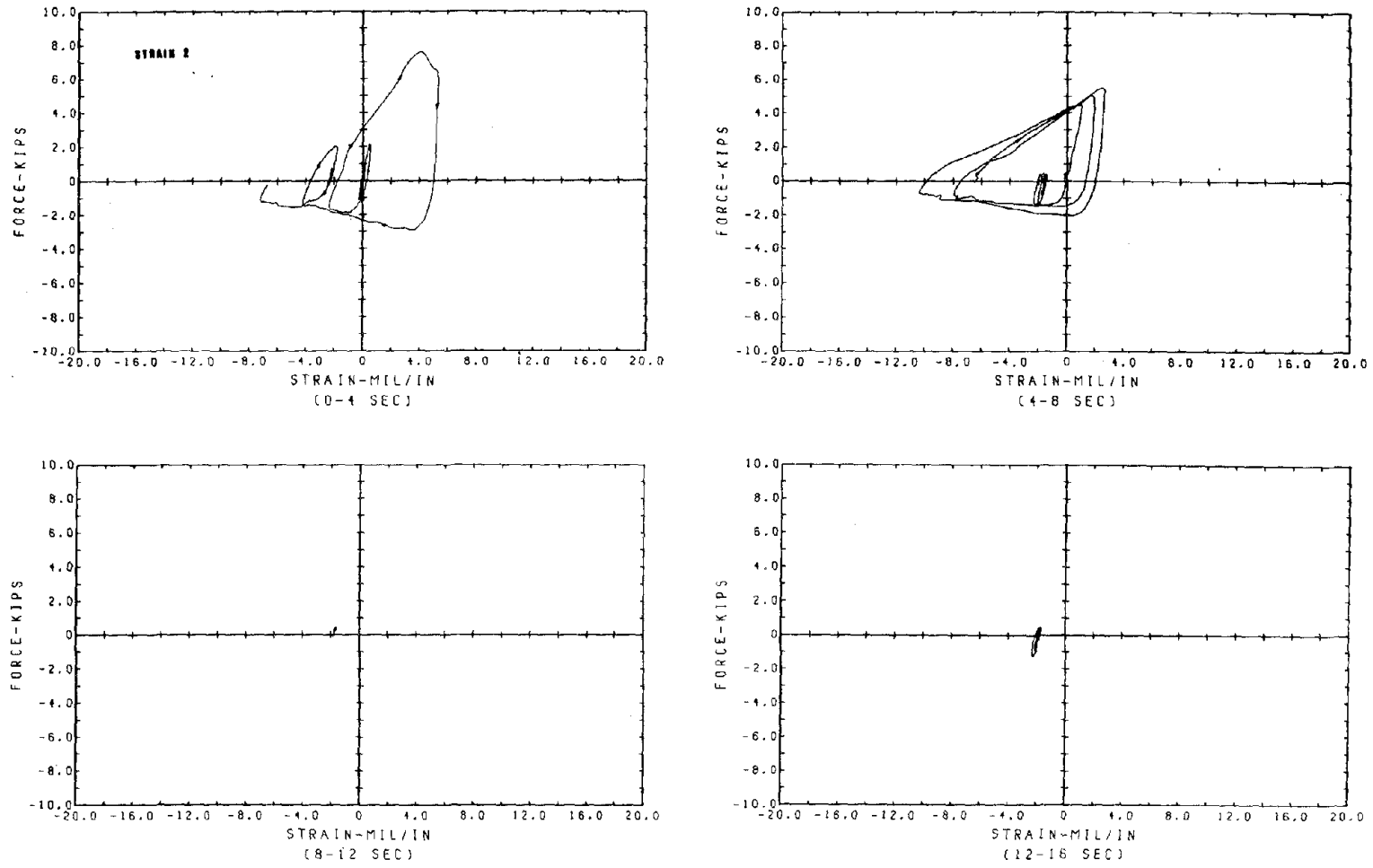

Fig. 5.49 Axial Force vs. Out-of-Plane Bending Strain of Brace 4 at the Diagonal Cross-Joint End. (Taft 360 II)

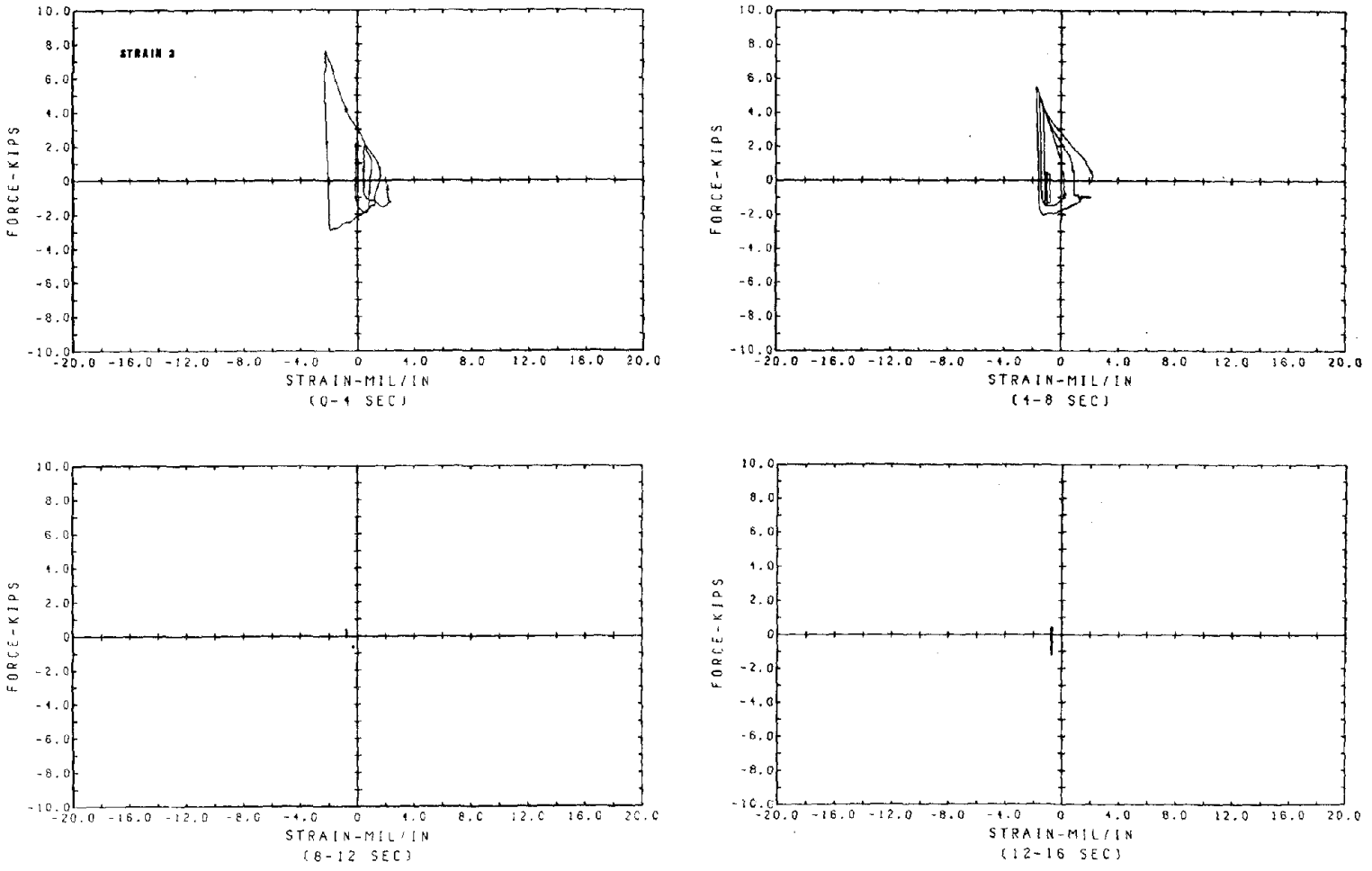

Fig. 5.50 Axial Force vs. In-Plane Bending Strain of Brace 4 at the Brace-to-Jacket Connection End. (Taft 360 II)

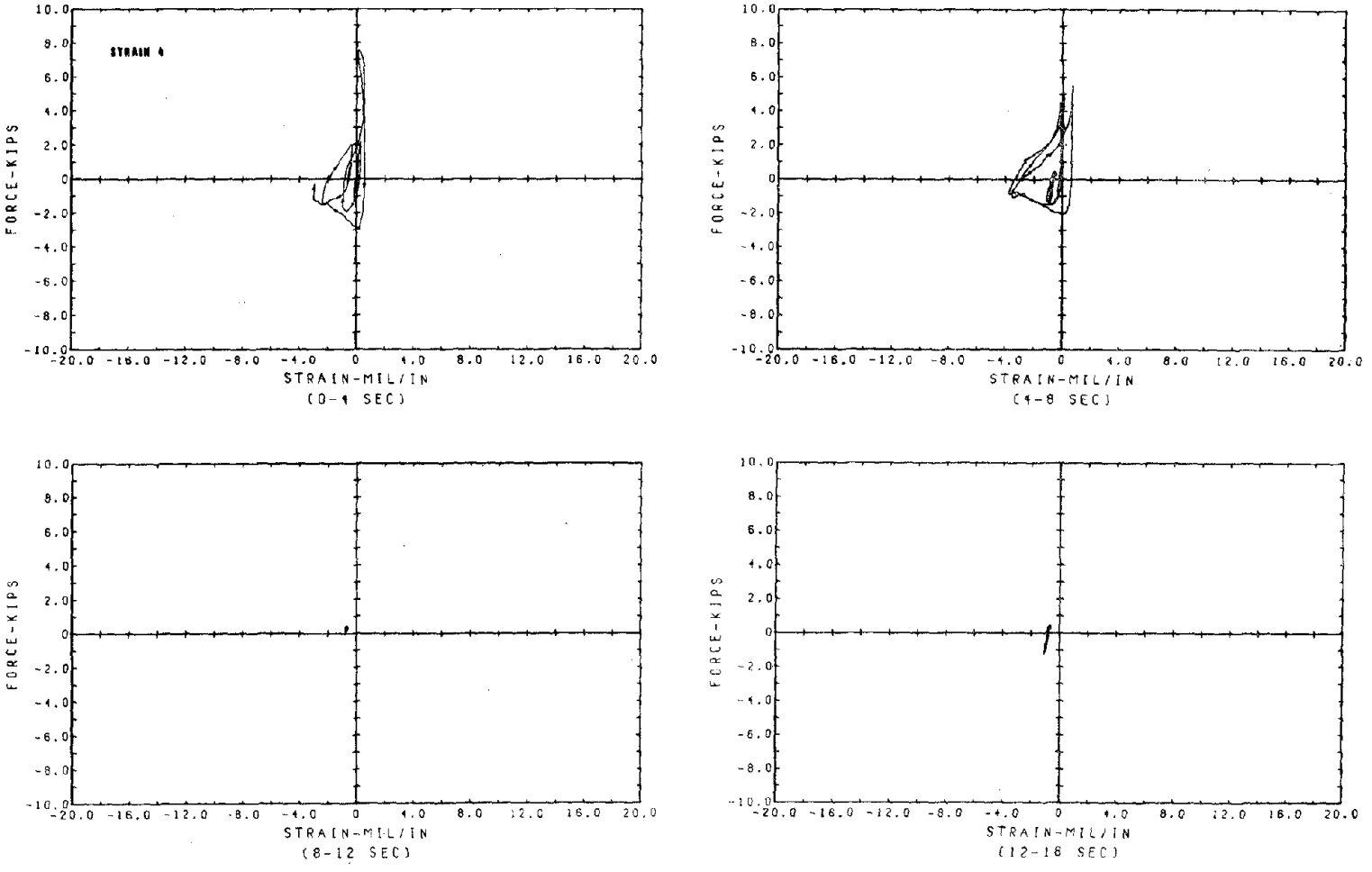

Fig. 5.51 Axial Force vs. In-Plane Bending Strain of Brace 4 at the Diagonal Cross-Joint End. (Taft 360 II)

6. CONCLUDING REMARKS

This investigation demonstrated the feasibility of dynamic testing of a two dimensional scale model of a typical fixed tubular x-braced offshore platform by means of a shaking table. The experimental data obtained on the overall seismic response of the test model subjected to various earthquake excitations comparable with the API "Strength Level", "Ductility Level", and "Maximum Credible" motions has been presented in this report. Based on those results, the following remarks and observations can be made:

1. The inelastic behavior of the test model demonstrated that for a properly designed braced frame, a moderate amount of energy dissipation can be achieved during severe earthquake input due to the inelastic buckling and tension yielding of bracing members.
2. Member buckling was initiated in the x-bracing members of the upper panel as expected, and it is important to note that the low strength of this panel limited the axial loads transmitted to the braces of the lower panel. Consequently, buckling did not progress to the bracing members of the lower panel during subsequent response cycles, and thus the force-displacement hysteresis loops for the complete frame obtained in this study were not as full as those obtained during the forced displacement inelastic cyclic test[11].
3. Buckling of the braces tended to be concentrated in one brace of a full diagonal, with a visible minor bowing of the adjoining brace along the same diagonal. Such behavior, which was also observed in the pseudo-dynamic cyclic test[11], would be expected due to differences in initial imperfections or secondary moments. As one brace of a full diagonal buckles, local failures made possible

by the high D/t ratio of the tubings reduce the buckling load in subsequent cycles, and thus, prevent inelastic deformation in the straighter brace.

4. When the test frame was subjected to the "Maximum Credible" earthquake, x-bracing members in the upper panel deteriorated rapidly due to inelastic buckling and local failures. But the resulting lateral forces in the damaged frame (a much softer structure) were reduced due to the smaller dynamic magnification for this reduced period system; consequently, there was no danger of collapse, even though the lateral force resistance was greatly reduced.
5. This test demonstrated again that survival of a structure subjected to severe earthquake motions depends almost entirely on its ability to accommodate the necessary lateral displacements while maintaining its vertical load carrying capacity. The ability to absorb energy during inelastic deformations may be useful in limiting the amplitude of dynamic displacements, but it is not essential to the survival of the structure if the imposed displacements can be accommodated by the vertical load carrying system.
6. Experimental results showed that there was significant interaction between the shaking table and the test model during this investigation. Such interaction was manifested by pitching motion of the shaking table, and it must be included in the mathematical modeling in order to achieve successful correlation with computer analyses. Unfortunately the interaction is a highly nonlinear mechanism, and must be defined numerically by trial and error procedures.

REFERENCES

1. American Petroleum Institute, "Recommended Practice for Planning, Designing, and Constructing Fixed Offshore Platforms," Dallas, Texas, 8th Ed., 1977; 9th Ed., 1977; 10th Ed., 1979; 11th Ed., 1980.

2. Sherman, D.R., "Tests of Circular Steel Tubes in Bending," Journal of the Structural Division, ASCE, Vol. 102, ST11, November 1976.

3. Bouwkamp, J.G., "Buckling and Post-buckling Strength of Circular Tubular Sections," Proc. 1975 Offshore Tech. Conference, OTC 2204.

4. Zayas, V.A., Popov, E.P., and Mahin, S.A., "Cyclic Inelastic Behavior of Tubular Steel Braces," Report No. UCB/EERC-80/16, Earthquake Engineering Research Center, University of California, Berkeley, 1980.

5. Sherman, D.R., "Cyclic Inelastic Behavior of Beam Columns and Struts," Preprint 3302, ASCE Convention and Exposition, Chicago, October 1978.

6. Briggs, M.J., and Maison, J.R., "Test of X-Braced Subassemblage," Preprint 3302, ASCE Convention and Exposition, Chicago, October 1978.

7. Marshall, P.W., "Post Buckling Behavior of Tubular Truss Elements," presented at 1976 Annual Meeting of Structural Stability Research Council (formerly CRC), Atlanta.

8. Gates, W.E., and Berger, E., "Documentation of New Elements in Non-linear Analysis Program DYNAS," Dames and Moore Report for Shell Oil Company, September 1976.

9. Marshall, P.W., Gates, W.E., and Anagnostopoulos, "Inelastic Dynamic Analysis of Tubular Offshore Structures," Proceedings, 1977 Offshore Tech. Conf., OTC 2908.

10. Litton, R.W., Pawsey, S.F., Stock, D.J., and Wilson, B.M., "Efficient Numerical Procedures for Nonlinear Seismic Response Analysis of Braced Tubular Structures," Preprint 3302, ASCE Convention and Exposition, Chicago, October 1978.

11. Zayas, V.A., Mahin, S.A., and Popov, E.P., "Cyclic Inelastic Behavior of Steel Offshore Structures," Report No. UCB/EERC-80/27, Earthquake Engineering Research Center, University of California, Berkeley, 1980.

12. Gates, W.E., Marshall, P.W., and Mahin, S.A., "Analytical Methods for Determining the Ultimate Earthquake Resistance of Fixed Offshore Structures," Proceeding, Offshore Technology Conference, OTC 2751, Houston, Texas, 1977.

13. Rea, D., and Penzien, J., "Dynamic Response of a 20' x 20' Shaking Table," Proceeding of the 5th World Conference on Earthquake Engineering, Rome, 1973.

14. Ghanaat, Y., "Study of X-Braced Steel Frame Structure Under Earthquake Simulation," EERC Report No. 80-08, Earthquake Engineering Research Center, University of California, Berkeley, April 1980.

15. Clough, R.W., and Ghanaat, Y., "Seismic Behavior of Diagonal Steel Wind Bracing," Proceedings of the 2nd U.S. National Conference on Earthquake Engineering, Stanford University, August, 1979.

16. Tang, D.T., "Earthquake Simulator Study of a Steel Frame Structure, Vol. II: Analytical Results," Report No. UCB/EERC-75-36, Earthquake Engineering Research Center, University of California, Berkeley, 1975.

17. Huckelbridge, A.A., and Clough, R.W., "Seismic Response of Uplifting Building Frame," Journal of the Structural Division, ASCE, Vol. No. ST8.

18. Nigam, N.C., and Jennings, P.C., "Digital Calculation of Response Spectra from Strong-Motion Earthquake Records," Earthquake Engineering Research Laboratory, California Institute of Technology, Pasadena, 1968.

APPENDIX A

LATERAL SUPPORT LINKAGES

LATERAL SUPPORT LINKAGES

The lateral support linkages used in the experiment were based on "Watt's mechanism" shown below. This mechanism consists of two lever arms attached at one end to the fixed points A and D and to a coupler member (BC) at the other end. All attachments are hinge type joints.

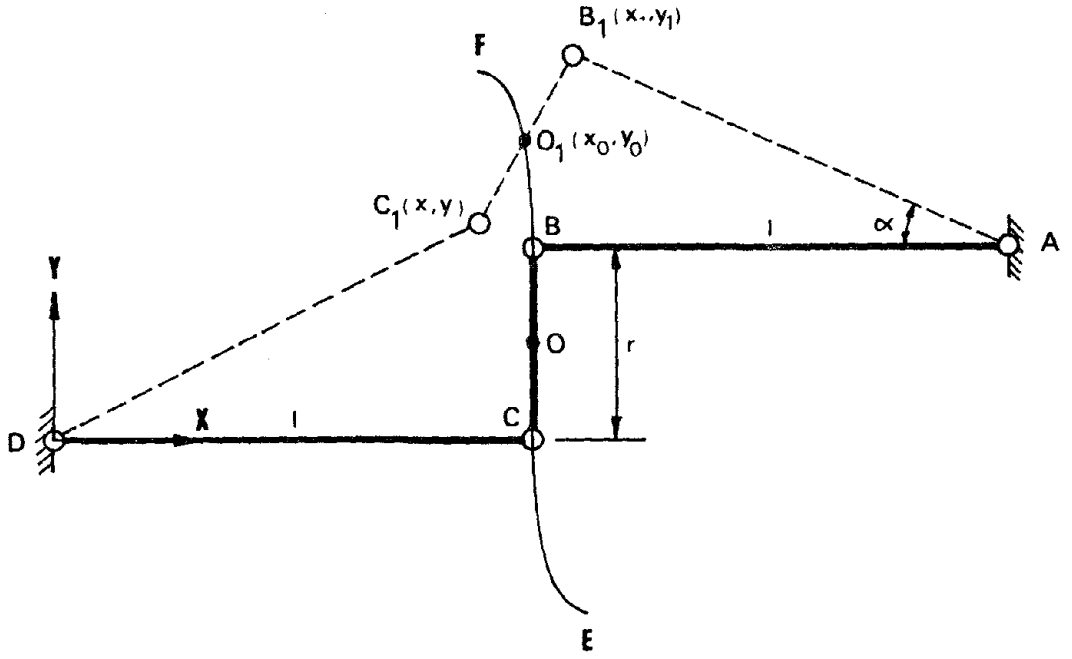

It can be shown that as the mechanism moves, point O (center of the coupler r) follows the path indicated as EF. This path is a straight line parallel to the orientation of the coupler for small movements of the mechanism, but becomes a curved line for larger movements.

Lateral movements associated with an angular movement α can be expressed as follows:

$$x_1 = 2\ell - \ell \cos\alpha \tag{1}$$

$$y_1 = r + \ell \sin\alpha. \tag{2}$$

Also using kinematics and the fact that all members are assumed inextensible we have

$$x^2 + y^2 = \ell^2 \tag{3}$$

$$(x-x_1)^2 + (y-y_1)^2 = r^2. \tag{4}$$

Eliminating x in equations (3) and (4) we obtain,

$$y^2 - 2\,B\,y + C = 0 \tag{5}$$

where

$$B = \frac{1}{2}\{\, y_1(\ell^2 + x_1^2 + y_1^2 - r^2)/(x_1^2 + y_1^2)\,\}$$

$$C = \frac{1}{4}\{\, [(\ell^2 + x_1^2 + y_1^2 - r^2)^2 - 4x_1^2\ell^2]/(x_1^2 + y_1^2)\,\}\ .$$

Only the smaller root of the quadratic equation (5) is significant, thus

$$y = B - \sqrt{B^2-C}\ . \tag{6}$$

Substituting y into equation (3), x is found to be

$$x = \sqrt{\ell^2 - (B-(B^2-C)^{1/2})^2}. \tag{7}$$

Therefore the position of point "0_1", the center point of the coupler member in the deformed configuration, is known and may be expressed as follows:

$$x_{0_1} = (x + x_1)/2 \tag{8}$$

$$y_{0_1} = (y + y_1)/2. \tag{9}$$

The relative position of point 0_1 with respect to the initial position 0 is given by

$$\Delta x = x_{0_1} - \ell \tag{10}$$

$$\Delta y = y_{0_1} - r/2. \tag{12}$$

Using the above formulation, (x_{0_1}, y_{0_1}) and $(\Delta x, \Delta y)$ were calculated for a wide range of angles "α" varying from -20° to $+20^\circ$, with results tabulated below. These numerical results show that Δx remains essentially zero for all angles in

the range $-7 \leq \alpha \leq 7^{o}$, corresponding to lateral movements of $-5.6 \leq \Delta y \leq 5.6$ in. In other words, point 0 moves on a straight line coincident with the coupler orientation for angles $-7^{o} \leq \alpha \leq 7^{o}$ and deviates gradually from the straight line as α becomes larger. The tabulated results are based on a 45.75 in. lever arm and a 16.0 in. coupler. Because the extent of the straight line path is a function of ℓ and r, any desired range can be obtained by proper selection of ℓ and r.

In dynamic testing of the 2D offshore frame, the lateral support linkages were designed to allow the test model to move freely in the longitudinal and vertical directions (plane of table motion) but would prevent lateral (out-of-plane) movements. They were designed based on "Watt's mechanism", but all attachments were provided by spherical bearing joints so that motions in a plane perpendicular to bracing arms were permitted (see Fig.A1 and the graph shown below). It can be shown that as the mechanism moves, point 0 (center of the coupler BC) travels in a yz plane passing through the coupler BC. The elliptical surface shown below is the upper bound for all possible positions of point 0 with essentially zero lateral movements (movement in x direction). The two diameters of the ellipse indicate the maximum acceptable travel range of point 0 in the y and z direction.

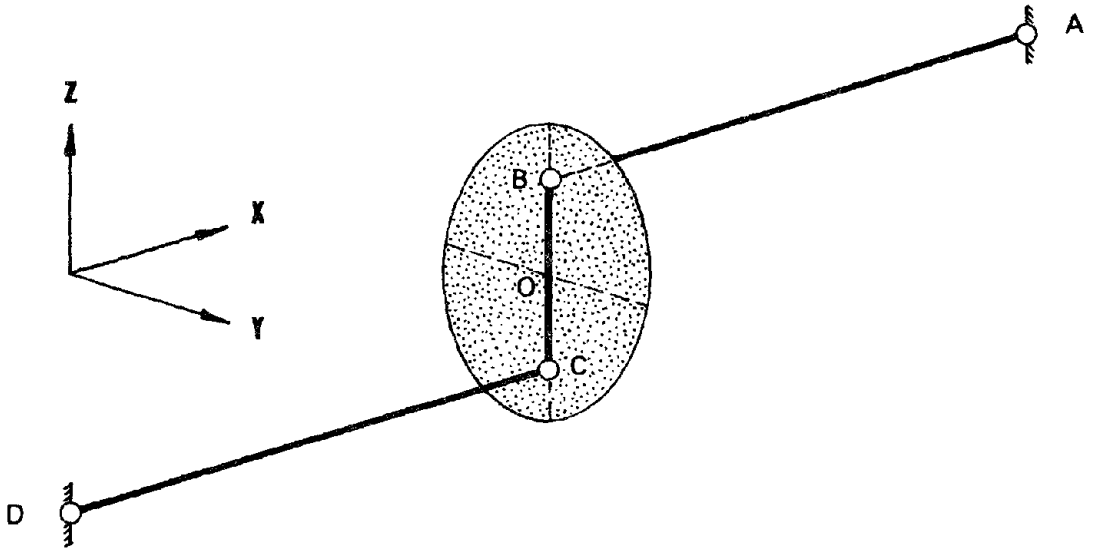

L=45.750 R=16.000

ALPHA	XO1	YO1	DX	DY
-20	45.903	-7.211	.153	-15.211
-19	45.870	-6.535	.120	-14.535
-18	45.843	-5.844	.093	-13.844
-17	45.820	-5.140	.070	-13.140
-16	45.802	-4.423	.052	-12.423
-15	45.788	-3.695	.038	-11.695
-14	45.777	-2.956	.027	-10.956
-13	45.769	-2.207	.019	-10.207
-12	45.762	-1.450	.012	-9.450
-11	45.758	-.686	.008	-8.686
-10	45.755	.085	.005	-7.914
-9	45.753	.862	.003	-7.137
-8	45.751	1.645	.001	-6.354
-7	45.750	2.431	.000	-5.568
-6	45.750	3.221	.000	-4.778
-5	45.750	4.014	.000	-3.985
-4	45.750	4.809	.000	-3.190
-3	45.750	5.605	.000	-2.394
-2	45.750	6.403	-.000	-1.596
-1	45.750	7.201	-.000	-.798
0	45.750	8.000	.000	.000
1	45.750	8.798	-.000	.798
2	45.750	9.596	-.000	1.596
3	45.750	10.394	-.000	2.394
4	45.749	11.192	-.000	3.192
5	45.749	11.989	-.000	3.989
6	45.749	12.786	-.000	4.786
7	45.749	13.582	-.000	5.582
8	45.748	14.379	-.001	6.379
9	45.746	15.176	-.003	7.176
10	45.744	15.975	-.005	7.975
11	45.741	16.774	-.008	8.774
12	45.736	17.576	-.013	9.576
13	45.729	18.381	-.020	10.381
14	45.719	19.189	-.030	11.189
15	45.705	20.003	-.044	12.003
16	45.687	20.823	-.062	12.823
17	45.663	21.652	-.086	13.652
18	45.631	22.492	-.118	14.492
19	45.588	23.347	-.161	15.347
20	45.532	24.221	-.217	16.221

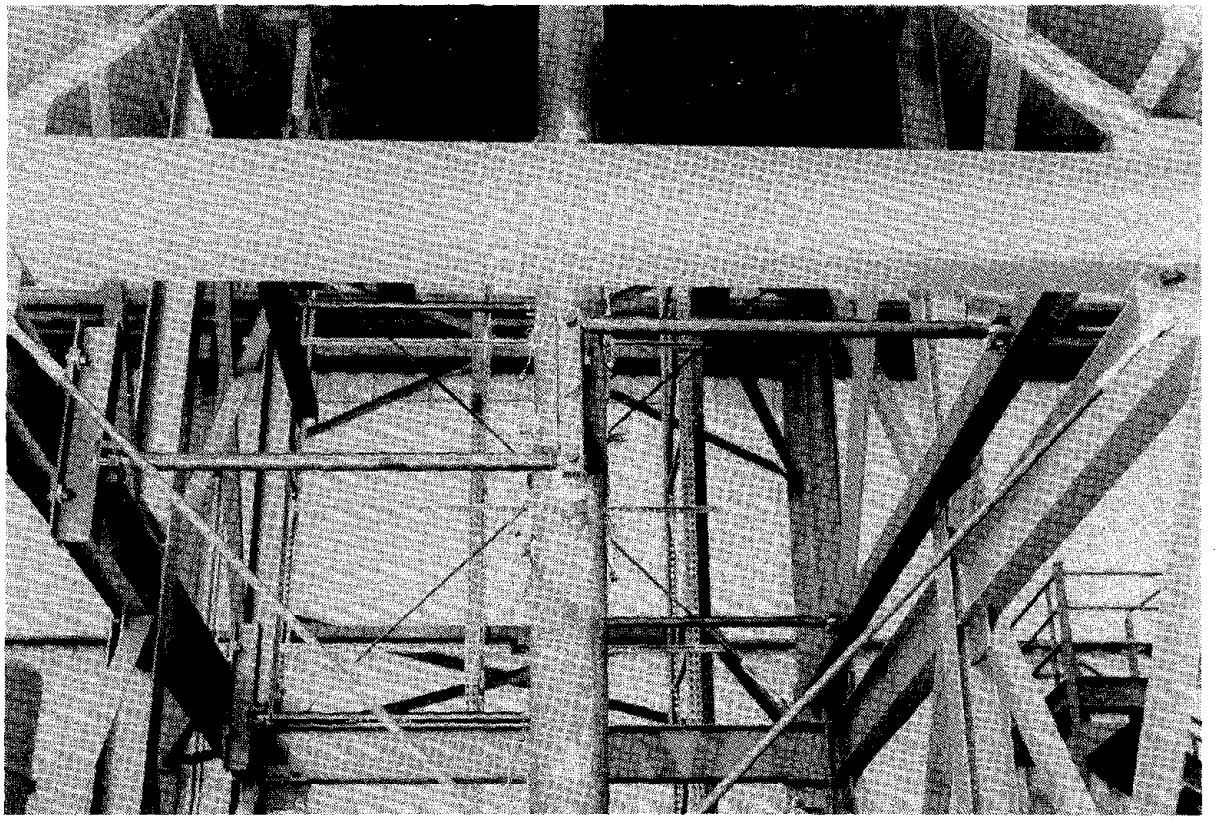

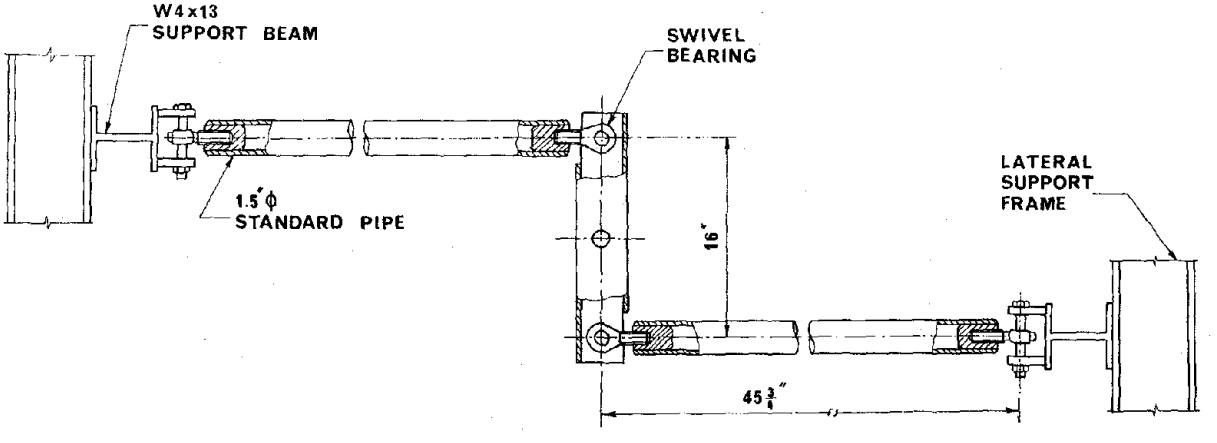

Fig. A1 Photograph and Drawing of Lateral Brace Mechanism used in the Test Model.

APPENDIX B

LIST OF DATA CHANNELS

Channel No.	Name	Maximum Measurable Data	Description
0	AV-H-T-DISP	9.92 in.	Average Horizontal Table Displacement
1	AV-V-T-DISP	2.53 in.	Average Vertical Table Displacement
2	AV-H-T-ACC	2.03 g	Average Horizontal Table Acceleration
3	AV-V-T-ACC	2.03 g	Average Vertical Table Acceleration
4	PITCH-ACC	10.1 rad/in^2	Table Angular Pitch Acceleration
5	ROLL-ACC	9.99 rad/in^2	Table Angular Roll Acceleration
6	TWIST-ACC	8.22 rad/in^2	Table Angular Twist Acceleration
7	BLANK	--	--
8	DISP-H1	10.0 in.	Horizontal Table Displacement at Actuator H1
9	DISP-H2	9.94 in.	Horizontal Table Displacement at Actuator H2
10	DISP-H3	10.0 in.	Horizontal Table Displacement at Actuator H3
11	FORCE-H1	128.0 kips	Force in Horizontal Actuator H1

Channel No.	Name	Maximum Measurable Data	Description
12	FORCE-H2	130.0 kips	Force in Horizontal Actuator H2
13	FORCE-H3	132.0 kips	Force in Horizontal Actuator H3
14	ACC-H1	2.05 g	Horizontal Table Acceleration at Actuator H1
15	ACC-H2	2.03 g	Horizontal Table Acceleration at Actuator H2
16	ACC-V1	2.06 g	Vertical Table Acceleration at Actuator V1
17	ACC-V2	2.04 g	Vertical Table Acceleration at Actuator V2
18	ACC-V3	2.07 g	Vertical Table Acceleration at Actuator V3
19	ACC-V4	2.03 g	Vertical Table Acceleration at Actuator V4
20	FORCE-V1	48.5 kips	Force in Vertical Actuator V1
21	FORCE-V2	48.8 kips	Force in Vertical Actuator V2
22	FORCE-V3	48.1 kips	Force in Vertical Actuator V3
23	FORCE-V4	48.5 kips	Force in Vertical Actuator V4
24	DISP-V1	2.58 in.	Vertical Table Displacement at Actuator V1

Channel No.	Name	Maximum Measurable Data	Description
25	DISP-V2	2.45 in.	Vertical Table Displacement at Actuator V2
26	DISP-V3	2.54 in.	Vertical Table Displacement at Actuator V3
27	DISP-V4	2.86 in.	Vertical Table Displacement at Actuator V4
28	BLANK	--	--
29	ACC-LNG	4.81 g	Deck Longitudinal Acceleration
30	ACC-TR1	4.67 g	Transverse Deck Acceleration 1
31	ACC-TR2	4.91 g	Transverse Deck Acceleration 2
32	DISP-TLNG	16.3 in.	Absolute Longitudinal Deck Displacement
33	DISP-UPLNG	15.1 in.	Absolute Longitudinal Frame Displacement at Upper Joint
34	DISP-LPLNG	8.30 in.	Relative Longitudinal Frame Displacement at Mid-Joint
35	DISP-BPLNG	16.6 in.	Absolute Longitudinal Frame Displacement at Lower-Joint
36	DISP-TTR1	16.6 in.	Relative Transverse Deck Displacement 1
37	DISP-TTR2	7.97 in.	Relative Transverse Deck Displacement 2

Channel No.	Name	Maximum Measurable Data	Description
38	DISP-UPTR	7.83 in.	Relative Transverse Displacement of the Upper Cross-Joint
39	DISP-LPTR	8.15 in.	Relative Transverse Displacement of the Lower Cross-Joint
40	DISP-LHB	1.07 in.	Axial Displacement of the Middle Horizontal Brace
41	DISP-UPB1	2.32 in.	Axial Displacement of the Brace 1
42	DISP-UPB2	2.53 in.	Axial Displacement of the Brace 2
43	DISP-UPB3	2.46 in.	Axial Displacement of the Brace 3
44	DISP-UPB4	2.39 in.	Axial Displacement of the Brace 4
45	DISP-LPB1	1.27 in.	Axial Displacement of the Brace 5
46	DISP-LPB2	1.25 in.	Axial Displacement of the Brace 6
47	DISP-LPB3	1.24 in.	Axial Displacement of the Brace 7
48	DISP-LPB4	1.38 in.	Axial Displacement of the Brace 8
49	BLANK	--	--
50	BLANK	--	--

Channel No.	Name	Maximum Measurable Data	Description
51	BLANK	--	--
52	AXST1-UPB1	4.77 milli in./in.	Axial Strain 1 in the Brace 1 Load Cell
53	AXST2-UPB1	4.82 milli in./in.	Axial Strain 2 in the Brace 1 Load Cell
54	AXST1-UPB2	4.86 milli in./in.	Axial Strain 1 in Brace 2 Load Cell
55	AXST2-UPB2	4.83 milli in./in.	Axial Strain 2 in Brace 2 Load Cell
56	AXST1-UPB3	4.81 milli in./in.	Axial Strain 1 in Brace 3 Load Cell
57	AXST2-UPB3	4.82 milli in./in.	Axial Strain 2 in Brace 3 Load Cell
58	AXST1-UPB4	4.82 milli in./in.	Axial Strain 1 in Brace 4 Load Cell
59	AXST2-UPB4	4.81 milli in./in.	Axial Strain 2 in Brace 4 Load Cell
60	AXST1-LPB1	4.82 milli in./in.	Axial Strain 1 in Brace 5 Load Cell
61	AXST2-LPB1	4.84 milli in./in.	Axial Strain 2 in Brace 5 Load Cell
62	AXST1-LPB2	4.92 milli in./in.	Axial Strain 1 in Brace 6 Load Cell
63	AXST2-LPB2	4.85 milli in./in.	Axial Strain 2 in Brace 6 Load Cell

Channel No.	Name	Maximum Measurable Data	Description
64	AXST1-LPB3	4.84 milli in./in.	Axial Strain 1 in Brace 7 Load Cell
65	AXST2-LPB3	4.90 milli in./in.	Axial Strain 2 in Brace 7 Load Cell
66	AXST1-LPB4	4.85 milli in./in.	Axial Strain 1 in Brace 8 Load Cell
67	AXST2-LPB4	4.90 milli in./in.	Axial Strain 2 in Brace 8 Load Cell
68	AXST1-TKB1	4.83 milli in./in.	Axial Strain 1 in K-Brace 1
69	AXST2-TKB1	4.84 milli in./in.	Axial Strain 2 in K-Brace 1
70	AXST1-TKB2	4.79 milli in./in.	Axial Strain 1 in K-Brace 2
71	AXST2-TKB2	4.83 milli in./in.	Axial Strain 2 in K-Brace 2
72	AXST1-UHB	9.76 milli in./in.	Axial Strain 1 in Upper Horizontal Brace
73	AXST2-UHB	9.75 milli in./in.	Axial Strain 2 in Upper Horizontal Brace
74	AXST1-LHB	4.82 milli in./in.	Axial Strain 1 in Lower Horizontal Brace Load Cell
75	AXST2-LHB	4.87 milli in./in.	Axial Strain 2 in Lower Horizontal Brace Load Cell
76	AXST1-BHB	4.89 milli in./in.	Axial Strain 1 in Bottom Horizontal Brace

Channel No.	Name	Maximum Measurable Data	Description
77	AXST2-BHB	4.82 milli in./in.	Axial Strain 2 in Bottom Horizontal Brace
78	BNDST1-UPB4	48.9 milli in./in.	Bending Strain 1 in Brace 4
79	BNDST2-UPB4	49.0 milli in./in.	Bending Strain 2 in Brace 4
80	BNDST3-UPB4	49.0 milli in./in.	Bending Strain 3 in Brace 4
81	BNDST4-UPB4	49.6 milli in./in.	Bending Strain 4 in Brace 4
82	BNDSTT-UPJ1	12.5 milli in./in.	Bending Strain in Top-End of the Upper Panel Jacket 1
83	BNDSTB-UPJ1	12.6 milli in./in.	Bending Strain in Bottom-End of the Upper Panel Jacket 1
84	BNDSTT-UPJ2	12.4 milli in./in.	Bending Strain in Top-End of the Upper Panel Jacket 2
85	BNDSTB-UPJ2	12.3 milli in./in.	Bending Strain in Bottom-End of the Upper Panel Jacket 2
86	BNDSTT-LPJ1	12.4 milli in./in.	Bending Strain in Top-End of the Lower Panel Jacket 1
87	BNDSTB-LPJ1	12.3 milli in./in.	Bending Strain in Bottom-End of the Lower Panel Jacket 1
88	BNDSTT-LPJ2	12.3 milli in./in.	Bending Strain in Top-End of the Lower Panel Jacket 2
89	BNDSTB-LPJ2	12.3 milli in./in.	Bending Strain in Bottom-End of the Lower Panel Jacket 2

Channel No.	Name	Maximum Measurable Data	Description
90	BNDSTT-BPJ1	12.4 milli in./in.	Bending Strain in Top-End of the Bottom Panel Jacket 1
91	BNDSTT-BPJ2	12.4 milli in./in.	Bending Strain in Top-End of the Bottom Panel Jacket 2
92	AXST-UPJ1	4.80 milli in./in.	Axial Strain in Upper Panel Jacket 1
93	AXST-UPJ2	4.83 milli in./in.	Axial Strain in Upper Panel Jacket 2
94	AXST-LPJ1	4.82 milli in./in.	Axial Strain in Lower Panel Jacket 1
95	AXST-LPJ2	4.81 milli in./in.	Axial Strain in Lower Panel Jacket 2
96	AXST-BPJ1	4.29 milli in./in.	Axial Strain in Bottom Panel Jacket 1
97	AXST-BPJ2	4.81 milli in./in.	Axial Strain in Bottom Panel Jacket 2
98	BLANK	--	---
99	BLANK	--	---
100	DISP-UCTR	16.4 in.	Absolute Longitudinal Displacement of the Upper Cross-Joint
101	DISP-LCTR	16.5 in.	Absolute Longitudinal Displacement of the Lower Cross-Joint

EARTHQUAKE ENGINEERING RESEARCH CENTER REPORTS

NOTE: Numbers in parentheses are Accession Numbers assigned by the National Technical Information Service; these are followed by a price code. Copies of the reports may be ordered from the National Technical Information Service, 5285 Port Royal Road, Springfield, Virginia, 22161. Accession Numbers should be quoted on orders for reports (PB --- ---) and remittance must accompany each order. Reports without this information were not available at time of printing. The complete list of EERC reports (from EERC 67-1) is available upon request from the Earthquake Engineering Research Center, University of California, Berkeley, 47th Street and Hoffman Boulevard, Richmond, California 94804.

UCB/EERC-77/01 "PLUSH - A Computer Program for Probabilistic Finite Element Analysis of Seismic Soil-Structure Interaction," by M.P. Romo Organista, J. Lysmer and H.B. Seed - 1977 (PB81 177 651)A05

UCB/EERC-77/02 "Soil-Structure Interaction Effects at the Humboldt Bay Power Plant in the Ferndale Earthquake of June 7, 1975," by J.E. Valera, H.B. Seed, C.F. Tsai and J. Lysmer - 1977 (PB 265 795)A04

UCB/EERC-77/03 "Influence of Sample Disturbance on Sand Response to Cyclic Loading," by K. Mori, H.B. Seed and C.K. Chan - 1977 (PB 267 352)A04

UCB/EERC-77/04 "Seismological Studies of Strong Motion Records," by J. Shoja-Taheri - 1977 (PB 269 655)A10

UCB/EERC-77/05 Unassigned

UCB/EERC-77/06 "Developing Methodologies for Evaluating the Earthquake Safety of Existing Buildings," by No. 1 - B. Bresler; No. 2 - B. Bresler, T. Okada and D. Zisling; No. 3 - T. Okada and B. Bresler; No. 4 - V.V. Bertero and B. Bresler - 1977 (PB 267 354)A08

UCB/EERC-77/07 "A Literature Survey - Transverse Strength of Masonry Walls," by Y. Omote, R.L. Mayes, S.W. Chen and R.W. Clough - 1977 (PB 277 933)A07

UCB/EERC-77/08 "DRAIN-TABS: A Computer Program for Inelastic Earthquake Response of Three Dimensional Buildings," by R. Guendelman-Israel and G.H. Powell - 1977 (PB 270 693)A07

UCB/EERC-77/09 "SUBWALL: A Special Purpose Finite Element Computer Program for Practical Elastic Analysis and Design of Structural Walls with Substructure Option," by D.Q. Le, H. Peterson and E.P. Popov - 1977 (PB 270 567)A05

UCB/EERC-77/10 "Experimental Evaluation of Seismic Design Methods for Broad Cylindrical Tanks," by D.P. Clough (PB 272 280)A13

UCB/EERC-77/11 "Earthquake Engineering Research at Berkeley - 1976," - 1977 (PB 273 507)A09

UCB/EERC-77/12 "Automated Design of Earthquake Resistant Multistory Steel Building Frames," by N.D. Walker, Jr. - 1977 (PB 276 526)A09

UCB/EERC-77/13 "Concrete Confined by Rectangular Hoops Subjected to Axial Loads," by J. Vallenas, V.V. Bertero and E.P. Popov - 1977 (PB 275 165)A06

UCB/EERC-77/14 "Seismic Strain Induced in the Ground During Earthquakes," by Y. Sugimura - 1977 (PB 284 201)A04

UCB/EERC-77/15 Unassigned

UCB/EERC-77/16 "Computer Aided Optimum Design of Ductile Reinforced Concrete Moment Resisting Frames," by S.W. Zagajeski and V.V. Bertero - 1977 (PB 280 137)A07

UCB/EERC-77/17 "Earthquake Simulation Testing of a Stepping Frame with Energy-Absorbing Devices," by J.M. Kelly and D.F. Tsztoo - 1977 (PB 273 506)A04

UCB/EERC-77/18 "Inelastic Behavior of Eccentrically Braced Steel Frames under Cyclic Loadings," by C.W. Roeder and E.P. Popov - 1977 (PB 275 526)A15

UCB/EERC-77/19 "A Simplified Procedure for Estimating Earthquake-Induced Deformations in Dams and Embankments," by F.I. Makdisi and H.B. Seed - 1977 (PB 276 820)A04

UCB/EERC-77/20 "The Performance of Earth Dams during Earthquakes," by H.B. Seed, F.I. Makdisi and P. de Alba - 1977 (PB 276 821)A04

UCB/EERC-77/21 "Dynamic Plastic Analysis Using Stress Resultant Finite Element Formulation," by P. Lukkunapvasit and J.M. Kelly - 1977 (PB 275 453)A04

UCB/EERC-77/22 "Preliminary Experimental Study of Seismic Uplift of a Steel Frame," by R.W. Clough and A.A. Huckelbridge 1977 (PB 278 769)A08

UCB/EERC-77/23 "Earthquake Simulator Tests of a Nine-Story Steel Frame with Columns Allowed to Uplift," by A.A. Huckelbridge - 1977 (PB 277 944)A09

UCB/EERC-77/24 "Nonlinear Soil-Structure Interaction of Skew Highway Bridges," by M.-C. Chen and J. Penzien - 1977 (PB 276 176)A07

UCB/EERC-77/25 "Seismic Analysis of an Offshore Structure Supported on Pile Foundations," by D.D.-N. Liou and J. Penzien 1977 (PB 283 180)A06

UCB/EERC-77/26 "Dynamic Stiffness Matrices for Homogeneous Viscoelastic Half-Planes," by G. Dasgupta and A.K. Chopra - 1977 (PB 279 654)A06

UCB/EERC-77/27 "A Practical Soft Story Earthquake Isolation System," by J.M. Kelly, J.M. Eidinger and C.J. Derham - 1977 (PB 276 814)A07

UCB/EERC-77/28 "Seismic Safety of Existing Buildings and Incentives for Hazard Mitigation in San Francisco: An Exploratory Study," by A.J. Meltsner - 1977 (PB 281 970)A05

UCB/EERC-77/29 "Dynamic Analysis of Electrohydraulic Shaking Tables," by D. Rea, S. Abedi-Hayati and Y. Takahashi 1977 (PB 282 569)A04

UCB/EERC-77/30 "An Approach for Improving Seismic - Resistant Behavior of Reinforced Concrete Interior Joints," by B. Galunic, V.V. Bertero and E.P. Popov - 1977 (PB 290 870)A06

UCB/EERC-78/01 "The Development of Energy-Absorbing Devices for Aseismic Base Isolation Systems," by J.M. Kelly and D.F. Tsztoo - 1978 (PB 284 978)A04

UCB/EERC-78/02 "Effect of Tensile Prestrain on the Cyclic Response of Structural Steel Connections, by J.G. Bouwkamp and A. Mukhopadhyay - 1978

UCB/EERC-78/03 "Experimental Results of an Earthquake Isolation System using Natural Rubber Bearings," by J.M. Eidinger and J.M. Kelly - 1978 (PB 281 686)A04

UCB/EERC-78/04 "Seismic Behavior of Tall Liquid Storage Tanks," by A. Niwa - 1978 (PB 284 017)A14

UCB/EERC-78/05 "Hysteretic Behavior of Reinforced Concrete Columns Subjected to High Axial and Cyclic Shear Forces," by S.W. Zagajeski, V.V. Bertero and J.G. Bouwkamp - 1978 (PB 283 858)A13

UCB/EERC-78/06 "Three Dimensional Inelastic Frame Elements for the ANSR-I Program," by A. Riahi, D.G. Row and G.H. Powell - 1978 (PB 295 755)A04

UCB/EERC-78/07 "Studies of Structural Response to Earthquake Ground Motion," by O.A. Lopez and A.K. Chopra - 1978 (PB 282 790)A05

UCB/EERC-78/08 "A Laboratory Study of the Fluid-Structure Interaction of Submerged Tanks and Caissons in Earthquakes," by R.C. Byrd - 1978 (PB 284 957)A08

UCB/EERC-78/09 Unassigned

UCB/EERC-78/10 "Seismic Performance of Nonstructural and Secondary Structural Elements," by I. Sakamoto - 1978 (PB81 154 593)A05

UCB/EERC-78/11 "Mathematical Modelling of Hysteresis Loops for Reinforced Concrete Columns," by S. Nakata, T. Sproul and J. Penzien - 1978 (PB 298 274)A05

UCB/EERC-78/12 "Damageability in Existing Buildings," by T. Blejwas and B. Bresler - 1978 (PB 80 166 978)A05

UCB/EERC-78/13 "Dynamic Behavior of a Pedestal Base Multistory Building," by R.M. Stephen, E.L. Wilson, J.G. Bouwkamp and M. Button - 1978 (PB 286 650)A08

UCB/EERC-78/14 "Seismic Response of Bridges - Case Studies," by R.A. Imbsen, V. Nutt and J. Penzien - 1978 (PB 286 503)A10

UCB/EERC-78/15 "A Substructure Technique for Nonlinear Static and Dynamic Analysis," by D.G. Row and G.H. Powell - 1978 (PB 288 077)A10

UCB/EERC-78/16 "Seismic Risk Studies for San Francisco and for the Greater San Francisco Bay Area," by C.S. Oliveira - 1978 (PB 81 120 115)A07

UCB/EERC-78/17 "Strength of Timber Roof Connections Subjected to Cyclic Loads," by P. Gülkan, R.L. Mayes and R.W. Clough - 1978 (HUD-000 1491)A07

UCB/EERC-78/18 "Response of K-Braced Steel Frame Models to Lateral Loads," by J.G. Bouwkamp, R.M. Stephen and E.P. Popov - 1978

UCB/EERC-78/19 "Rational Design Methods for Light Equipment in Structures Subjected to Ground Motion," by J.L. Sackman and J.M. Kelly - 1978 (PB 292 357)A04

UCB/EERC-78/20 "Testing of a Wind Restraint for Aseismic Base Isolation," by J.M. Kelly and D.E. Chitty - 1978 (PB 292 833)A03

UCB/EERC-78/21 "APOLLO - A Computer Program for the Analysis of Pore Pressure Generation and Dissipation in Horizontal Sand Layers During Cyclic or Earthquake Loading," by P.P. Martin and H.B. Seed - 1978 (PB 292 835)A04

UCB/EERC-78/22 "Optimal Design of an Earthquake Isolation System," by M.A. Bhatti, K.S. Pister and E. Polak - 1978 (PB 294 735)A06

UCB/EERC-78/23 "MASH - A Computer Program for the Non-Linear Analysis of Vertically Propagating Shear Waves in Horizontally Layered Deposits," by P.P. Martin and H.B. Seed - 1978 (PB 293 101)A05

UCB/EERC-78/24 "Investigation of the Elastic Characteristics of a Three Story Steel Frame Using System Identification," by I. Kaya and H.D. McNiven - 1978 (PB 296 225)A06

UCB/EERC-78/25 "Investigation of the Nonlinear Characteristics of a Three-Story Steel Frame Using System Identification," by I. Kaya and H.D. McNiven - 1978 (PB 301 363)A05

UCB/EERC-78/26 "Studies of Strong Ground Motion in Taiwan," by Y.M. Hsiung, B.A. Bolt and J. Penzien - 1978 (PB 298 436)A06

UCB/EERC-78/27 "Cyclic Loading Tests of Masonry Single Piers: Volume 1 - Height to Width Ratio of 2," by P.A. Hidalgo, R.L. Mayes, H.D. McNiven and R.W. Clough - 1978 (PB 296 211)A07

UCB/EERC-78/28 "Cyclic Loading Tests of Masonry Single Piers: Volume 2 - Height to Width Ratio of 1," by S.-W.J. Chen, P.A. Hidalgo, R.L. Mayes, R.W. Clough and H.D. McNiven - 1978 (PB 296 212)A09

UCB/EERC-78/29 "Analytical Procedures in Soil Dynamics," by J. Lysmer - 1978 (PB 298 445)A06

UCB/EERC-79/01 "Hysteretic Behavior of Lightweight Reinforced Concrete Beam-Column Subassemblages," by B. Forzani, E.P. Popov and V.V. Bertero - April 1979(PB 298 267)A06

UCB/EERC-79/02 "The Development of a Mathematical Model to Predict the Flexural Response of Reinforced Concrete Beams to Cyclic Loads, Using System Identification," by J. Stanton & H. McNiven - Jan. 1979(PB 295 875)A10

UCB/EERC-79/03 "Linear and Nonlinear Earthquake Response of Simple Torsionally Coupled Systems," by C.L. Kan and A.K. Chopra - Feb. 1979(PB 298 262)A06

UCB/EERC-79/04 "A Mathematical Model of Masonry for Predicting its Linear Seismic Response Characteristics," by Y. Mengi and H.D. McNiven - Feb. 1979(PB 298 266)A06

UCB/EERC-79/05 "Mechanical Behavior of Lightweight Concrete Confined by Different Types of Lateral Reinforcement," by M.A. Manrique, V.V. Bertero and E.P. Popov - May 1979(PB 301 114)A06

UCB/EERC-79/06 "Static Tilt Tests of a Tall Cylindrical Liquid Storage Tank," by R.W. Clough and A. Niwa - Feb. 1979 (PB 301 167)A06

UCB/EERC-79/07 "The Design of Steel Energy Absorbing Restrainers and Their Incorporation into Nuclear Power Plants for Enhanced Safety: Volume 1 - Summary Report," by P.N. Spencer, V.F. Zackay, and E.R. Parker - Feb. 1979(UCB/EERC-79/07)A09

UCB/EERC-79/08 "The Design of Steel Energy Absorbing Restrainers and Their Incorporation into Nuclear Power Plants for Enhanced Safety: Volume 2 - The Development of Analyses for Reactor System Piping,""Simple Systems" by M.C. Lee, J. Penzien, A.K. Chopra and K. Suzuki "Complex Systems" by G.H. Powell, E.L. Wilson, R.W. Clough and D.G. Row - Feb. 1979(UCB/EERC-79/08)A10

UCB/EERC-79/09 "The Design of Steel Energy Absorbing Restrainers and Their Incorporation into Nuclear Power Plants for Enhanced Safety: Volume 3 - Evaluation of Commercial Steels," by W.S. Owen, R.M.N. Pelloux, R.O. Ritchie, M. Faral, T. Ohhashi, J. Toplosky, S.J. Hartman, V.F. Zackay and E.R. Parker - Feb. 1979(UCB/EERC-79/09)A04

UCB/EERC-79/10 "The Design of Steel Energy Absorbing Restrainers and Their Incorporation into Nuclear Power Plants for Enhanced Safety: Volume 4 - A Review of Energy-Absorbing Devices," by J.M. Kelly and M.S. Skinner - Feb. 1979(UCB/EERC-79/10)A04

UCB/EERC-79/11 "Conservatism In Summation Rules for Closely Spaced Modes," by J.M. Kelly and J.L. Sackman - May 1979(PB 301 328)A03

UCB/EERC-79/12 "Cyclic Loading Tests of Masonry Single Piers; Volume 3 - Height to Width Ratio of 0.5," by P.A. Hidalgo, R.L. Mayes, H.D. McNiven and R.W. Clough - May 1979(PB 301 321)A08

UCB/EERC-79/13 "Cyclic Behavior of Dense Course-Grained Materials in Relation to the Seismic Stability of Dams," by N.G. Banerjee, H.B. Seed and C.K. Chan - June 1979(PB 301 373)A13

UCB/EERC-79/14 "Seismic Behavior of Reinforced Concrete Interior Beam-Column Subassemblages," by S. Viwathanatepa, E.P. Popov and V.V. Bertero - June 1979(PB 301 326)A10

UCB/EERC-79/15 "Optimal Design of Localized Nonlinear Systems with Dual Performance Criteria Under Earthquake Excitations," by M.A. Bhatti - July 1979(PB 80 167 109)A06

UCB/EERC-79/16 "OPTDYN - A General Purpose Optimization Program for Problems with or without Dynamic Constraints," by M.A. Bhatti, E. Polak and K.S. Pister - July 1979(PB 80 167 091)A05

UCB/EERC-79/17 "ANSR-II, Analysis of Nonlinear Structural Response, Users Manual," by D.P. Mondkar and G.H. Powell July 1979(PB 80 113 301)A05

UCB/EERC-79/18 "Soil Structure Interaction in Different Seismic Environments," A. Gomez-Masso, J. Lysmer, J.-C. Chen and H.B. Seed - August 1979(PB 80 101 520)A04

UCB/EERC-79/19 "ARMA Models for Earthquake Ground Motions," by M.K. Chang, J.W. Kwiatkowski, R.F. Nau, R.M. Oliver and K.S. Pister - July 1979(PB 301 166)A05

UCB/EERC-79/20 "Hysteretic Behavior of Reinforced Concrete Structural Walls," by J.M. Vallenas, V.V. Bertero and E.P. Popov - August 1979(PB 80 165 905)A12

UCB/EERC-79/21 "Studies on High-Frequency Vibrations of Buildings - 1: The Column Effect," by J. Lubliner - August 1979 (PB 80 158 553)A03

UCB/EERC-79/22 "Effects of Generalized Loadings on Bond Reinforcing Bars Embedded in Confined Concrete Blocks," by S. Viwathanatepa, E.P. Popov and V.V. Bertero - August 1979(PB 81 124 018)A14

UCB/EERC-79/23 "Shaking Table Study of Single-Story Masonry Houses, Volume 1: Test Structures 1 and 2," by P. Gülkan, R.L. Mayes and R.W. Clough - Sept. 1979 (HUD-000 1763)A12

UCB/EERC-79/24 "Shaking Table Study of Single-Story Masonry Houses, Volume 2: Test Structures 3 and 4," by P. Gülkan, R.L. Mayes and R.W. Clough - Sept. 1979 (HUD-000 1836)A12

UCB/EERC-79/25 "Shaking Table Study of Single-Story Masonry Houses, Volume 3: Summary, Conclusions and Recommendations," by R.W. Clough, R.L. Mayes and P. Gülkan - Sept. 1979 (HUD-000 1837)A06

UCB/EERC-79/26 "Recommendations for a U.S.-Japan Cooperative Research Program Utilizing Large-Scale Testing Facilities," by U.S.-Japan Planning Group - Sept. 1979(PB 301 407)A06

UCB/EERC-79/27 "Earthquake-Induced Liquefaction Near Lake Amatitlan, Guatemala," by H.B. Seed, I. Arango, C.K. Chan, A. Gomez-Masso and R. Grant de Ascoli - Sept. 1979(NUREG-CR1341)A03

UCB/EERC-79/28 "Infill Panels: Their Influence on Seismic Response of Buildings," by J.W. Axley and V.V. Bertero Sept. 1979(PB 80 163 371)A10

UCB/EERC-79/29 "3D Truss Bar Element (Type 1) for the ANSR-II Program," by D.P. Mondkar and G.H. Powell - Nov. 1979 (PB 80 169 709)A02

UCB/EERC-79/30 "2D Beam-Column Element (Type 5 - Parallel Element Theory) for the ANSR-II Program," by D.G. Row, G.H. Powell and D.P. Mondkar - Dec. 1979(PB 80 167 224)A03

UCB/EERC-79/31 "3D Beam-Column Element (Type 2 - Parallel Element Theory) for the ANSR-II Program," by A. Riahi, G.H. Powell and D.P. Mondkar - Dec. 1979(PB 80 167 216)A03

UCB/EERC-79/32 "On Response of Structures to Stationary Excitation," by A. Der Kiureghian - Dec. 1979(PB 80166 929)A03

UCB/EERC-79/33 "Undisturbed Sampling and Cyclic Load Testing of Sands," by S. Singh, H.B. Seed and C.K. Chan Dec. 1979(ADA 087 298)A07

UCB/EERC-79/34 "Interaction Effects of Simultaneous Torsional and Compressional Cyclic Loading of Sand," by P.M. Griffin and W.N. Houston - Dec. 1979(ADA 092 352)A15

UCB/EERC-80/01 "Earthquake Response of Concrete Gravity Dams Including Hydrodynamic and Foundation Interaction Effects," by A.K. Chopra, P. Chakrabarti and S. Gupta - Jan. 1980(AD-A087297)A10

UCB/EERC-80/02 "Rocking Response of Rigid Blocks to Earthquakes," by C.S. Yim, A.K. Chopra and J. Penzien - Jan. 1980 (PB80 166 002)A04

UCB/EERC-80/03 "Optimum Inelastic Design of Seismic-Resistant Reinforced Concrete Frame Structures," by S.W. Zagajeski and V.V. Bertero - Jan. 1980(PB80 164 635)A06

UCB/EERC-80/04 "Effects of Amount and Arrangement of Wall-Panel Reinforcement on Hysteretic Behavior of Reinforced Concrete Walls," by R. Iliya and V.V. Bertero - Feb. 1980(PB81 122 525)A09

UCB/EERC-80/05 "Shaking Table Research on Concrete Dam Models," by A. Niwa and R.W. Clough - Sept. 1980(PB81 122 368)A06

UCB/EERC-80/06 "The Design of Steel Energy-Absorbing Restrainers and their Incorporation into Nuclear Power Plants for Enhanced Safety (Vol 1A): Piping with Energy Absorbing Restrainers: Parameter Study on Small Systems," by G.H. Powell, C. Oughourlian and J. Simons - June 1980

UCB/EERC-80/07 "Inelastic Torsional Response of Structures Subjected to Earthquake Ground Motions," by Y. Yamazaki April 1980(PB81 122 327)A08

UCB/EERC-80/08 "Study of X-Braced Steel Frame Structures Under Earthquake Simulation," by Y. Ghanaat - April 1980 (PB81 122 335)A11

UCB/EERC-80/09 "Hybrid Modelling of Soil-Structure Interaction," by S. Gupta, T.W. Lin, J. Penzien and C.S. Yeh May 1980(PB81 122 319)A07

UCB/EERC-80/10 "General Applicability of a Nonlinear Model of a One Story Steel Frame," by B.I. Sveinsson and H.D. McNiven - May 1980(PB81 124 877)A06

UCB/EERC-80/11 "A Green-Function Method for Wave Interaction with a Submerged Body," by W. Kioka - April 1980 (PB81 122 269)A07

UCB/EERC-80/12 "Hydrodynamic Pressure and Added Mass for Axisymmetric Bodies," by F. Nilrat - May 1980(PB81 122 343)A08

UCB/EERC-80/13 "Treatment of Non-Linear Drag Forces Acting on Offshore Platforms," by B.V. Dao and J. Penzien May 1980(PB81 153 413)A07

UCB/EERC-80/14 "2D Plane/Axisymmetric Solid Element (Type 3 - Elastic or Elastic-Perfectly Plastic) for the ANSR-II Program," by D.P. Mondkar and G.H. Powell - July 1980(PB81 122 350)A03

UCB/EERC-80/15 "A Response Spectrum Method for Random Vibrations," by A. Der Kiureghian - June 1980(PB81 122 301)A03

UCB/EERC-80/16 "Cyclic Inelastic Buckling of Tubular Steel Braces," by V.A. Zayas, E.P. Popov and S.A. Mahin June 1980(PB81 124 885)A10

UCB/EERC-80/17 "Dynamic Response of Simple Arch Dams Including Hydrodynamic Interaction," by C.S. Porter and A.K. Chopra - July 1980(PB81 124 000)A13

UCB/EERC-80/18 "Experimental Testing of a Friction Damped Aseismic Base Isolation System with Fail-Safe Characteristics," by J.M. Kelly, K.E. Beucke and M.S. Skinner - July 1980(PB81 148 595)A04

UCB/EERC-80/19 "The Design of Steel Energy-Absorbing Restrainers and their Incorporation into Nuclear Power Plants for Enhanced Safety (Vol 1B): Stochastic Seismic Analyses of Nuclear Power Plant Structures and Piping Systems Subjected to Multiple Support Excitations," by M.C. Lee and J. Penzien - June 1980

UCB/EERC-80/20 "The Design of Steel Energy-Absorbing Restrainers and their Incorporation into Nuclear Power Plants for Enhanced Safety (Vol 1C): Numerical Method for Dynamic Substructure Analysis," by J.M. Dickens and E.L. Wilson - June 1980

UCB/EERC-80/21 "The Design of Steel Energy-Absorbing Restrainers and their Incorporation into Nuclear Power Plants for Enhanced Safety (Vol 2): Development and Testing of Restraints for Nuclear Piping Systems," by J.M. Kelly and M.S. Skinner - June 1980

UCB/EERC-80/22 "3D Solid Element (Type 4-Elastic or Elastic-Perfectly-Plastic) for the ANSR-II Program," by D.P. Mondkar and G.H. Powell - July 1980(PB81 123 242)A03

UCB/EERC-80/23 "Gap-Friction Element (Type 5) for the ANSR-II Program," by D.P. Mondkar and G.H. Powell - July 1980 (PB81 122 285)A03

UCB/EERC-80/24 "U-Bar Restraint Element (Type 11) for the ANSR-II Program," by C. Oughourlian and G.H. Powell July 1980(PB81 122 293)A03

UCB/EERC-80/25 "Testing of a Natural Rubber Base Isolation System by an Explosively Simulated Earthquake," by J.M. Kelly - August 1980(PB81 201 360)A04

UCB/EERC-80/26 "Input Identification from Structural Vibrational Response," by Y. Hu - August 1980(PB81 152 308)A05

UCB/EERC-80/27 "Cyclic Inelastic Behavior of Steel Offshore Structures," by V.A. Zayas, S.A. Mahin and E.P. Popov August 1980(PB81 196 180)A15

UCB/EERC-80/28 "Shaking Table Testing of a Reinforced Concrete Frame with Biaxial Response," by M.G. Oliva October 1980(PB81 154 304)A10

UCB/EERC-80/29 "Dynamic Properties of a Twelve-Story Prefabricated Panel Building," by J.G. Bouwkamp, J.P. Kollegger and R.M. Stephen - October 1980(PB82 117 128)A06

UCB/EERC-80/30 "Dynamic Properties of an Eight-Story Prefabricated Panel Building," by J.G. Bouwkamp, J.P. Kollegger and R.M. Stephen - October 1980(PB81 200 313)A05

UCB/EERC-80/31 "Predictive Dynamic Response of Panel Type Structures Under Earthquakes," by J.P. Kollegger and J.G. Bouwkamp - October 1980(PB81 152 316)A04

UCB/EERC-80/32 "The Design of Steel Energy-Absorbing Restrainers and their Incorporation into Nuclear Power Plants for Enhanced Safety (Vol 3): Testing of Commercial Steels in Low-Cycle Torsional Fatigue," by P. Spencer, E.R. Parker, E. Jongewaard and M. Drory

UCB/EERC-80/33 "The Design of Steel Energy-Absorbing Restrainers and their Incorporation into Nuclear Power Plants for Enhanced Safety (Vol 4): Shaking Table Tests of Piping Systems with Energy-Absorbing Restrainers," by S.F. Stiemer and W.G. Godden - Sept. 1980

UCB/EERC-80/34 "The Design of Steel Energy-Absorbing Restrainers and their Incorporation into Nuclear Power Plants for Enhanced Safety (Vol 5): Summary Report," by P. Spencer

UCB/EERC-80/35 "Experimental Testing of an Energy-Absorbing Base Isolation System," by J.M. Kelly, M.S. Skinner and K.E. Beucke - October 1980(PB81 154 072)A04

UCB/EERC-80/36 "Simulating and Analyzing Artificial Non-Stationary Earthquake Ground Motions," by R.F. Nau, R.M. Oliver and K.S. Pister - October 1980(PB81 153 397)A04

UCB/EERC-80/37 "Earthquake Engineering at Berkeley - 1980," - Sept. 1980(PB81 205 874)A09

UCB/EERC-80/38 "Inelastic Seismic Analysis of Large Panel Buildings," by V. Schricker and G.H. Powell - Sept. 1980 (PB81 154 338)A13

UCB/EERC-80/39 "Dynamic Response of Embankment, Concrete-Gravity and Arch Dams Including Hydrodynamic Interaction," by J.F. Hall and A.K. Chopra - October 1980(PB81 152 324)A11

UCB/EERC-80/40 "Inelastic Buckling of Steel Struts Under Cyclic Load Reversal," by R.G. Black, W.A. Wenger and E.P. Popov - October 1980(PB81 154 312)A08

UCB/EERC-80/41 "Influence of Site Characteristics on Building Damage During the October 3, 1974 Lima Earthquake," by P. Repetto, I. Arango and H.B. Seed - Sept. 1980(PB81 161 739)A05

UCB/EERC-80/42 "Evaluation of a Shaking Table Test Program on Response Behavior of a Two Story Reinforced Concrete Frame," by J.M. Blondet, R.W. Clough and S.A. Mahin

UCB/EERC-80/43 "Modelling of Soil-Structure Interaction by Finite and Infinite Elements," by F. Medina - December 1980(PB81 229 270)A04

UCB/EERC-81/01 "Control of Seismic Response of Piping Systems and Other Structures by Base Isolation," edited by J.M. Kelly - January 1981 (PB81 200 735)A05

UCB/EERC-81/02 "OPTNSR - An Interactive Software System for Optimal Design of Statically and Dynamically Loaded Structures with Nonlinear Response," by M.A. Bhatti, V. Ciampi and K.S. Pister - January 1981 (PB81 218 851)A09

UCB/EERC-81/03 "Analysis of Local Variations in Free Field Seismic Ground Motions," by J.-C. Chen, J. Lysmer and H.B. Seed - January 1981 (AD-A099508)A13

UCB/EERC-81/04 "Inelastic Structural Modeling of Braced Offshore Platforms for Seismic Loading," by V.A. Zayas, P.-S.B. Shing, S.A. Mahin and E.P. Popov - January 1981(PB82 138 777)A07

UCB/EERC-81/05 "Dynamic Response of Light Equipment in Structures," by A. Der Kiureghian, J.L. Sackman and B. Nour-Omid - April 1981 (PB81 218 497)A04

UCB/EERC-81/06 "Preliminary Experimental Investigation of a Broad Base Liquid Storage Tank," by J.G. Bouwkamp, J.P. Kollegger and R.M. Stephen - May 1981(PB82 140 385)A03

UCB/EERC-81/07 "The Seismic Resistant Design of Reinforced Concrete Coupled Structural Walls," by A.E. Aktan and V.V. Bertero - June 1981(PB82 113 358)A11

UCB/EERC-81/08 "The Undrained Shearing Resistance of Cohesive Soils at Large Deformations," by M.R. Pyles and H.B. Seed - August 1981

UCB/EERC-81/09 "Experimental Behavior of a Spatial Piping System with Steel Energy Absorbers Subjected to a Simulated Differential Seismic Input," by S.F. Stiemer, W.G. Godden and J.M. Kelly - July 1981

UCB/EERC-81/10 "Evaluation of Seismic Design Provisions for Masonry in the United States," by B.I. Sveinsson, R.L. Mayes and H.D. McNiven - August 1981

UCB/EERC-81/11 "Two-Dimensional Hybrid Modelling of Soil-Structure Interaction," by T.-J. Tzong, S. Gupta and J. Penzien - August 1981(PB82 142 118)A04

UCB/EERC-81/12 "Studies on Effects of Infills in Seismic Resistant R/C Construction," by S. Brokken and V.V. Bertero - September 1981

UCB/EERC-81/13 "Linear Models to Predict the Nonlinear Seismic Behavior of a One-Story Steel Frame," by H. Valdimarsson, A.H. Shah and H.D. McNiven - September 1981(PB82 138 793)A07

UCB/EERC-81/14 "TLUSH: A Computer Program for the Three-Dimensional Dynamic Analysis of Earth Dams," by T. Kagawa, L.H. Mejia, H.B. Seed and J. Lysmer - September 1981(PB82 139 940)A06

UCB/EERC-81/15 "Three Dimensional Dynamic Response Analysis of Earth Dams," by L.H. Mejia and H.B. Seed - September 1981 (PB82 137 274)A12

UCB/EERC-81/16 "Experimental Study of Lead and Elastomeric Dampers for Base Isolation Systems," by J.M. Kelly and S.B. Hodder - October 1981

UCB/EERC-81/17 "The Influence of Base Isolation on the Seismic Response of Light Secondary Equipment," by J.M. Kelly - April 1981

UCB/EERC-81/18 "Studies on Evaluation of Shaking Table Response Analysis Procedures," by J. Marcial Blondet - November 1981

UCB/EERC-81/19 "DELIGHT.STRUCT: A Computer-Aided Design Environment for Structural Engineering," by R.J. Balling, K.S. Pister and E. Polak - December 1981

UCB/EERC-81/20 "Optimal Design of Seismic-Resistant Planar Steel Frames," by R.J. Balling, V. Ciampi, K.S. Pister and E. Polak - December 1981

UCB/EERC-82/01 "Dynamic Behavior of Ground for Seismic Analysis Lifeline Systems," by T. Sato, A. Der Kiureghian - Jaunary 1982

UCB/EERC-82/02 "Shaking Table Tests of a Tubular Steel Frame Model," by Y. Ghanaat, R. W. Clough - January 1982